UNIVERSITY OF SOUTHAMPTON

School of Ocean and Earth Sciences

Bio-optical modeling for ecosystems in case II waters

by

Violeta Sanjuan Calzado

Thesis for the degree of Doctor of Philosophy

May 2009

Graduate School of Ocean and Earth Sciences

This PhD dissertation by

Violeta Sanjuan Calzado

has been produced under the supervision of the following persons

Supervisor

Prof. Ian S. Robinson

Member of Advisory Panel

Prof. John Sheperd

DECLARATION OF AUTHORSHIP

I, Violeta Sanjuan Calzado, declare that the thesis entitled 'Bio optical modeling for ecosystems in case II waters', and the work presented in the thesis are both my own, and have been generated by me as the result of my own original research. I confirm that:

- this work was done wholly or mainly while in candidature for a research degree at this University;
- where any part of this thesis has previously been submitted for a degree or any other qualification at this University or any other institution, this has been clearly stated;
- where I have consulted the published work of others, this is always clearly attributed;
- where I have quoted from the work of others, the source is always given. With the exception of such quotations, this thesis is entirely my own work;
- I have acknowledged all main sources of help;
- where the thesis is based on work done by myself jointly with others, I have made clear exactly what was done by others and what I have contributed myself;
- none of this work has been published before submission,

Signed: ……..

Date:…….

The real voyage of discovery consists not in seeking new landscapes but in having new eyes.

Marcel Proust (1871 - 1922)

UNIVERSITY OF SOUTHAMPTON

ABSTRACT

FACULTY OF SCIENCE

SCHOOL OF OCEAN AND EARTH SCIENCE

Doctor of Philosophy

BIO-OPTICAL MODELLING FOR ECOSYSTEM MODELS IN CASE II WATERS

By Violeta Sanjuan Calzado

This thesis presents a thorough critique of bio-optical models and the validity of the parameters used to describe the inherent optical properties (IOP) of the ocean that define model behaviour. The context of this critique is to assess the feasibility of coupling optical and ecosystem models so that the optical model can adequately predict the underwater light field. The study explores each step of the forward bio-optical-ecosystem model in case II waters. An available data set of optical measurements from the Irish Sea is used to evaluate the errors and uncertainty of measured optical properties, and to explore the sensitivity of the predicted radiance field to uncertainties in the model parameters.

The initialization of the bio-optical model is given by IOPs or concentrations of optically active constituents (OAC) and specific IOPs (SIOPs) derived from IOPs. Constituent concentrations and type determine optical water types. In this dataset, two distinctive water types are found in the region in different areas and seasons; chlorophyll dominated waters and mineral dominated waters. Uncertainty in IOPs and constituents are quantified in order to derive uncertainty ranges in SIOPs used in bio-optical models. Traditional SIOPs calculation significantly enlarges its apparent variability due to error propagation affecting the sensitivity of the bio-optical model. To overcome this, a new statistical method is presented which can reduce error propagation in the derivation of SIOPs from IOPs. The potential impact in reflectance of error propagation in optical modelling is studied for SIOPs obtained from both methods and a variety of water types.

Finally, predefined SIOPs values from literature are evaluated for the best optical description of the area. Real limitations are present when using literature values due to the lack of published data and in particular scattering and backscattering coefficients. Current definitions of constituent IOPs are also mismatched to those OAC found in ecosystem models and this prevents the feasibility of coupling forward optical modelling within ecosystem models. The conclusion is reached that further advances in the bio-optics field need to be made before such an approach is feasible, especially in the case of optically complex (Case II) waters.

Contents

Acknowledgements ..... **vi**

List of figures ..... **viii**

List of tables ..... **x**

Symbols ..... **xi**

Abbreviations ..... **xiii**

Chapter 1. Introduction **1**

1.1 Aim of this thesis 1

1.2 Coupling bio-optics and ecosystem models 3

1.3 Implications: remote sensing data assimilation 4

1.4 Outline of the thesis 6

Chapter 2. Optical theory and fundamental definitions in ocean optics **9**

2.1 The radiance field 9

2.2 Apparent Optical Properties 11

2.3 Inherent Optical Properties 12

2.4 Elastic and inelastic scattering 15

Fluorescence 17

2.5 Radiative transfer equation 18

2.6 Relations among AOP and IOP. Bio-optical models 19

Bio-optical models 19

Chapter 3. Bio-optics: parameterization of inherent optical properties **22**

3.1 Optically Active Constituents in the water 22

3.2 Water 23

3.3 Coloured Dissolved Organic Matter 25

3.4 Suspended Particulate Matter 27

3.5 Phytoplankton 30

Packaging effect 33

3.6 Issues associated with measurements of IOPs and constituents 34

Filter pad measurements 35

Pigment measurements 38

In situ spectrophotometers 39

Review 4

Chapter 4. Characterization of optical data: modeling the Irish Sea 43

4.1 Introduction 43

Topography 44

Hydrography 46

4.2 Cruises 47

4.3 Data acquisition 49

Operation of the AC-9 49

Hydroscat 49

Filter pad measurements 50

Pigment measurements 50

Constituents 52

4.4 Distribution of constituents 52

4.5 IOP distributions and optical water types 54

4.6 Constituent IOP's. 57

Minerals and detritus 57

Phytoplankton 60

CDOM 62

4.7 A four component model for the Irish Sea 63

Chapter 5. Uncertainties on constituent IOPs: A new approach to reduce uncertainties in optical data 65

5.1 Introduction 65

5.2 Variability of constituent IOPs 66

5.3 Quantifying uncertainties 71

Geometric mean regression 73

IOP uncertainty 74

Constituent uncertainty 77

5.4 Variability accounted by measurement uncertainty 79

5.5 An alternative approach: regression SIOPs 81

5.6 Summary 86

Chapter 6. Impact of SIOPs and water types in radiance field 88

6.1 Introduction 88

6.2 SIOPs to define the underwater light field: Regression SIOPs vs point-by-point SIOPs 89

6.3 Case Scenarios. Impact of SIOPs in different water types 99

6.4 Significance of SIOPs in the radiance field 105

Chapter 7. The use of IOPs from the published literature 108

7.1 Introduction 108

7.2 Phytoplankton absorption coefficient 109

Prieur and Sathyendranath (1981) 110

Bricaud et al., (1995) 111

Ciotti et al., (2002) 112

7.3 MSS absorption coefficient 115

Bowers et al., (1996) 116

7.4 Detritus absorption coefficient 119

Babin et al., (2003) 119

7.4 Absorption by CDOM 122

Tilstone et al., (2005) 123

7.5 Phytoplankton scattering coefficient 125

Loisel and Morel, (1998) 125

Gould et al., (1999) 126

7.6 Mineral scattering coefficient 129

Stavn and Richter, 2008 130

7.7 Backscattering ratio 132

Petzold, 1972 132

7.8 Overview 133

Chapter 8. Conclusions 135

8.1 Overview 135

8.2 Summary of achievements 135

8.3 Alternatives to radiative transfer modelling 139

8.4 Conclusion: The feasibility of linking optical and ecosystem models 140

8.5 Implications for remote sensing 142

Appendix A 143

References 152

Acknowledgements

I would like to start these acknowledgments by thanking my supervisor, Prof Ian Robinson for his support during this PhD. He always believed in my ability and skills to produce quality research in ocean optics, even with the hard conditions that this research faced. He always gave me encouragement to carry on with this work and believed in me. Thanks for your support.

I don't have enough words to thank Dr. David McKee, from the University of Strathclyde, friend and mentor; this thesis would not have been possible without his advice and innumerable discussions about this thesis and work produced and published jointly. I would like to thank also his fantastic family for their support during my intensive work trips to Glasgow to discuss this research. They always opened their house to me. Also to the hydrological optics group of the University of Strathclyde, in particular Prof. Alex Cunningham and Ian Brown, with whom I had great feedback for the analysis and processing of the dataset presented in this thesis work.

I would like to thank also the World University Network (WUN) exchange program, who gave me the opportunity of working for 5 months with the Scripps Photobiology Group headed by Dr. Greg Mitchell. He and his team provided me the resources and support I needed to start this research and gave me excellent training in ocean optics. Thanks Greg. A big thanks to all the professors I had during the Ocean Optics 2006 course at the Darling Marine Center in Maine, sponsored by NASA, an authentic privilege. Curt Mobley, Mary Jane Perry, Colin Roesler and Emmanuel Boss trained us with state of the art technology and research in this field;. Ocean optics elite and top class people. Thanks.

From my institution, I would like to thank the Laboratory of Satellite Oceanography who hosted me during this research and in particular to Peter Challenor who gave me key advice on this research. To friends that came and most left during this time but will always be there; Adriana, Xana, Martin Gutowski, Sara Benetti, Ivona, Katarzyna, Yolanda, Jackie, Monique and Pedro, Debora and Martin Mella.

To my family, my mother and Walter, for your love and support. I would not have made it without you. Thanks.

This PhD was funded by MERSEA and CASIX.

List of figures

Figure 1.1. Diagram of a bio-optical/ecosystem model. 2

Figure 1.2. Flow chart of the reserach. 6

Figure 2.1. Schematic representation of the radiance field. 11

Figure 2.2. Schematic representation of a volume of water. 13

Figure 2.3. Rayleigh and Mie scattering. 16

Figure 2.4. Relations among AOP and IOP. 20

Figure 4.1. Map of the Irish Sea. 45

Figure 4.2. Profiles of salinity, temperature and chlorophyll. 47

Figure 4.3. Profiles of salinity, temperature and chlorophyll. 48

Figure 4.4. Histograms of the concentrations of OAC 53

Figure 4.5. Total absorption spectra and b_{bp}470. 54

Figure 4.6. Water types classification. 56

Figure 4.7. Map of water types location stations. 57

Figure 4.8. MSS vs chlorophyll 58

Figure 4.9. Detrital absorption coefficient for Group A and B 59

Figure 4.10. a_{det}* in Group B. 60

Figure 4.11. a_{ph}, a_{cdom}, mean b_{ph}, mean b_{mss}. 61

Figure 5.1. a_{chl}*, a_{det}*, a_{mss}*, and a_{cdom}*. Mean b_{chl}* and b_{mss}* 70

Figure 5.2. a_{ph} 440 vs Chla concentration. 72

Figure 5.3. GMR analysis and error estimates for a_{ph}, a_{det}, and a_{mss} 75

Figure 5.4. GMR analysis and error estimates for a_{cdom}, b_{ph}, and b_{mss}. 76

Figure 5.5. GMR analysis for Chl a concentration. 77

Figure 5.6. Combined uncertainty for a_{chl}*, a_{det}*, a_{mss}*, a_{cdom}*, b_{chl}* and b_{mss}*. 80

Figure 5.6. Regression analysis for a_{ph}440 vs Chl a 81

Figure 5.7. a_{chl}*, a_{det}* and a_{mss}* in regression and point –by-point approach. 83

Figure 5.8. b_{chl}* and b_{mss}* calculated in regression and point –by-point approach. 84

Figure 6.1. Radiance reflectance from a_{chl}*, a_{det}*, a_{mss}* and a_{cdom}* in point-by-point and regression analysis. 92

Figure 6.2. Radiance reflectance from b_{chl}*, b_{mss}*, bb/b_{chl} and bb/b_{mss} in point-by-point and regression analysis. 93

Figure 6.3. %Δ on radiance reflectance for a_{chl}*, a_{det}*, a_{mss}*, a_{cdom}*, b_{chl}* and b_{mss}* in point-by-point and regression approach..... 95

Figure 6.3. (cont.) %Δ on radiance reflectance for bb/b_{chl} and bb/b_{mss} in point-by-point and regression approach. 96

Figure 6.4. %Δ on radiance reflectance from SIOPs in point-by-point and regression analysis. . 99

Figure 6.5. Total absorption from SIOP variation in each case scenario and % Δ. 102

Figure 6.6. % Δ in total absorption from SIOP variation in its particular case scenario. 103

Figure 6.7. %Δ on radiance reflectance from SIOPs in point-by-point and regression analysis. 104

Figure 6.8. Impact of variation of *a**, *b** and *bb/b* in radiance reflectance. 105

Figure 7.1. a_{chl}* , a_{ph} and radiance reflectance from Irish Sea, Prieur 81, Bricaud 95 and Ciotti 02 parameterizations. 115

Figure 7.2. a_{mss}* , a_{mss} and radiance reflectance from Irish Sea data and Bowers 96. 118

Figure 7.3. Snap from Babin 2003 and Irish Sea data. a_{det} 440 vs SPM Irish Sea data. 122

Figure 7.4. a_{det} and radiance reflectance from Babin'03 and Irish Sea dataset. 122

Figure 7.5 a_{cdom}*,a_{cdom}* and radiance reflectance from this Irish Sea data and Tilstone 05. 125

Figure 7.6 b_{chl}*, b_{chl}* and radiance reflectance from Irish Sea data, Loisel-Morel 98 and Gould 99. 129

Figure 7.7 b_{mss}* , b_{mss} and radiance reflectance from Irish Sea data and Stavn 08..... 132

Figure 7.8 *bb/b* from Petzolds and Irish Sea data in radiance reflectance. 134

List of tables

Table 3.1. Taxonomic pigments and cell size. (Vidussi et al., 2001) 31

Table 5.1. SIOPs variation in point-by-point and regression analysis. 85

Table 6.1. Δ range of radiance reflectance from SIOPs in point-by-point and regression analysis at a reference wavelength. %Δ of radiance reflectance on the entire spectra 98

Table 6.2. Case scenarios generated for HYDROLIGHT runs. 100

Table 6.3. Variability of SIOPs, variation on total *a* and *b* and variation on radiance reflectance. 106

Symbols

a	Absorption coefficient	$[m^{-1}]$
b	Scattering coefficient	$[m^{-1}]$
c	Attenuation coefficient	$[m^{-1}]$
λ	Wavelength	[nm]
VSF	Volume scattering function	$[sr^{-1}\ m^{-1}]$
b_p	Particle scattering coefficient	$[m^{-1}]$
b_b/b	Backscattering ratio	[-]
b_b	Backscattering coefficient	$[m^{-1}]$
P	Scattering phase function	[-]
ω_0	scattering albedo	[-]
L	Radiance	$[W \cdot m^{-2} \cdot sr^{-1}]$
E_d	Downwelling irradiance	$[Wm^{-2}nm^{-1}]$
$\widetilde{\mu}_d$	Average cosine of irradiance	[-]
R	Irradiance reflectance	[-]
Rrs	Remote sensing reflectance	$[sr^{-1}]$
a_{ph}	Phytoplankton absorption coefficient	$[m^{-1}]$
a_{chl}^*	Chlorophyll specific absorption coefficient	$[m^2(mg\ Chl\ a)^{-1}]$
a_{det}	Detritus specific absorption coefficient	$[m^{-1}]$
a_{det}^*	Detritus specific absorption coefficient	$[m^2(mg\ Chl\ a)^{-1}]$
a_{cdom}	Coloured dissolved organic matter specific absorption coefficient	$[m^{-1}]$
a_{cdom}^*	Coloured dissolved organic matter specific absorption coefficient	$[m^{-2}]$
a_{mss}	Mineral suspended sediment absorption coefficient	$[m^{-1}]$
a_{mss}^*	Mineral suspended sediment specific absorption coefficient	$[m^2\ g^{-1}]$
b_{ph}	Phytoplankton scattering coefficient	$[m^{-1}]$
b_{chl}^*	Chlorophyll specific scattering coefficient	$[m^2(mg\ Chl\ a)^{-1}]$

b_{mss}	Mineral suspended sediment scattering coefficient	[m^{-1}]
b_{mss}*	Mineral suspended sediment specific scattering coefficient	[m^2 g^{-1}]
Q_a	Absorption efficiency factor	[-]
Q_b	Scattering efficiency factor	[-]
β	Path length amplification factor	[-]
Chl a	Chlorophyll a concentration	[mg m^{-3}]

Abbreviations

OAC	Optically Active Constituents
IOP	Inherent Optical Properties
SIOP	Specific Inherent Optical Properties
SPM	Suspended Particulate Matter
DOM	Dissolved Organic Matter
CDOM	Colored Dissolved Organic Matter
HPLC	High Performance Liquid Chromatography
AC-9	Absorption-Attenuation-9
MSS	Mineral Suspended Sediment
GMR	Geometric Mean Regression
NAP	Non Algal Particles
HICO	Hyperspectral Imager for the Coastal Ocean

Chapter 1

Introduction

1.1 Aim of this thesis

The work described in this thesis explores the feasibility of bio-optical modelling of the light field within ecosystems having complex, Case II, optical characteristics.

The modelling of biogeochemical processes in natural waters has developed over the last two decades to the stage where hindcasting and forecasting of ecosystem behaviour is considered feasible. Ecosystem models seek to reproduce and predict biogeochemical cycles in the ocean where the model is constrained by physical parameters such as, wind, currents, density and light. The hydrodynamic and hydrographic aspects of the physical environment of marine ecosystems can generally be defined with confidence using ocean circulation models, which are largely independent of the ecosystem itself and represent the external forcing of the system. On the other hand the physical optics which determines the light environment are not independent of the ecosystem. Because light interacts with particles which are defined by the biogeochemical processes, the specification of the optical behaviour of the seawater and its contents should be considered as a crucial element of an ecosystem model, although this is often overlooked because of the complexity of modelling the biogeochemical interactions themselves.

It is therefore the aim of this work to analyze and improve the incorporation of optics into ecosystem models in order to produce an adequate and realistic representation of the light field in which the uncertainties are properly characterised and understood.

Many light dependent processes occur within an ecosystem and these can govern the dynamics of important elements of the model; photosynthesis determining primary production rates, photo-oxidation defining the sources or sink of carbon, etc. The addition of light dependent processes depends very much upon the complexity of the model. Even though light is the principal physical process to define life and other co-related processes, it is typically approximated as a simple factor, enormously limiting the dynamics of the light field that ultimately drive the ecosystem model. Furthermore, when light interacts with particles, state variables of the ecosystem model will be dynamically changing according to the absorption and scattering processes occurring.

Therefore, for an accurate definition of ecosystem model processes an adequate characterization of the light field driving the ecosystem dynamics is necessary. This can be given by a parallel bio-optical model instantaneously defining light variations and their repercussion on the ecosystem model. Some of the state variables in the ecosystem model (phytoplankton, dissolved organic carbon, non-algal particles) as well as the water itself are the principal optically active constituents (OAC) in natural waters that define the underwater light field by absorption and scattering processes. The absorption and scattering processes of these OAC are given by the inherent optical properties (IOP) of these constituents.

Constituent IOPs are the initialization parameter in forward bio-optical modelling and radiative transfer modelling which defines the radiance field. But light is a constantly changing property, and in order to couple optical modelling with ecosystem models an accurate definition of IOPs and an assessment of every step in the forward optical model is needed (figure 1.1). Given the current state of the art in optical oceanography, the outstanding challenge is to define these processes in complex coastal and Case II waters - those where phytoplankton is not the main OAC as it is in Case I waters - and where particles and dissolved organic matter have a significant impact on the underwater radiance field.

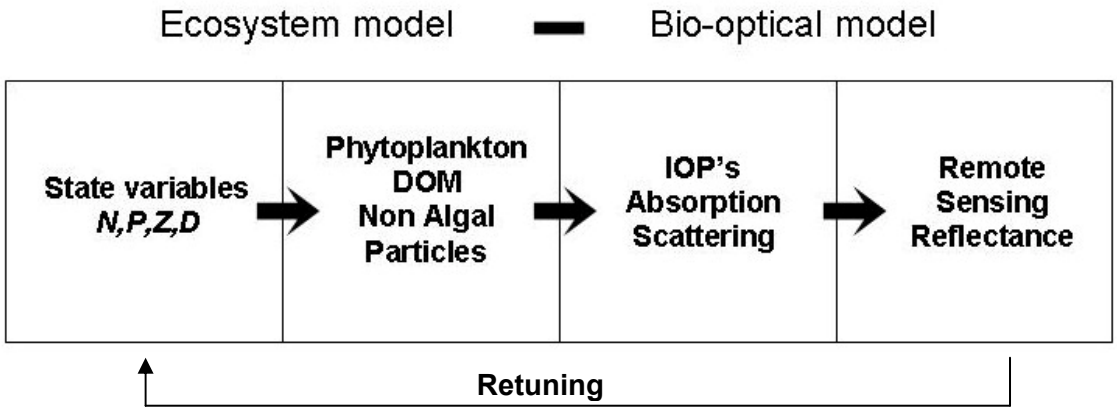

Figure 1.1. Diagram of a bio-optical/ecosystem model.

To meet this challenge, the study reported in this thesis addressed the following objectives:

- IOPs from OAC are comprehensively studied and defined to set up an adequate input for the bio-optical modelling according to the OAC within the ecosystem model.
- The effect of IOPs uncertainty in the input parameters and different optical water types is also studied to analyze the impact on the underwater light field.
- When optical observations are not available, IOPs from literature are identified that characterize the OAC from the ecosystem model in a Case II water environment.

1.2 Coupling bio-optics and ecosystem models

Many studies have been performed to model the underwater light field based on absorption and scattering processes of OAC. There is a wide literature on parameterization of absorption and scattering properties of OAC. Several studies have also computed remote sensing reflectance from absorption and scattering of OAC using bio-optical modelling and radiative transfer modelling. Outputs from the optical model are then assessed against in-situ radiometry, observations or remote sensing data in a closure exercise. Many issues arise when undertaking

closure exercises (Chang et al., 2003); uncertainties in input data, instrument corrections in optical data, assessment of the bio-optical algorithm to be used, and uncertainties on in-situ radiometry or remote sensing data. The way these factors impinge on optical modelling determine the performance of the bio-optical model but are rarely mentioned let alone taken into account. The work in this thesis precisely tackles possible sources of error affecting the output of the optical model.

Fuji et al. (2007), have published the first discussion of a coupled optical-ecosystem model. In that work, based on the state variables of the ecosystem model, absorption and scattering processes of OAC are calculated and radiative transfer modelling is applied to retrieve remote sensing reflectance. However some important issues are not addressed; uncertainties in IOP retrieval, adequacy of constituent IOPs used in relation to the state variables of the ecosystem model, and sensitivity studies of the optical characterization in IOPs used in different water types. These points are explicitly addressed in this thesis. Ultimately optical modelling is a closure exercise in itself and so the issues affecting closure exercises are important factors that need to be considered in this work as well. This exercise is even harder in coastal environments, where the complexity of constituents within the water makes the computation of a bio-optical model particularly challenging.

1.3 Implications: remote sensing data assimilation

Ecosystem model outputs are often assessed and sometimes tuned with remote sensing products because of their excellent information content in terms of area coverage and near-real time acquisition, which provides an instantaneous assessment of the ecosystem dynamics in an operational base. Remote sensing has proved to be a reliable tool in many scenarios and provides accurate geophysical parameters. However a high degree of uncertainty is still present when the geophysical parameters are transformed into biogoechemical parameters. This is the case of products from ocean colour sensors, where the geophysical parameter (radiance) is

converted into a biogeochemical parameter such as chlorophyll, atmospheric dust, etc... Satellite derived chlorophyll products are used as a proxy for primary production in ecosystem modelling. Their use can have major implications for the ecosystem model assessment and operation.

Ocean colour products used to estimate chlorophyll concentration in open ocean waters have shown a reasonable agreement with in situ data, but have also presented a high degree of uncertainty in shelf seas and coastal regions, typically greatly overestimating chlorophyll.

Chlorophyll products are generated based on a direct relationship between chlorophyll (as an indicator of primary production and light absorption) and water leaving radiance which is measured by the satellite. Ocean colour algorithms are derived based on remote sensing reflectance ratios at single wavelengths of max/min absorption of chlorophyll. A similar procedure is applied to obtain satellite products from other OAC such as total suspended matter (TSM), and particulate organic carbon (POC). This technique typically relates remote sensing reflectance with the OAC of interest in a one to one approach, discarding the effect of any other light interacting particles and weights the algorithm over the most common case scenarios encountered in oceanographic environments.

This approach leads to a high uncertainty when such observations come from complex oceanographic environments (coastal regions, upwelling systems, etc) which contain a variety of light interacting particles. The representation of these areas and a description of the ecological interactions occurring within ecosystem models are great challenges in themselves, which can be made harder when inaccurate ocean colour products are used to check the performance of the model.

By using coupled optical-ecosystem models, modelled reflectance from the optical-ecosystem model could be directly assimilated with satellite remote sensing reflectance. This approach would eliminate added uncertainty from remote sensing products and create a direct comparison interface. In an operational approach, the optical-ecosystem model can be re-assessed in a near-real time approach, dynamically readjusting the OAC within the ecosystem model according to remote sensing data assimilations. This approach also generates hyperspectral optical signatures

of the biogeochemical interactions ongoing in the ecosystem model. The traditional use of band ratio algorithms considerably limits the representation of such interactions. New generation satellites such as HICO (Hyperspectral Imager for the Coastal Ocean) provide a hyperspectral signature of the ocean colour. The data produced from such sensors can potentially change the approach of how remote sensing data has traditionally been used.

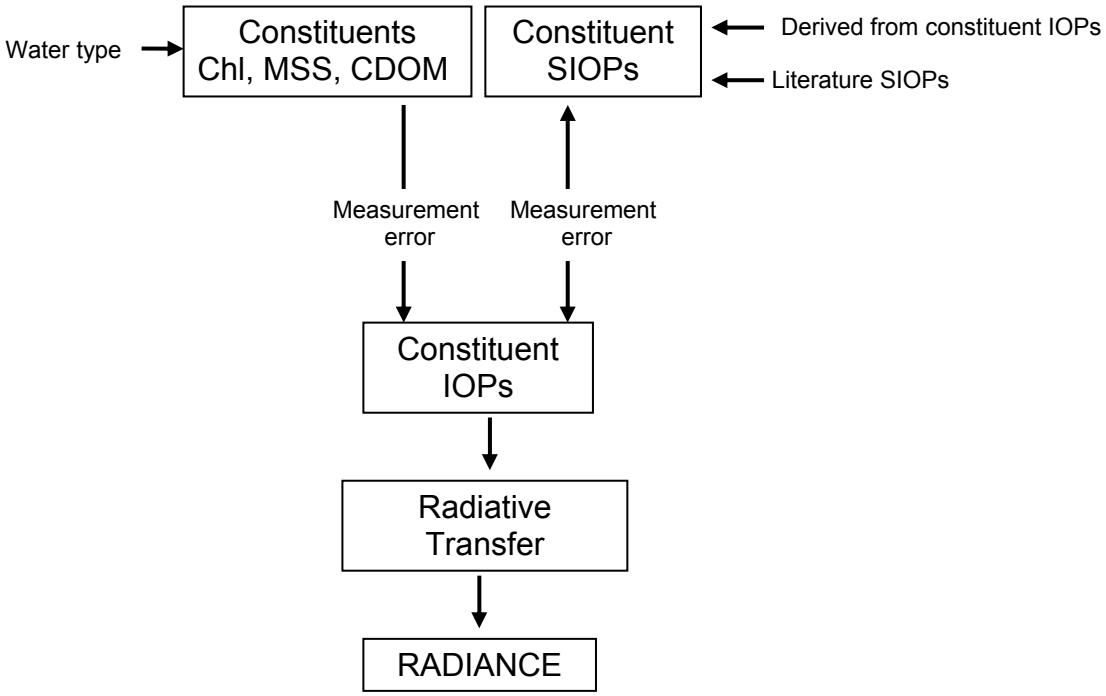

Figure 1.2. Flow chart of the research.

1.4 Outline of the thesis

This thesis consists of two distinctive parts. The first chapters introduce a solid background in optics and in particular the bio-optics referred to in the later chapters. The review includes state of the art algorithms and parameterisations of OAC which will be critically discussed. The second part of this work demonstrates each step of the forward optical model as in figure 1.2, using previously summarized and discussed parameterisations with an independent dataset from coastal and Case II waters.

As a beginning, chapter 2 provides brief background information in optical theory, stressing the optical quantities related to this work. IOPs and AOPs related with bio-optical modelling are summarized and described. Elastic and inelastic scattering are important when computing the underwater light field and a description of them is given here as well. The solution of the radiative transfer equation is presented which calculates the radiance field. Finally, relationships between IOPs and AOPs and simple bio-optical models to retrieve reflectance are also presented.

Chapter 3 provides a comprehensive overview in bio-optics. This chapter centres on the four main components interacting with light in the sea and its optical properties; phytoplankton, coloured dissolved organic matter, suspended particles and water itself. An extensive literature review is provided on the retrieval of the optical properties of these constituents as well as a critical discussion of calculation techniques and methodological issues.

Chapter 4 begins the substantive data analysis of the work and introduces the optical dataset from the Irish Sea used in this study. An overview of the region's oceanography is given together with a quantitative description of the optical properties. These prompt a discussion about the different optical water types found in the seawater and their relationship to its biogoechemical composition. Finally, a bio-optical model is introduced to describe the optical behaviour that characterises this region.

Chapter 5 introduces the issue of uncertainty in optical data. It discusses the variability in optical data, which is partly due to natural variability of the optical measurement itself and is partly a consequence of uncertainty in data measurements. Estimates of such uncertainty are given. The core of this chapter considers the statistical methods used to calculate derived optical quantities (specific IOPs) from IOPs and the error propagation when deriving SIOPs from IOPs. Finally it presents an alternative statistical method to derive SIOPs from IOPs which greatly reduces the variability due to error propagation.

Chapter 6 studies the propagation of uncertainties when IOPs are used in optical modelling. It presents simulations of IOP error propagation using a radiative transfer model (Hydrolight). Different case scenarios are introduced to test SIOP error propagation and the relevance of SIOPs in different water types. Ultimately this chapter presents sensitivity studies of reflectance spectra to error propagation and to variable biogeochemical environments, revealing the relevance of SIOPs to the quality of optical modelling.

Chapter 7 evaluates the suitability of different constituent parameterizations of IOPs when real time optical data are not available for input in the bio-optical model. Parameterisations of the main OAC are reviewed and tested to establish their suitability when used in bio-optical modelling in an optical Case II environment.

Finally, the thesis concludes with a summary of achievements of this work and their implications for the feasibility of coupled bio-optical – ecosystem models, together with some recommendations. It also presents a critical review on whether the actual research in bio-optics can support such a complex exercise and proposes some future research lines to materialize the possibility of coupling optics and ecosystem models.

Chapter 2

Optical theory and fundamental definitions in ocean optics

This chapter summarises those aspects of underwater optical theory which underpin the rest of the thesis, identifying the variables and defining the optical properties that are used throughout. A more complete and systematic treatment of underwater optics can be found in standard texts like Mobley (1994) or Spinrad (1994), on which this chapter is based.

2.1 The radiance field

As sunlight enters the ocean, it interacts with the particulates and dissolved materials within the water, as well as the water molecules themselves. These interactions produce two physical processes; absorption and scattering that will determine the underwater light field or *radiance*. Radiance, L, is the measure of light energy leaving an extended source in a particular direction. The definition of radiance is given by flux per unit area per unit of solid angle in a given direction in W m^{-2} sr^{-1}:

$$L = \frac{\Phi}{\Omega A \cos\theta} \tag{2.1}$$

where Φ is the radiant flux or power, defined as the time rate of radiant energy flow as measured in watts (or joules per second), θ is the angle between the surface normal and the specified direction, A is the area of the source (m^2), and Ω is the solid angle (sr) subtended by the measurement. Spectral radiance is measured per unit wavelength and defines the variation of L with λ. Since radiance is a quantity difficult to measure, most light field measurements involve integrals of the radiance distribution. The planar irradiance represents the energy flux impinging on a plane from one side. Considering the integral of radiance coming from the upper or lower side of a horizontal plane leads to the definition of downwelling irradiance:

$$E_d(z,\lambda) = \int_{\Omega_d} L(z,\theta,\phi,\lambda)\cos\theta d\Omega \tag{2.2}$$

and upwelling irradiance:

$$E_u(z,\lambda) = -\int_{\Omega_u} L(z,\theta,\phi,\lambda)\cos\theta d\Omega \tag{2.3}$$

in Wm^{-2} nm^{-1}, where Ω_d and Ω_u represent integration over the lower and upper hemisphere respectively and z represents depth. Another useful optical property is scalar irradiance, denoted by E_0 when radiance is integrated over the whole sphere and by E_{0d} or E_{0u} when radiance is integrated over the lower or upper hemisphere:

$$E_0(z,\lambda) = \int_{\Omega} L(z,\theta,\phi,\lambda)d\Omega \tag{2.4}$$

$$E_{0d}(z,\lambda) = \int_{\Omega_d} L(z,\theta,\phi,\lambda)\cos\theta d\Omega \tag{2.5}$$

$$E_{0u}(z,\lambda) = \int_{\Omega_u} L(z,\theta,\phi,\lambda)\cos\theta d\Omega \tag{2.6}$$

where θ defines the direction of the measurement from the vertical. The average cosine of the downwelling radiance field is represented by:

$$\tilde{\mu}_d(z,\lambda) = \frac{E_d(z,\lambda)}{E_{0d}(z,\lambda)} \tag{2.7}$$

and similarly for the upwelling field. Its maximum value is 1 when all the radiance is vertically downwards or upwards. It reduces as the light field becomes more directionally diffuse.

As shown in figure 2.1, when irradiance from the sun (both the direct solar radiance and irradiance from solar radiation scattered by the atmosphere) reaches the sea surface some is reflected at the surface, to produce the reflected light field with radiance L_r, and some, L_t, is transmitted through the surface where it interacts with the water and its contents. This interaction generates the upwelling radiance field L_u measured just below the sea surface, and this becomes the water leaving radiance L_w, after transmission through the surface and into the atmosphere. Note that the upwelling radiance measured in the atmosphere above the sea surface is the sum of the water leaving radiance and reflected radiance. The water leaving radiance is the optical property of interest since it is the result of the underwater light interacting with marine particles.

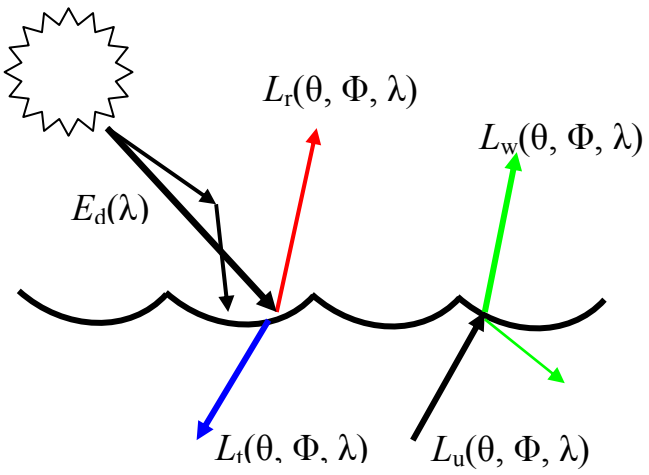

Figure 2.1. Schematic representation of the radiance field in relation to the sea surface.

2.2 Apparent Optical Properties

Apparent optical properties, AOP's, are used to characterise the integrated optical response of a water body when it is illuminated. The AOP's depend both on the optical properties of the medium and on the directional structure of the light field. Some radiometric quantities, such as irradiance, can change greatly depending on the radiance field. However, there are certain ratios of radiometric quantities that are relatively insensitive to environmental factors. An ideal AOP changes only slightly with external environmental changes, but changes sufficiently with the optical response of the medium to be able to characterize one water body and distinguish it from another.

One of the most used AOP's is the *spectral irradiance reflectance* at a depth z that provides the ratio of spectral upwelling to downwelling plane irradiances. In field measurements, $R(z,\lambda)$ is commonly evaluated just below the water surface, $R(0^-, \lambda)$, or above the water surface, $R(0^+, \lambda)$.

$$R(z,\lambda) = \frac{E_u(z,\lambda)}{E_d(z,\lambda)} \tag{2.8}$$

R being dimensionless. For measurements in remote sensing a hybrid variable is used which provides the ratio of the light leaving through the surface in direction (θ,Φ) to the incident downwelling light (figure 2.1). This is the remote sensing reflectance, usually defined in the nadir-viewing direction:

$$R_{rs}(\theta,\phi,\lambda) \equiv \frac{L_w(z=0;\theta,\phi,\lambda)}{E_d(z=0,\lambda)}. \quad (2.9)$$

measured in sr^{-1}. R_{rs} presents very little dependence on sun angle and strong dependence on water optical properties, absorption and scattering, which makes it an ideal AOP in optical modelling.

The most widely-used AOP in ecological models for light penetration is the downwelling diffuse attenuation coefficient K_d .K_d is essentially the attenuation with depth experienced by sunlight. Its value depends on depth, sun angle, sky conditions, and shadowing by objects on the surface, as well as the absorption and scattering of light by the water and its contents. However as depth increases, the influence of the surface illumination characteristics decreases, and K_d eventually reaches an asymptotic value that is in fact an IOP. Thus the distinction between IOPs and AOP's can sometimes be misleading.

Under typical conditions, the various radiances and irradiances decrease exponentially with depth. The *spectral downwelling diffuse attenuation coefficient* for spectral downwelling plane irradiance, $K_d(z;\lambda)$, is measured in $m^{-1}$and is expressed, for a particular wavelength of light, as:

$$K_d(z,\lambda) = -E_d(z,\lambda)\frac{dE_d}{dz} \quad (2.10)$$

A similar expression defines the upwelling diffuse attenuation coefficient, K_u, which in general is not the same as the downwelling coefficient, especially near the surface.

2.3 Inherent Optical Properties

The scattering and absorption properties of a natural water body are called its Inherent Optical Properties (IOPs). These are optical properties that depend only upon the medium, and are independent of the light field within the medium. There are also other IOPs such as index of refraction, beam attenuation coefficient and single scattering albedo.

To define some of these quantities let us consider a volume ΔV of water, of thickness Δr, illuminated by a narrow collimated beam of monochromatic light of spectral radiant power $\Phi_i(\lambda)$, where part of the incident power, $\Phi_a(\lambda)$, is absorbed within the volume of water (see

figure 2.2). Some part $\Phi_s(\lambda)$ is scattered out of the beam at an angle ψ, and the remaining power $\Phi_t(\lambda)$ is transmitted though the volume with no change in direction. Then $\Phi_s(\lambda)$ is the total power scattered into all directions.

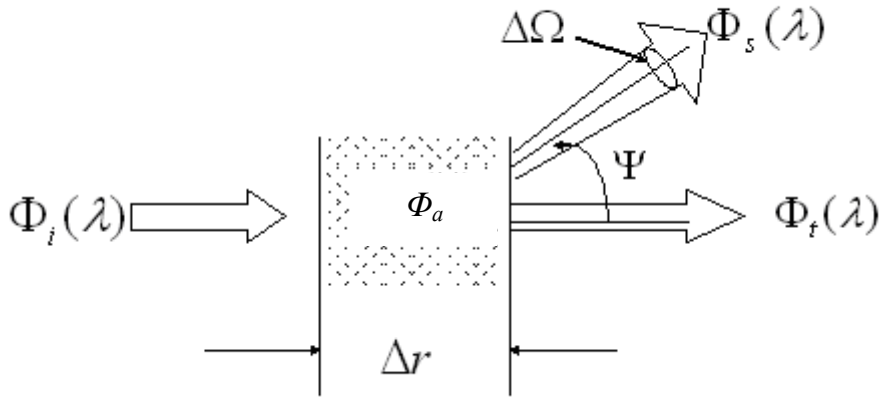

Fig 2.2. Schematic representation of a narrow collimated beam illuminating a volume of water (Mobley, 1994).

The *spectral absorptance A(λ)* is defined as the fraction of incident power that is absorbed within the volume:

$$A(\lambda) \equiv \frac{\Phi_a(\lambda)}{\Phi_i(\lambda)} \tag{2.11}$$

and the *spectral scatterance B(λ)* is the fractional of the incident power that is scattered out of the beam:

$$B(\lambda) \equiv \frac{\Phi_s(\lambda)}{\Phi_i(\lambda)}. \tag{2.12}$$

The spectral transmittance *T(λ)* is:

$$T(\lambda) \equiv \frac{\Phi_t(\lambda)}{\Phi_i(\lambda)} \tag{2.13}$$

and

$$A(\lambda) + B(\lambda) + T(\lambda) = 1 \tag{2.14}$$

The inherent optical properties of interest for this work are the spectral absorption and scattering coefficients, which are respectively the spectral absorptance and scatterance per unit distance in the medium. The *spectral absorption coefficient a(λ)* is defined as:

$$a(\lambda) \equiv \lim_{\Delta r \to 0} \frac{A(\lambda)}{\Delta r} \tag{2.15}$$

And the *spectral scattering coefficient b(λ)* is:

$$b(\lambda) \equiv \lim_{\Delta r \to 0} \frac{B(\lambda)}{\Delta r} \tag{2.16}$$

The *spectral beam attenuation coefficient c(λ)* is defined as:

$$c(\lambda) \equiv a(\lambda) + b(\lambda) \tag{2.17}$$

where *c, a* and *b* are measured in m^{-1}.

ψ is the *scattering angle*; its values lie in the interval $0 \le \psi \le \pi$. $B(\psi;\lambda)$ is the fraction of incident power scattered out of the beam through an angle ψ into a solid angle $\Delta\Omega$ centred on ψ. The angular scatterance per unit distance and unit solid angle, $B(\psi;\lambda)$, is:

$$\beta(\psi;\lambda) \equiv \lim_{\Delta r \to 0} \lim_{\Delta\Omega \to 0} \frac{B(\psi;\lambda)}{\Delta r \Delta\Omega} = \lim_{\Delta r \to 0} \lim_{\Delta\Omega \to 0} \frac{\Phi_s(\psi;\lambda)}{\Phi_i \Delta r \Delta\Omega} \tag{2.18}$$

The spectral power scattered into the given solid angle $\Delta\Omega$ is just the spectral radiant intensity scattered into direction ψ times the solid angle: $\Phi_s(\lambda) = I_s(\lambda)\cdot\Delta\Omega$. Moreover, if the incident power $\Phi_i(\lambda)$ falls on an area ΔA, then the corresponding incident irradiance is $E_i(\lambda) = \Phi_i(\lambda)/\Delta A$. Noting that $\Delta V = \Delta r \cdot \Delta A$ is the volume of water that is illuminated by the incident beam gives:

$$\beta(\psi;\lambda) = \lim_{\Delta v \to 0} \frac{I_s(\psi;\lambda)}{E_i(\lambda)\Delta V} \tag{2.19}$$

which is the volume scattering function, also VSF, and gives the scattered intensity per unit of incident irradiance per unit of volume of water (sr^{-1} m^{-1}). The spectral scattering coefficient is the result of integrating $\beta(\psi;\lambda)$ over all directions:

$$b(\lambda) = \int \beta(\psi;\lambda) d\Omega = 2\pi \int_0^{\pi} \beta(\psi;\lambda) \sin\psi d\psi \tag{2.20}$$

This integration is often divided into forward scattering, $0 \le \psi \le \pi/2$, and backward scattering $\pi/2 \le \psi \le \pi$. The corresponding spectral forward and backward scattering coefficients are respectively:

$$b_f(\lambda) \equiv 2\pi \int_0^{\pi/2} \beta(\psi;\lambda) \sin\psi d\psi \tag{2.21}$$

$$b_b(\lambda) \equiv 2\pi \int_{\pi/2}^{\pi} \beta(\psi;\lambda) \sin\psi d\psi \tag{2.22}$$

For the scope of this work the most important scattering process is the backward scattering coefficient also called backscattering coefficient.

Another inherent optical property commonly used in hydrologic optics is the spectral single scattering albedo, ω_0, dimensionless, defined as:

$$\omega_0 = b/c \tag{2.23}$$

In waters where the beam attenuation is due primarily to scattering, the value of ω_0 approaches 1 whereas in those where the beam attenuation is due primarily to absorption, ω_0 is close to zero.

The scattering phase function, $P(\psi,\lambda)$, (sr^{-1}) specifies the angular dependence of the scattering without regard to its magnitude.

$$P = \beta / b \tag{2.24}$$

In practice, any measure of β is extremely difficult. An approximate way to represent the direction of scattering is to use the backscattering ratio, B (Mobley, Sundman et al. 2002):

$$B = b_b / b \tag{2.25}$$

which represents the probability that a photon will be scattered through an angle $\psi \geq 90^\circ$ in any scattering event.

2.4 Elastic and inelastic scattering

Since different components can be found in the water, when light interacts with them it can lead to different responses. There are different scattering interactions according to the nature of the particle. Rayleigh scattering is applied when the interaction is elastic and the photon energies of the scattered photons are not changed. Scattering in which the scattered photons have either a higher or lower photon energy is called Raman inelastic scattering. A loss of energy results in a shift to longer wavelengths and vice versa. Usually this kind of scattering involves exciting some vibrational mode of the molecules, giving lower scattered photon energy, or scattering of

an excited vibrational state of a molecule which adds its vibrational energy to the incident photon. This type of scattering is involved in phytoplankton fluorescence.

Like Rayleigh scattering, Raman scattering depends upon the polarizability of the molecules. For polarizable molecules, the incident photon energy can excite vibrational modes of the molecules, yielding scattered photons which are diminished in energy by the amount of the vibrational transition energies. Raman spectroscopy also has application in remote monitoring for pollutants. For example, the scattering produced by a laser beam directed to the plume of a waste pipeline can be used to monitor the effluent for levels of molecules which will produce recognizable Raman lines. This laser produces scattered light which includes one or more "sidebands" that are offset by rotational and/or vibrational energy differences which can also provide information about the type of pollutant. Raman scattering is significant in the study of different optically active constituents of the water in Case II situations (Mobley, 1994).

The scattering from molecules and very tiny particles (< 1/10 wavelength) is predominantly Rayleigh scattering. When the particle size is comparable to or bigger in diameter than the incident wavelength, Mie theory is used to compute scattering. This scattering produces a pattern like an antenna lobe, with a sharper and more intense forward lobe for larger particles (figure 2.3).

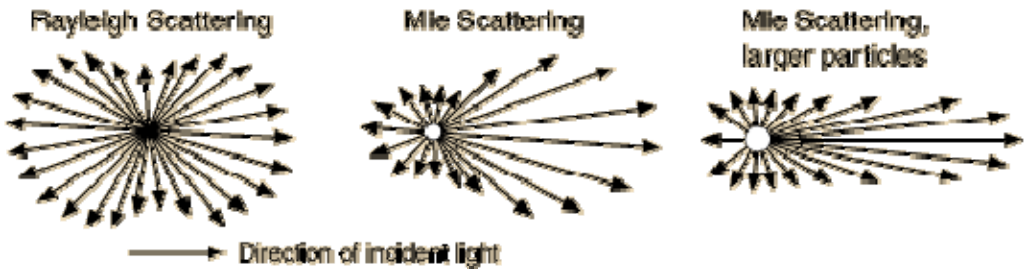

Figure 2.3. Directional dispersion of light in Rayleigh and Mie scattering.

Mie theory is used to compute scattering for particles in a homogeneous medium whose index of refraction is real. Mie theory assumes that the particles are sufficiently diluted so that scattering is independent, and that particles are spherical and homogeneous. Mie scattering is not wavelength dependent and the solutions are given in terms of absorption and scattering cross-sections.

Fluorescence

Different components in the water can generate luminescence, but one of the most significant processes is chlorophyll fluorescence from phytoplankton.

Light energy absorbed by chlorophyll can be used to drive photosynthesis. Excess energy can be dissipated as heat or it can be re-emitted as light. These three processes occur in competition. Fluorescence is the process of re-emission of absorbed energy as a photon, when an electron relaxes from an electronic exited state. The fraction of energy absorbed at shorter wavelengths is re-emitted as a photon at longer wavelengths. The total amount of chlorophyll fluorescence is about 1% or 2% of total light absorbed. Fluorescence, *F*, is expressed as:

$$F = E(\lambda) \cdot conc \cdot \Phi_f \quad \text{or} \quad F = E(\lambda) \cdot a(\lambda) \cdot \Phi_f \tag{2.26}$$

where $E(\lambda)$ is the excitation energy, *conc* is concentration, $a(\lambda)$ is phytoplankton absorption, and Φ_f is quantum yield of fluorescence (moles photon fluoresced / moles photon absorbed). Φ_f depends on temperature and environment, physiological state, etc... Typical values of Φ_f chlorophyll *a* fluorescence in vitro are ~0.33 and ~<0.03-0.05 in vivo (living cell).

In coastal environments, where the water leaving radiance signal can be significantly attenuated by the components in the water, the fraction of water-leaving radiance due to fluorescence could be significant. The radiance due to fluorescence is expressed as (Huot et al., 2005):

$$dL_f(\lambda_{em}, z) = \frac{1}{4\pi} \cdot \frac{\varphi}{C_f} \cdot Q_a^*(\lambda_{em}) \cdot A_{abs}(z) \cdot e^{-a_f(\lambda_{em}) \cdot z} \cdot dz \tag{2.27}$$

where the factor $1/4\pi$ (sr^{-1}) converts an isotropic fluorescence field to radiance; C_f (nm) is the ratio of the emission in the whole fluorescence band to that observed over $\Delta\lambda$; Q_a* is a parameter accounting for emitted radiation at λ_{em} not reabsorbed within the cell; $A_{abs}(z)$ is the flux absorbed by phytoplankton at depth z ($mol^{-3}sr^{-1}$); and a_f is the attenuation coefficient for upwelling fluoresced radiance at 678 nm.

Other sources of fluorescence in natural waters are from phycoerithrins, coloured dissolved organic matter (CDOM) and bioluminescence.

2.5 Radiative transfer equation

The radiance distribution is related to the inherent optical properties through the *radiative transfer equation*, RTE. In a medium where the IOPs depend only on depth, where inelastic processes are ignored and there are no internal sources, the RTE is

$$\cos\theta \frac{dL(z,\lambda,\theta,\phi)}{dz} = -c(z,\lambda)\cdot L(z,\lambda,\theta,\phi) + \int_{4\pi} \beta(z,\lambda,\theta',\phi' \to \theta,\phi)\cdot L(z,\lambda,\theta',\phi')d\Omega' \tag{2.28}$$

where $d\Omega = \sin\theta' d\theta' d\phi'$ and the 4π on the integral means that the integration is to be carried out over all θ' and ϕ'. The first term on the right hand side represents the loss of radiance in the direction (θ,ϕ) by scattering and absorption, while the second term provides the gain in radiance due to scattering of radiance from all other directions (θ',ϕ') into the direction (θ,ϕ).

Analytical solutions to the RTE are possible only in the simplest case for which scattering is negligible, when $\omega_0 = 0$ (equation 2.23). Otherwise it must be solved with numerical solutions. The most complete and accurate is the *successive orders of scattering solution* used in radiative transfer modelling such as the Hydrolight model. The basic idea is to successively compute the radiance that is scattered once, twice... and then to sum these contributions to obtain the total radiance.

Adopting this approach, the radiance can be explained in a power series in ω_0:

$$L(z,\theta,\phi) = L^{(0)}(z,\theta,\phi) + \omega_0 L^{(1)}(z,\theta,\phi) + \omega_0 L^{(2)}(z,\theta,\phi) + \ldots \tag{2.29}$$

The RTE is satisfied if the individual $L^{(n)}$ satisfy

$$\cos\theta \frac{dL^{(0)}}{dz} = -L^{(0)}$$

$$\cos\theta \frac{dL^{(1)}}{dz} = -L^{(1)} + \int PL^{(0)'}d\Omega'$$

$$\cos\theta \frac{dL^{(2)}}{dz} = -L^{(2)} + \int PL^{(1)'}d\Omega'$$

:

$$\cos\theta \frac{dL^{(n)}}{dz} = -L^{(n)} + \int PL^{(n-1)'} d\Omega' \tag{2.30}$$

2.6 Relations among AOP and IOP. Bio-optical models

Manipulating the RTE gives us some relations between AOP and IOP that are exact when no contributions from internal sources are present (Spinrad et al., 1994):

$$a \le K_d \widetilde{\mu}_d \le c \tag{2.31}$$

$$\widetilde{\mu} = \frac{a}{K_{net}} = \frac{a \cdot (1-R)}{K_d - R \cdot K_u} \tag{2.32}$$

$$R = \frac{K_d - a \cdot \widetilde{\mu}_d}{K_u + a \cdot \widetilde{\mu}_d} \tag{2.33}$$

Figure 2.4 from Mobley (1994) shows some other relationships that can be obtained upon simplification of the radiative transfer equation that relate IOPs and AOPs.

Bio-optical models

Relationships between IOPs and AOPs are also used to explain OAC in the water and radiance field. Calculation of the radiance field is given by the RTE, which ultimately can be approximated as a ratio of backscattering and absorption to radiance (Gordon et al., 1988):

$$\frac{R}{Q} = \sum_{i-1}^{2} l_i \left(\frac{b_b}{a + b_b} \right)^i \tag{7.30}$$

where l_1 = 0.0949 and l_2 = 0.0794. Q is defined as the ratio of the upwelling radiance to the upwelling irradiance towards the zenith. Q equals π for a totally diffuse radiance distribution and appears to be between 4 and 5 for radiance distributions observed in nature (Austin 1979).

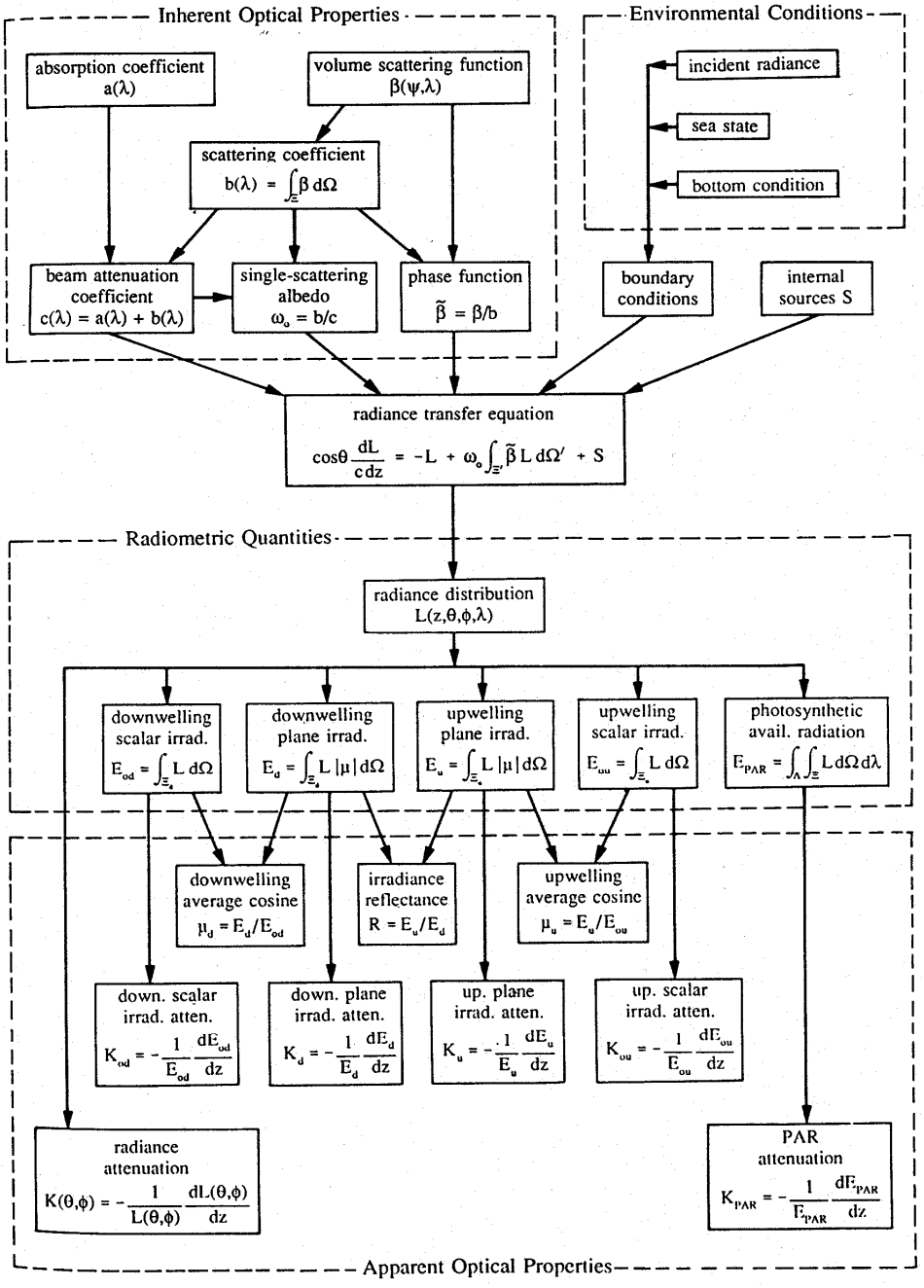

Figure 2.4. Relations among AOP and IOP (Mobley, 1994).

Variations on this parameterization have been presented in further studies where absorption and backscattering have been defined in terms of the individual OAC contributions. Garver and Siegel (1997) presented a revision of this model which has been widely used in inversion exercises from reflectance to IOPs (IOCCG 2006). Lee et al. (2002), also presented a bio-optical model for IOP retrieval derived from the RTE. In contrast to the Garver model, the IOPs are not defined as spectral parameterizations from literature and it is developed for IOPs retrieval from remote sensing reflectance from different sensors.

The brief optical theory introduced in this chapter is sufficient to provide the basis for the subsequent work in this thesis.

Chapter 3

Bio-optics: parameterization of inherent optical properties

3.1 Optically Active Constituents in the water

The inherent optical properties of the water, absorption, scattering and backscattering can be expressed as a function of the optically active constituents in the water (OAC). The most relevant OAC are phytoplankton, coloured dissolved organic matter (CDOM) or gelbstoff and suspended particulate matter (SPM) as well as water itself. In the context of linking a bio-optical model to an ecosystem model, these components can usually be found as state variables of the ecosystem model itself with the exception of CDOM, which is a fraction of the dissolved organic matter (DOM) represented in the model. Thus, the light field that defines the biogeochemical interactions within the ecosystem model, driven by the processes of absorption (a) and scattering (b), can in principle be expressed as the sum of the individual constituent parts of *a* and *b*:

$$\begin{aligned} a &= a_w + a_{ph} + a_{cdom} + a_{spm} \\ b &= b_w + b_{ph} + b_{spm} \end{aligned} \tag{3.1}$$

where CDOM does not contribute to the scattering signal. Turbulence, viruses and bubbles (Stramski et al., 2001; Stramski and Tegowski, 2001) can also have a significant impact on the scattering coefficient of clear sea water in the open ocean, but it is usually very difficult to measure. For the context and aim of this work these will not be discussed further since their effect is unlikely to be relevant for optical modelling in coastal environments where phytoplankton, SPM and CDOM have a stronger optical signature.

This chapter discusses the absorption and scattering properties of water (Section 3.2), CDOM (3.3), SPM (3.4) and phytoplankton (3.5). After this a review on measurement techniques of

these OACs is presented (3.6), leading to a critical review of sources of uncertainty in constituent IOPs.

3.2 Water

Sea water plays a significant role in total absorption and scattering properties (Sullivan et al., 2006). Pure water presents a tetrahedral structure, distorted because of the two non-bonding electron pairs which create an angle H-O-H of 104.5°. The polar nature of the molecule allows hydrogen bonds to create dimers, trimers and larger clusters. The strength of the hydrogen bonds is dependent on temperature, with higher thermal motion tending to break the clusters. Also in seawater, the presence of inorganic salts (such as NaCl, KCl, MgSO4, and CaSO4) causes larger, more tightly bound clusters and therefore affects the characteristics of absorption and scattering of light by water. When light of wavelengths longer than 450 nm is absorbed, the energy is transferred to one or more of the vibrational modes of the O-H bond. As the temperature decreases the number of hydrogen bonds increases which causes the absorption peaks to shift to longer wavelengths. The variations in absorption and scattering are due to changes in density which in the sea depends on temperature, salinity and pressure.

Water absorbs weakly in the blue and green regions of the spectrum but increases from about 550 nm and is significant in the red (Kirk, 1994). Measurements of absorption coefficient in the visible region are difficult because of the low absorption values in this part of the spectrum. At wavelengths greater than 580 nm, scattering by water molecules becomes essentially insignificant when compared to absorption. Thus, the attenuation of light at wavelengths greater than 580 nm becomes essentially a consequence of molecular absorption. For values of λ in the range of 400-520 nm, scattering is dominant compared to absorption by water molecules. Sea water has two principal features that provide the scattering property; fluctuations of the orientation of the water molecules and the presence of dissolved inorganic salts. These salts are usually present in their dissociated form due to the bipolarity of the water molecule. The

fluctuations of the orientation of the molecule are caused by changes in density, so it depends on temperature, pressure and salinity. However since these fluctuations are minor, a standard backscattering coefficient is usually adopted for pure seawater.

The backscattering coefficient for pure seawater can be calculated theoretically (Morel, 1974) from electrodynamics and thermodynamic considerations. The scattering of sea water is assumed to be isotropic. The directional scattering at visible wavelengths by water molecules was modelled by Morel as:

$$\beta_{sw}(\theta) = \beta_{sw}(90^{\circ})(1+0.835)\cos^2\theta \tag{3.2}$$

where $\beta_{sw}(\theta)$ is the volume scattering function at wavelength λ and scattering angle θ and $\beta_{sw}(90^{\circ})$ is the volume scattering function at wavelength λ and scattering angle 90°. The value of $\beta_w(90^{\circ})$ has been estimated at λ = 550 nm as 0.93×10^{-4} m^{-1} sr^{-1}. From this equation it is seen that β (180°) = β (0°). Therefore scattering in the backward direction is assumed to equal scattering in the forward direction.

$$b_w = 2b_{bw} = 2b_{fw} \tag{3.3}$$

The total scattering coefficient is given by:

$$b_w = 16.06\left(\frac{\lambda_0}{\lambda}\right)^{4.32}\beta_w(90°;\lambda_0) \tag{3.4}$$

Smith and Baker, (1981) also made a careful study of the spectral absorption and scattering coefficient in the range 200 nm ≤ λ ≤ 800 nm. They assumed negligible absorption by salt ions and no inelastic scattering for natural waters. With these assumptions the absorption coefficient can be expressed as (based in radiative transfer theory):

$$a_w(\lambda) \le K_d(\lambda) - 1/2b_{sw}(\lambda) \tag{3.5}$$

Standard values for absorption coefficient are usually taken from accurate measurements of the absorption coefficient using an integrating cavity absorption meter with high sensitivity independent of backscattering effects (Pope and Fry, 1997). Scattering estimates are usually

taken from Smith and Baker (1981), who derived values for scattering and backscattering based on Morel's equations.

3.3 Coloured Dissolved Organic Matter

Definitions for absorption by dissolved organic matter (DOM) are based entirely on methodology. DOM includes the matter contained in seawater that passes through a small pore size filter, usually a polycarbonate membrane filter with a 0.2 μm pore size. The fraction of DOM with optical activity in the water is called colored dissolved organic matter (CDOM), with alternative names of gelbstoff, yellow substance or gilvin. Ratios of CDOM to DOM are highly variable (Siegel et al., 2002) hence it is difficult to define the absorption coefficient of DOM in an ecosystem model.

CDOM contains humic and fulvic acids (Kowalczuk, 1999), associated with decomposition of vegetal tissue that provides a characteristic yellowish appearance. Humic and fulvic acids have been largely documented from inland sources, associated with terrigenous activity and therefore, when incorporated in the sea shows high salinity gradients (Nelson and Guarda, 1995). The origin of CDOM in coastal waters therefore may in some areas be river discharge, but in oceanic water away from the coastal zone, CDOM is probably entirely due to phytoplankton cell breakdown and zooplankton messy feeding. Jerlov, (1976) noticed the presence of CDOM in the upwelling region west of South America, and attributed it purely to marine origin since this area is practically devoid of river or inland discharge. Some products of the humic substance are phenols derived from lignin, a structural polymer present only in land plants with a very low degradation rate. Meyers-Schulte and Hedges (1986), measuring lignin-specific phenols concluded that 10 % of the humic material in the eastern equatorial Pacific is terrestrially derived. Since this part of the ocean is not greatly affected by river and inland discharges, it is likely that some of the CDOM comes from the slow degradation of material from land plants.

In coastal regions which are strongly influenced by river discharge CDOM can also affect the amount and quality of the photosynthetically active radiation available to phytoplankton, decreasing primary productivity and affecting ecosystem structure. In remote sensing applications, the individual absorption spectra of CDOM, detritus and Chlorophyll *a* overlap, making it very difficult to distinguish the separate contributions of each one of these components in Case II waters to the total reflectance spectra.

CDOM, from an optical classification point of view, is described as those dissolved substances that absorb light at the blue end of the spectrum. This is a rough classification regardless of its chemical nature or ecological origin. CDOM absorption spectra follow a decreasing exponential pattern and are usually fitted to an exponential expression for purposes of data smoothing and to reduce the effect of instrumental noise. Maximum values are found at the shortest wavelengths in the visible domain, decreasing towards a minimum in the yellow region of the spectra.

CDOM together with the pigment composition and nonliving material determines the shape of the absorption spectra in the visible domain. Absorption by CDOM can be parameterised as an exponential expression such as (Bricaud et al., 1981; Carder et al., 1989) :

$$a_{cdom}(\lambda) = a_{cdom}(\lambda_0)\exp[-S(\lambda - \lambda_0)] \tag{3.6}$$

where the coefficient S, called the 'mean slope', can be calculated by fitting each sample to an exponential expression using a reference wavelength (λ_0 = 440 nm). Bricaud et al. (1981), observed a slope value of 0.014 ± 0.0032 $m^{-1}nm^{-1}$ and noted a spread of values for the absorption coefficient for CDOM between 0.06 and 4.2 m^{-1} at 375 nm, although values over 1 m^{-1} were found only in the Baltic Sea or in highly contaminated areas.

Specific absorption values of fulvic and humic acids extracted from marine waters have also been studied. The mass-specific absorption coefficient of fulvic acids has been reported to be low because of the aliphatic carbons which are built into its structure, having a high slope coefficient, with highest values of (0.018-0.020) recorded in marine waters. In contrast, the specific absorption coefficient of humic acids is reportedly high because of strongly absorbing aromatic circles built into its structure, with a low slope coefficient around 0.010 (Kowalczuk,

1999). However in natural waters, a solution of variable fractions of fulvic and humic acids forms the CDOM. Thus the final slope value of CDOM would vary between these values.

Concerning the choice of reference wavelength, later studies have shown the convenience of using λ of 350 nm or lower for natural waters, in order to define UV light levels in natural waters. Remote sensing studies in which absorption by CDOM competes with that by phytoplankton pigments in the blue region often employ a reference value for a_{cdom} at 440 nm (Carder et al., 1989).

CDOM can also generate fluorescence when excited in the UV region and can be used to identify particular chromomorphic substances in CDOM (Coble, 1996).

3.4 Suspended Particulate Matter

Suspended particulate matter (SPM) is defined as the entire unpigmented fraction retained on a Whatman GF/F filter with an approximate effective pore size of 0.7 μm. This suspended matter consists of the seston, which includes mineral particles of terrigenous origin, plankton (that includes zooplankton, algae, bacteria and algal fungi), and detritus (residual products of the decomposition of phytoplankton and zooplankton cells as well as macrophytic plants along with their excretions). SPM absorption is measured after pigment extraction of phytoplanktonic cells; however phytoplankton detritus and cellular by-products are accounted as part of the SPM pool. Phytoplankton pigments and suspended particulate matter are separated by different extractive methods that will be discussed later.

The presence of terrigenous suspended particles in the SPM is a consequence of river discharge, resuspension, shore erosion or long and short range aeolic transport of atmospheric particulates followed by dry deposition. These particles are diverse in shape and size. Suspended terrigenous matter generally has negligible impact in open ocean waters except for dust plumes episodes,

but is very significant in coastal waters, where it can comprise 40-80 % of the suspended matter (Kirk, 1994).

Other components of the suspended matter to be taken into account are iron and manganese hydroxides and calcium carbonate. Substantial concentrations of these components can produce significant absorption and scattering in the water. Precipitates of these components will depend not only on their chemical composition but also on the environmental pH (Bukata et al., 1995). An example of where these components are significant is in coccolithophore blooms.

The absorption properties of SPM depend very much on the constituents measured. Absorption properties of non-living organic material can be substantially different to the absorption properties of inorganic material such as mineral particles.

The spectral form of the absorption by SPM follows an exponential profile and it is commonly agreed to fit absorption values to an exponential expression such as:

$$a_{spm}(\lambda) = a_{spm}(400)\exp\left[-S_{spm}\cdot(\lambda-400)\right] \tag{3.7}$$

where S_{spm} is the slope coefficient of the exponential equation in $m^{-1}nm^{-1}$. The value of S_{spm} varies according to region and water type sampled. Different values have been proposed for the slope coefficient; Roesler et al., (1989) propose a value of S_{spm} = 0.011 found on the Washington coast. Babin et al., (2003) found an average of S_{spm} = 0.0123 $m^{-1}nm^{-1}$ with SD = 0.0013 nm^{-1} in coastal European waters. It has also been suggested that the similarity between the exponential spectral shapes of a_{spm} and a_{cdom} is because these two components may share some common chromophores (Babin et al., 2003).

The differentiation between different sources of SPM could provide a more accurate characterization of its absorption coefficient but methodologically this is extremely difficult. SPM contains particles both from organic and inorganic origins. Some studies have shown that the absorption coefficient of mineral particles presents approximately an exponential profile, but the absorption values can be significantly different from those observed in detrital particles of

organic origin (Babin and Stramski, 2004). An unclear definition of the SPM pool can lead to substantial error when attempting parameterizations of its absorption and scattering coefficient. Furthermore when attempting to couple optical and ecosystem models the sources of SPM in the optical model cannot be identified in the ecosystem model. Babin et al., (2003) discussed the possibility of attributing organic or inorganic origin to SPM samples based on the slope coefficient, S_{spm}. In that study, low slope values were found in samples with high mineral content and high slope values were found for those with organic origin. However, this type of classification may be affected by variations in the chemical composition of mineral particles.

These problems are also present when parameterising the scattering coefficient of SPM which implies certain assumptions. Rigorous modelling would be impossible since particles vary in terms of particle size, shape and refractive index. Usually marine particles are modelled using Mie scattering theory assuming that the particles are homogeneous, with a given refractive index, and a Junge type power law function for the particle size distribution (Ulloa et al., 1994), where the distribution is fitted to a hyperbolic curve. It is also assumed that the backscattering ratio is wavelength independent when particles are not strongly pigmented (Ulloa et al., 1994). Then, the particle scattering coefficient is parameterised as (Babin et al., 2003):

$$b_p(\lambda) = b_p(\lambda_0) \cdot \left(\frac{\lambda}{\lambda_0} \right)^{-\gamma} \tag{3.8}$$

where λ_0 is the reference wavelength, usually 555 nm where absorption is minimum, and γ is related to the slope parameter of the Junge-type model. This parameterization for particles includes any particle in the water column, including the effect of phytoplankton and its photosynthetic pigments. Recent studies discuss the use of the commonly assumed power law distribution as a descriptor for the particle size distribution in natural waters (McKee et al., *in press*), and it has been shown that pigmented particles have a spectrally variable backscattering ratio. This could significantly affect the validity of this type of parameterisation and its effect when used to compute the radiance field.

Parameterizations of the backscattering coefficient for non-algal particle scattering are difficult to find because of the problems related with separation of different types of particles contributing to the SPM pool.

3.5 Phytoplankton

Phytoplankton has a strong optical influence in Case I waters and determine the shape of the total absorption spectrum. They have a wide range of size, type and cell structures. They can be found as individual species or larger chains of associated unicellular organisms. The coloration of phytoplankton cells is dependent upon their pigment composition (Bukata et al., 1995). Different pigment compositions result in green algae or Chlorophyta (dark green), red algae or Rhodophyta (dark red), blue-green algae or Cyanophyta (olive green, yellow-green, pink, violet or brown), and dinoflagelates or Pyrrophyta (reddish), diatoms or Bacilariophyceae (brownish) among others.

According to their pigment composition, the absorption coefficient of phytoplankton can vary greatly. To differentiate between taxonomic groups, a classification based on indicative or 'diagnostic' pigments is often used (Babin et al., 2003). Usually phytoplankton species are grouped into three size classes in which phytoplankton species have similar pigment composition. Picoplankton represents phytoplankton cells under 2 μm, nanoplankton represents cells between 2-20 μm and microplankton cells greater than 20 μm.

These groups are defined according to their concentration of pigment composition or diagnostic pigments (table 3.1) as (Vidussi et al., 2001); (Babin et al., 2003):

$$Picoplankton(\%) = \frac{[zeaxanthin] + [chlorophyllb + [divinyl - chloropyllb]]}{[diagnostic \cdot pigments]} \times 100 \quad (3.9)$$

$$Nanoplankton(\%) = \frac{[alloxanthin] + [19'BFucoxanthin] + [19'Fucoxanthin]}{[diagnostic \cdot pigments]} \times 100 \quad (3.10)$$

$$Microplankton(\%) = \frac{[fucoxanthin]+[peridinin]}{[diagnostic \cdot pigments]} \times 100 \quad (3.11)$$

Table 3.1. Taxonomic pigments and cell size. (Vidussi et al., 2001)

Diagnostic pigments	***Taxonomic significance***	***Size µm***
Zeaxanthin	Cyanobacteria and prochlorophytes	<2
Divinyl – chlorophyll a	Prochlorophytes	<2
Chlorophyll b + Divinyl-chlorohyll b	Green flagellates and prochlorophytes	<2
19' hexanoyloxyfucoxanthin	Chromophytes nanoflagellates	2-20
19' butanoyloxyfucoxanthin	Chromophytes nanoflagellates	2-20
Alloxanthin	Cryptophytes	2-20
Fucoxanthin	Diatoms	>20
Peridinin	Dinoflagellates	>20

This classification was developed for open ocean waters but it has also shown good agreement when used in coastal areas (Babin et al., 2003). Recently, new studies have proposed the use of phytoplankton absorption and its spectral shape as unique indicators for taxonomic groups (Hirata et al., 2008).

Chlorophyll and related pigments strongly absorb the light in the red and blue parts of the spectrum, and thus, when concentrations are high, predominate in determining the spectral absorption of sea water. Absorption by chlorophyll maxima in the blue and the red regions of the spectra peaks at 430 and 665 nm. Chlorophyll concentration usually refers to the sum of chlorophyll *a*, the main pigment in cells and pheophytin *a*. Chlorophyll concentrations vary in the range from < 0.01 mg/m^3 in the clearest ocean waters to 10 mg/m^3 in productive coastal upwelling regions to > 100 mg/m^3 in eutrophic estuaries or lakes (Kirk, 1994).

Even though the pigment concentration and type does not generate the totality of the absorption signal, the phytoplankton absorption coefficient, a_{ph}, is sometimes referred to as the chlorophyll

absorption coefficient, a_{chl}, since chlorophyll is the most common pigment present in phytoplankton species.

The mass specific absorption coefficient of phytoplankton, a_{ph}*, is expressed in terms of chlorophyll *a* and divinyl a concentration. The specific absorption coefficient varies between species as well as within species grown under different environmental conditions of irradiance, nutrients and temperature. High values of a_{ph}* have reportedly been found in warm, low pigmented surface waters (Sosik and Mitchell, 1995). This variability both between and within species is due to differences in taxonomic pigments and pigment efficiency.

Phytoplankton cells are generally much larger than the wavelength of visible light and are efficient scatterers especially via diffraction, thus strongly influencing the total scattering properties of sea water. Large particles scatter strongly at small forward angles, and thus contribute less to the backscattering coefficient. Therefore the larger phytoplankton contribute less to backscatter (Kirk, 1994). Phytoplankton cells that contain on their external structure silicate and calcium can scatter considerably as is the case for diatoms and coccolithophores. The calcite of coccolitophores produces a strong scattering signal which creates a milky appearance in oceanic waters (Balch et al., 1996).

Reynolds et al., (2001) developed a parameterisation for particle backscattering coefficient based on phytoplankton content in the form:

$$b_b(\lambda) = \left[b_{bw}(\lambda_0) + b_{bp}(\lambda_0\right] \cdot \left(\frac{\lambda_0}{\lambda}\right)^{\gamma} \tag{3.12}$$

where γ is a dimensionless parameter describing the spectral dependency of total backscattering relative to a reference wavelength, λ_0, here 555 nm, and b_{bp} for phytoplankton is defined as:

$$b_{bp}(555) = 10^{-3} \cdot Chl^{0.667} \tag{3.13}$$

these numbers being for the Ross Sea, with r^2=0.85.

Total scattering and backscattering is commonly measured with volume scattering meters, but measurements involving only phytoplankton are extremely difficult due to the presence of different OAC in the water. As shown in equation 13, relationships between phytoplankton backscattering and chlorophyll content are usually applied for the retrieval of b_{bp} for phytoplankton.

Another source of scattering in phytoplankton cells is fluorescence. The fluorescence peak appears at 685 nm due to the emission by chlorophyll *a* which absorbs visible light and re-emits or fluoresces red light. Fluorescence signal strongly depends on the quantum yield of fluorescence whose determination is difficult and often values from previous literature are taken. The assumption of a fixed quantum yield of fluorescence can lead to substantial errors on the fluorescence retrieval (Letelier and Abbott, 1996). Further explanation of fluorescence equations and efficiency is provided in chapter 2.4.

Packaging effect

The estimation of phytoplankton absorption coefficient, a_{ph}, faces the problem of determining the absorption coefficients for each pigment in vivo. Pigment absorption presents significant differences when measured in the cell, in vivo, or extracted, in vitro. Photosynthetic pigments are present in the cells in the tilakoids of the chloroplasts, in 'packages' which can limit its energy absorption efficiency. When pigments are extracted they can absorb at their maximum efficiency rate and in vitro pigment absorption values are usually greater than in vivo values (Bricaud et al., 1995). Even though this technique is commonly used in bio-optics, it is not representative of real pigment absorption in natural waters.

The package effect is defined as the ratio of the specific absorption coefficient of pigmented cells to the specific absorption coefficient of the same cellular matter dispersed into a solution. The package effect is measured as (Morel and Bricaud, 1981; Sathyendranath et al., 1987):

$$Q_a^* = 1.5 \cdot Q_a(\rho') / \rho' \tag{3.14}$$

where Q_a, the mean efficiency factor for absorption by phytoplanktonic cells, is a function of the parameter ρ':

$$Q_a = 1 + \frac{2\exp(-\rho')}{\rho'} + \frac{2[\exp(-\rho') - 1]}{\rho'^2} \tag{3.15}$$

and ρ' is the product of the cellular matter absorption, a_{cm}, and the cell size d:

$$\rho' = a_{cm} d \tag{3.16}$$

Q^*_a continuously decreases from 1 (no package effect) to 0 (maximal package effect) with increasing ρ' values. The decrease of $a_{ph}^*(\lambda)$ with increasing chlorophyll has been attributed to an increase of packaging effect from oligotrophic to eutrophic waters (Yentsch and Phinney, 1989).

Package effects are most extreme in large highly pigmented cells because of attenuation by surrounding pigment molecules. This results in lower a_{ph}^* with flatter peaks for phytoplankton cells which have significant package effects due to larger cell size or higher intracellular chlorophyll *a* concentrations (Sosik and Mitchell, 1995).

As well as a reduced packaging effect in oligotrophic waters (Bricaud and Stramski, 1990), a shift has been observed in the absorption blue peak by 6-8 nm to longer wavelengths (Bricaud et al., 1995; Bricaud and Stramski, 1990) corresponding to the shift of the in vivo absorption maximum of divinyl Chl a (around 447 nm) compared with that of Chl a (around 440 nm).

3.6 Issues associated with measurements of IOPs and constituents

As in other disciplines, advances in science and on technical instrumentation have led to a constant evolution of optical definitions. In modern optical oceanography, Jerlov, (1976) stated definitions for absorption and scattering coefficients in terms of the additive contribution of constituents in dissolved or particulate form as in equation 3.1. It must be noted that in this

approach the classification of the constituents is based purely on a methodological perspective rather than according to the natural optical properties. This dependence on the methodology for separating the different constituents, together with the different methods proposed to calculate the coefficients, leads to inconsistency in the calculations. This can be critical for accuracy when optical parameters are used to derive other optical quantities. This section presents a detailed review of the methods to retrieve optical parameters, and the correction factors applied to optical parameters to adjust for their sensitivity to different measurement methods. It also develops a critical discussion about the latest research into optical instrumentation accuracy, corrections factors for filter pad measurements, pigment measurements and in situ spectrophotometers.

Filter pad measurements

In oceanographic applications, the definitions of CDOM and SPM are operationally based on filtration of seawater with a certain type of filter. Since parameterisations of these coefficients are based on methodology any issue related with the retrieval method can greatly influence them.

Dissolved organic matter includes the matter contained in seawater that passes through a small pore size filter, typically a 0.2 μm polycarbonate membrane filter and SPM absorption corresponds to the fraction retained in a 0.7 μm GF/F filter. Therefore there is a fraction corresponding to particles sized between 0.2 and 0.7 μm that are not accounted for in the absorption coefficient. Furthermore, the definition of pore size in filter pad measurements is purely nominal; when aggregates are formed on the retained fraction in the filter pad, the effective pore size in the filtration method can be reduced.

The use of different measurement techniques for a and b involves some mismatch between the particulate assemblages contributing to the particulate absorption and scattering (a_p and b_p). When measuring absorption with the filter pad technique, a_p includes the fraction of particles

retained on a Whatman GF/F filter and b_p is determined from measurements of unfiltered water with in situ scattering meters. While a_p excludes particulates that pass through the filter, b_p includes the contribution of all colloidal particles.

Secondly, a and b include contributions of all suspended particles regardless of their origin, size, shape or composition. Although the fraction of SPM is often divided into phytoplankton and non-algal particles, this is still insufficient to explain the different optical behaviour of particulates. Even though the role of phytoplankton is usually computed as another coefficient, this classification is still insufficient to explain the diverse optical responses to the different constituents of the water in the ocean. A more accurate division for the absorption and scattering coefficient is needed that will characterise its diverse composition.

Another problem arises when separating living from non-living contributions. One of the most widely used techniques to separate living from non-living particles was proposed by Kishino et al., (1985). A fixed volume of water is filtered on a membrane filter (usually Whatman GF/F filters) for preconcentration, since particle concentration is generally low, and then resuspended in a small volume. Methanol is used as a bleaching agent to extract most of the photosynthetic pigments of natural phytoplankton. Absorption is measured before and after the bleaching process and the difference between these two measurements provides the absorption for phytoplankton. Modifications on this technique have been applied to the chemical components used for extraction and sodium hypochlorite is currently the most widely used.

After the chemical extraction, the residual absorption is due to unpigmented particles, but also to non-extractable pigments (phycobilins) and to ‘bleached’ cells. The difference of absorption before and after the extraction is due not only to in vivo pigments, but also to extractable pheopigments and detrital carotenoids. This method shows in general an efficiency of 90% in the pigment extraction. Detrital particles contain a negligible amount of extractable pigments, but in the euphotic zone it is possible to obtain detrital particles that contain photosynthetic pigments in decomposed form (pheopigments) extractable with sodium hypoclorite. This technique is widely used to extract the major part of the photosynthetic pigments of natural

phytoplankton. Stramski, (1990) pointed out the possible pigment degradation related with this technique which introduces errors on the absorption measurements.

Other problems arise when applying correction factors. Filter pad measurements are affected by scattering from particles and filter pad fibres that amplify the mean path length that the photons travel through the filter particle system, artificially enhancing the derived absorption coefficients. The required correction factor is known as the "β path length amplification factor". It is also defined as the ratio of the optical thickness of the diffusing material to its geometric thickness (Kiefer and SooHoo, 1982). The path length amplification factor is assumed to be wavelength independent and it is calculated as (Kishino et al., 1985):

$$\beta = OD_f \,/\, OD_{cuv} \tag{3.17}$$

where OD_f represents the optical density of the sample measured in the filter pad and OD_{cuv} is the optical density of the same sample measured in suspension in a cuvette.

Different correction factors have been proposed in the literature; 2.43 to 4.71, (Kishino et al., 1985); 2.63 to 4.06, (Gallegos et al., 1990). It has also been suggested that there is a possible wavelength dependence of β, significant at low absorbance (Mitchell and Kiefer, 1984). Two different approaches are commonly used to calculate β:

The theoretical approach (Roesler, 1998): assuming that the filter creates an isotropic light field, the optical path length is two times the geometric path length.

The empirical approach (Mitchell, 1990): the relationship between the optical path length, OD_f, and the geometrical path length, OD_{cuv}, is non linear of the form:

$$OD_f corrected = C_1 \cdot OD_f + C_2 \cdot OD_f^2 \tag{3.18}$$

With C_1 = 0.29 to 0.48 and C_2 = 0.05 to 0.75

Consensus in this topic has not been reached, although new measurement techniques of absorption by particles have been proposed (Allali et al., 1995) that may overcome problems with the β factor correction.

A different technique for separating living from non-living fractions was proposed by Iturriaga and Siegel, (1989) using efficiency factors for absorption of individual living and detrital particles. Using multiple regressions it can be partitioned into phytoplankton and detrital components. This technique, as well as requiring multiple measurements, is restricted to particles bigger than 2.5 μm, and is not efficient for field studies where smaller particles are common.

Filter pad measurements are also corrected for any light scattered by particles outside the acceptance angle of the detector. This is achieved by subtracting the optical density measured in the near-IR (usually 750 nm) from the measured optical density spectrum (Babin and Stramski, 2004; Mitchell and Kiefer, 1988). This correction is certainly valid for phytoplankton cells where absorption in the near-IR is zero, but when measuring SPM absorption in highly loaded filter pads the absorption coefficient might be significant in this region of the spectrum (Bowers and Mitchelson-Jacob, 1996). This correction could be a significant source of error when measuring absorption coefficients with the filter pad technique in coastal turbid environments.

Pigment measurements

High Performance liquid Chromatography (HPLC) is the most widely recommended technique for determining pigments in natural waters. Uncertainty on their retrievals has been reported to be 7% for total Chl *a*, whereas for other pigments it has been observed to be 21.5% on average (Claustre et al., 2004). This technique provides a very good accuracy for chlorophyll measurements but measures pigments in vitro, and hence overestimates the real pigment efficiency observed in field measurements.

The trichromatic equations of (Jeffrey and Humphrey, 1975), is another *in vitro* technique to retrieve pigment concentration. It converts algal absorbance spectra from acetone extracts of pigments from cells retained on filter pads. Two different methods are suggested in their protocols to retrieve chlorophylls and phaeopigments.

Method 1*:* For mixed phytoplankton populations of Chls *a, b,* c_1 and c_2, chlorophylls can be calculated as:

$$\begin{aligned} Chlorophyll_a &= 11.85 \cdot E_{664} - 1.54 \cdot E_{647} - 0.08 \cdot E_{630} \\ Chlorophyll_b &= -5.43 \cdot E_{664} + 21.03 \cdot E_{647} - 2.66 \cdot E_{630} \\ Chlorophyll_{c_1+c_2} &= -1.67 \cdot E_{664} - 7.60 \cdot E_{647} + 24.52 \cdot E_{630} \end{aligned} \quad (3.19)$$

where E stands for absorbance of the sample at different wavelengths obtained as above and corrected by the 750 reading. Then total content of chlorophyll is obtained as:

$$Chl_a \quad (mg/m^3) = \frac{Chlorophyll_a \cdot v}{V \cdot l} \quad (20)$$

where v is the volume of acetone in ml used for chemical extraction of pigments, V is the volume of seawater filtered through the filter pad, l is the path length of the cuvette (cm) and *Chl a* is the spectrophotometric measure of chlorophyll *a* as above.

Method 2: This method was originally described to retrieve phaeopigments, but can provide chlorophyll *a* as well.

$$Chl_a \quad (mg/m^3) = \frac{26.7(665_0 - 665_a) \cdot v}{V \cdot l} \quad (21)$$

where 665_0 is the extinction at 665 nm before pigment extraction, 665_a is the extinction at 665 nm after pigment extraction, v is the volume of acetone used in ml, V is the volume of seawater filtered and l is the path length of the cuvette.

In situ spectrophotometers

In situ spectrophotometers are also widely used in field observations for absorption and attenuation measurements. Some of the most commonly used are the AC-s or AC-9

commercialized by Wetlabs (Inc.), which was used for this study. Absorption and attenuation is measured in a dual tube spectrophotometer. Correction factors are applied to these data for temperature and salinity effects on the sample referenced against the blank measured in the lab, typically ultra pure fresh water and at lab temperature. Both temperature and salinity affect the molecular structure of the water, and therefore its optical properties.

Pegau et al., (1997) studied the effect of temperature and salinity on field measurements of spectrophotometers and presented a correction equation for absorption and attenuation measurements:

$$\begin{aligned} a_{mts} &= a_m - \left[\Psi_t * (t - t_r) + \Psi_{sa} * S\right] \\ c_{mts} &= c_m - \left[\Psi_t * (t - t_r) + \Psi_{sc} * S\right] \end{aligned} \tag{22}$$

Where a_{mts} and c_{mts} stands for measured absorption and attenuation corrected for temperature and salinity effects, a_m and c_m are measured absorption and attenuation, Ψ_t is the correction coefficient for temperature effect, Ψ_{sa} and Ψ_{sc} are the correction coefficients for salinity effect on absorption and attenuation respectively.

AC-9 measurements are usually corrected for any scattering effect produced within the absorption tube. There is usually assumed to be zero absorption at 715 nm and a wavelength independent scattering correction (Zaneveld et al., 1994). Absorption at 715 nm is used as the scattering correction factor applied to the total spectrum as:

$$a(\lambda) = a_{TS}(\lambda) - b(\lambda) \cdot \frac{a_{TS}(715)}{b(715)} \tag{23}$$

where $a_{TS}(\lambda)$ indicates temperature and salinity corrected absorption observations, $b(\lambda) = c_{TS}(\lambda) - a_{TS}(\lambda)$, and $b(715) = c_{TS}(715) - a_{TS}(715)$.

It has been previously discussed that assuming zero absorption at the near IR could lead to substantial sources of error, particularly in mineral dominated environments where mineral absorption is not negligible at the near infra-red region of the spectrum. Assuming a similar

correction for in situ absorption-attenuation meters and applying this correction factor to the whole spectrum could have a massive impact on the data accuracy.

Recent studies have proposed different scattering correction factors for absorption attenuation meters that do not imply zero absorption at 715 nm (McKee et al., 2008). The correction factor proposed by Zaneveld also assumes a wavelength independent scattering phase function. It was previously stated that recent studies question the wavelength independence of the backscattering ratio (McKee et al., 2009) which is used to approximate the scattering phase function (Mobley et al., 2002).

Review

Optical theory currently extends far beyond our real capability for measuring optical properties. The optical variables used in hydrological optics are constrained by the capability of the present measurement techniques, and constituent IOPs as presently defined do not describe well enough their optical behaviour. Current standard protocols for ocean optics measurements (Mueller et al., 2003) are outdated and still insufficient to explain bio-optics with respect to fundamental optics and the physical processes involved in the interaction of light with particles. Moreover, questioning the validity of certain basic assumptions in hydrological optics is a healthy exercise although the community does not seem ready to discuss it.

Recent studies about wavelength dependence of the particle backscattering ratio can have major implications when this parameter is further used in models of the underwater light field for remote sensing and primary productivity. Furthermore, the implications for historic measurements of optical properties will be crucial and a re-evaluation of correction factors applied to these measurements will need to be performed.

A similar situation exists with correction factors applied on filter pad data such as the β factor which is still under discussion and can vary the measurement by an order of magnitude. The

scattering correction factor applied in filter pad data will also have major implications when SPM is measured in coastal environments, as it is for this work. Finally the greatest problem at the moment is the unclear definition of the individual assemblages contributing to each constituent IOP which presently makes impossible a clear connection between bio-optics and ecosystem modeling.

Following, chapter 4 introduces the dataset used in this study. In the chapter, an optical water type classification is applied that can help to differentiate IOPs signature for different OAC based on their optical characteristics. The effect of added uncertainty on IOPs data from methodological and correction factors is also evaluated in chapter 5 and 6. In chapter 5, IOPs and constituent uncertainties are further discussed and quantified. The potential impact of these in the radiance field is presented in chapter 6.

Chapter 4

Characterization of optical data: modeling the Irish Sea

4.1 Introduction

Attempting bio-optical modelling in coastal and complex Case II waters is the most difficult scenario for optical modelling. It requires access to a complete optical dataset containing coastal and Case II samples, which has been carefully quality controlled, in order to study error estimates and uncertainties in bio optical modelling. Complete optical datasets are very scarce and difficult to obtain. For the purpose of this study it was also crucial to be able to assess the reliability of the data acquisition process and to have full information about the sampling procedure. The data made available to the author for use in this thesis were collected in the Irish Sea during optical oceanography cruises by the University of Strathclyde. This region provides an excellent context for optically complex waters, where both Case I type and Case II type waters can be found in different areas and seasons and non-algal materials have a significant impact on optical properties (Bowers and Mitchelson-Jacob, 1996).

This chapter introduces the dataset, with an overview of the oceanographic area sampled, discussing the topography and hydrography of the region. The methodology section discusses the sampling procedure, instruments used and corrections applied to the data acquired from the various instruments. The biogeochemical content of the region and the related optical properties, as determined from the cruise data are presented and discussed. What emerges from consideration of the optical behaviour of the Irish Sea is that there exists a clear distinction between different optical water types based on their biogeochemical composition and reflected in their optical response. This novel classification is used to set a model to describe the optical

properties of the region. The chapter concludes with a discussion of the implication from this result that optical models need to be chosen to match the character of the ecosystem.

The data used here were provided courtesy of the University of Strathclyde (Prof. Alex Cunningham and Dr. David McKee) and collected by them during four cruises between 2001 and 2002, in different locations of the Irish Sea (see Figure 4.1). This optical dataset includes biogeochemical constituents, IOP and radiometry, collected and processed by Dr McKee. (McKee and Cunningham, 2005, 2006; McKee et al., 2007).

Topography

The Irish Sea, a shallow shelf sea lying between the islands of Ireland and Great Britain, provides a wide range of water types in a relatively small geographical area. The Irish Sea region covers approximately 51˚-55˚ N and 3˚- 8˚W. The Irish Sea consists of a deeper channel in the west, with shallower embayments in the east. The channel is open-ended, forming part of a loop connected at both ends to the Atlantic Ocean, in the south via the Celtic Sea and St. George's Channel, and in the north via the North Channel and the Malin Shelf Sea. Hence the Irish Sea receives Atlantic water and influences through both entrances. The channel is about 300 km long and 30 – 50 km wide, with a minimum depth of 80 m and a maximum exceeding 275 m in Beaufort's Dyke in the North Channel. The two principal shallower embayments, each with depths less than 50 m are Cardigan Bay in the south and the eastern Irish Sea (to the east of the Isle of Man) in the north, and there is also the smaller Caernarfon Bay. The width of the Irish Sea varies between 75 and 200 km but decreases to 30 km in the North Channel.

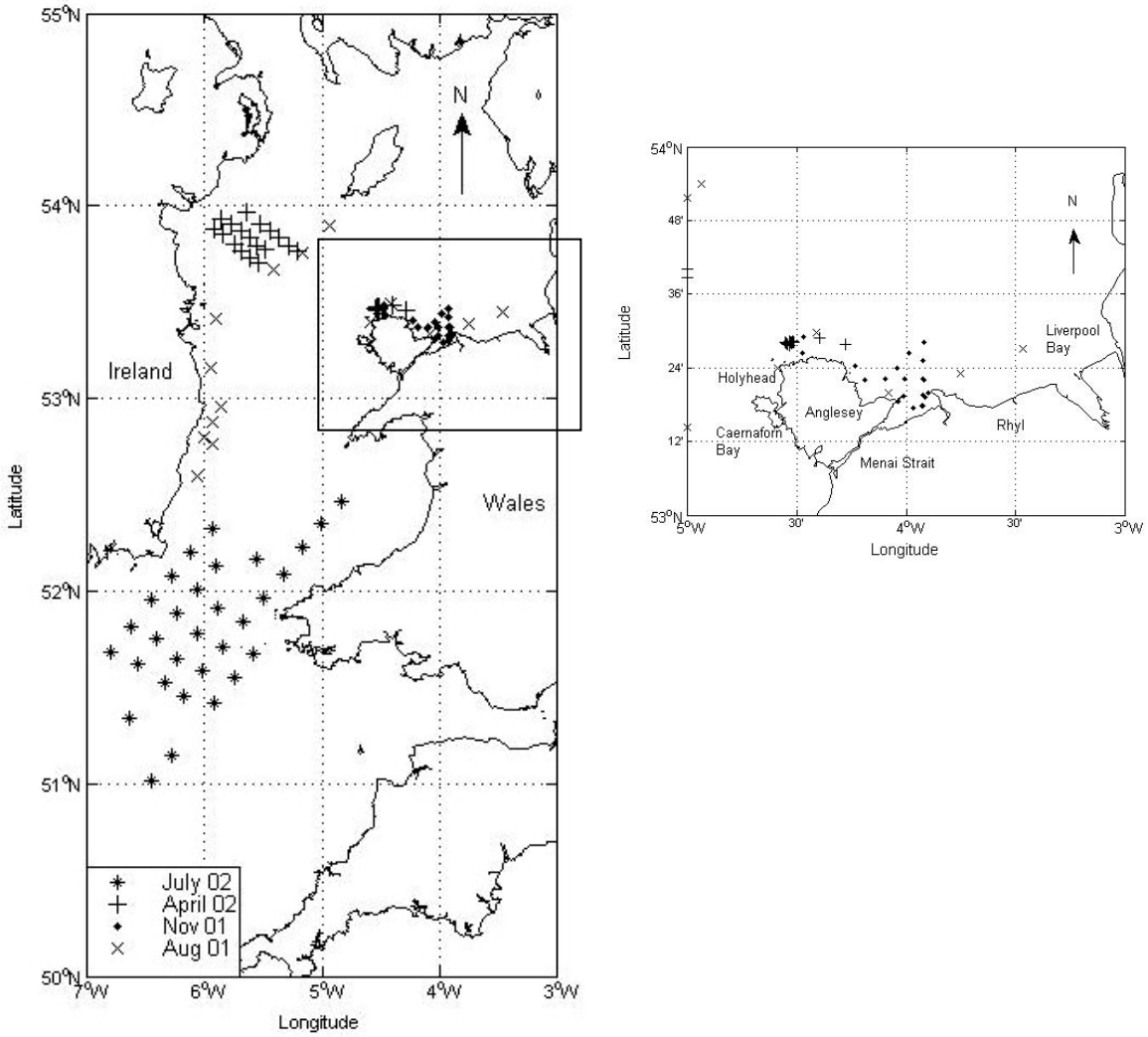

Figure 4.1. Map of the Irish Sea and location of the stations of the entire dataset

Hydrography

The complexity of the Irish Sea is a consequence of regional differences in tidal mixing, freshwater inflow and bathymetry that create distinct hydrographical regions (Gowen et al., 1995). Coastal regions of the eastern Irish Sea are characterized by low salinity water that reflects the high volume of freshwater inflow (Bowden, 1955). Offshore waters of the western Irish Sea become seasonally stratified each year from May until October, showing strong nearbed density gradients (Gowen et al., 1995; Horsburgh et al., 2000). In spring, salinity has a dominant influence on the density structure, but from June until October temperature controls the density stratification (Horsburgh et al., 2000).

Differences in tidal mixing result in the formation of offshore mixed and stratified regions in the NW Irish Sea during spring and summer. The northern coastal and offshore mixed regions are characterized and distinguished from the southern coastal and summer stratified regions by the presence of more saline, cool nearsurface water and incomplete depletion of dissolved inorganic nutrients (Gowen et al., 1995).

As stratification develops (typically in late April and May), cold water becomes isolated below the thermocline, and the density gradients associated with this ‘cold water dome’ drive a near surface gyre (Hill et al., 1994). The low turbulence in the stratified region together with the retentive nature of the gyre, creates conditions for a sedimentary environment (Trimmer et al., 2003), and waters in this region tend to be Case I or close to Case I in spring and summer. To the south and north of the stratified region, particularly in St. George’s Channel and the North Channel, tidal mixing is sufficient to ensure that the water column is vertically mixed throughout most of the year. Stratified western Irish Sea waters are separated from these mixed waters by tidal mixing fronts. The most pronounced of these is the western Irish Sea front which runs approximately from the southwest tip of the Isle of Man to Dublin (Simpson and Hunter, 1974).

4.2 Cruises

Figure 4.1 shows locations of the sampling stations occupied during four optical cruises made between 2001 and 2002.

During the first cruise, in August 2001, stations were taken along the western boundary of the Irish Sea from Wicklow to Howth, and across the Irish Sea, towards the Isle of Man, following the tidal mixing front southwest of the Isle of Man. Figure 4.2 (left) shows temperature, salinity and chlorophyll profiles for the tidal mixing front in the front region. The region is shown to be strongly stratified, with a consistent gradient of density where stratification is developed due to temperature (Horsburgh et al., 2000). The shallow embayment of Liverpool Bay was sampled as well (figure 4.2, right) where salinity is significantly lower due to freshwater inputs from rivers Clwyd, Dee and Alyn mainly, and also from the Conwy area.

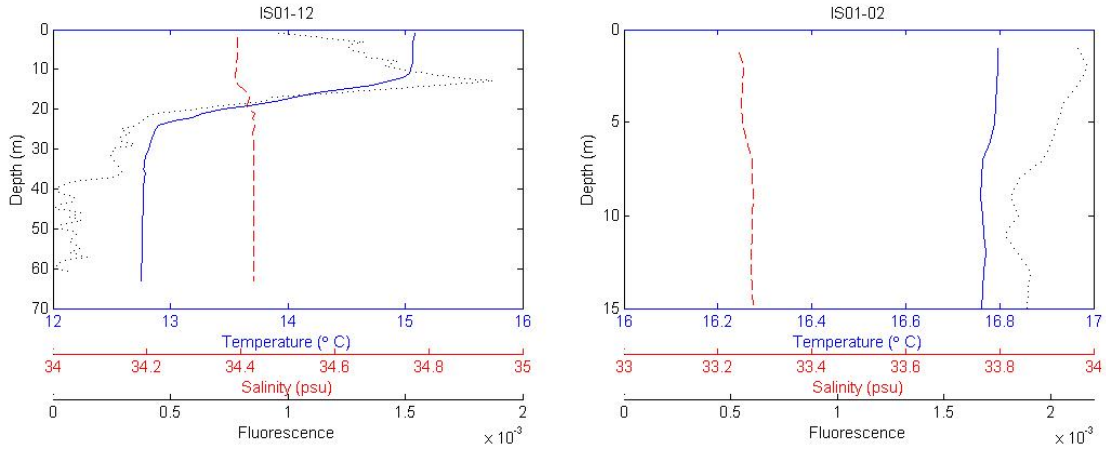

Figure 4.2. Profiles of salinity (red dashed line), temperature in degrees C (blue solid line) and fluorescence (dotted grey line) from two stations taken in August 2001. Profiles correspond to a station taken along the tidal mixing front southwest of the Isle of Man (IS01-12, left), and to a station taken in Liverpool Bay (IS01-2, right).

On the second cruise in November 2001, stations were taken in Liverpool bay, from Rhyl to the north of Anglesey Island and around Holyhead. Waters in this region, especially the mouths of the Dee and Mersey estuaries, north of Anglesey and the Menai Strait, tend to be more Case II

and have a higher content of TSM, especially in winter and autumn (Bowers et al., 1996; Bowers and Mitchelson-Jacob, 1996). Strong winds and shallow stations generated high mineral resuspension. Liverpool Bay has a strong influence of river inputs with low salinity values in the uppermost surface layer, but in this case CDOM levels were not as strong as in other regions of the Irish Sea.

The third cruise was carried out in April 2002, mainly sampling the gyre southwest of the Isle of Man, where due to the retentive nature of the gyre, Case I waters are more typically found. The gyre presents the onset of thermal stratification – a key process producing the stable surface layer where the spring bloom can take place (Hill et al., 1994). Salinity values were higher than expected in that region which could indicate a calibration problem; however these data won't be used in further analysis in this thesis. This is shown in figure 4.3 (left). Some stations were also taken in Liverpool Bay, from Rhyl to the north of Anglesey Island.

The fourth cruise in July 2002 was sampled through the Celtic Sea, St George's Channel and a few stations in Cardigan Bay. This region is strongly influenced by tidal mixing; tidal currents induce resuspension of sediments (Bowers et al., 1998). To the south of this region in the Celtic Sea, thermal stratification develops in summer (figure 4.3, right) (Buchan et al., 1967).

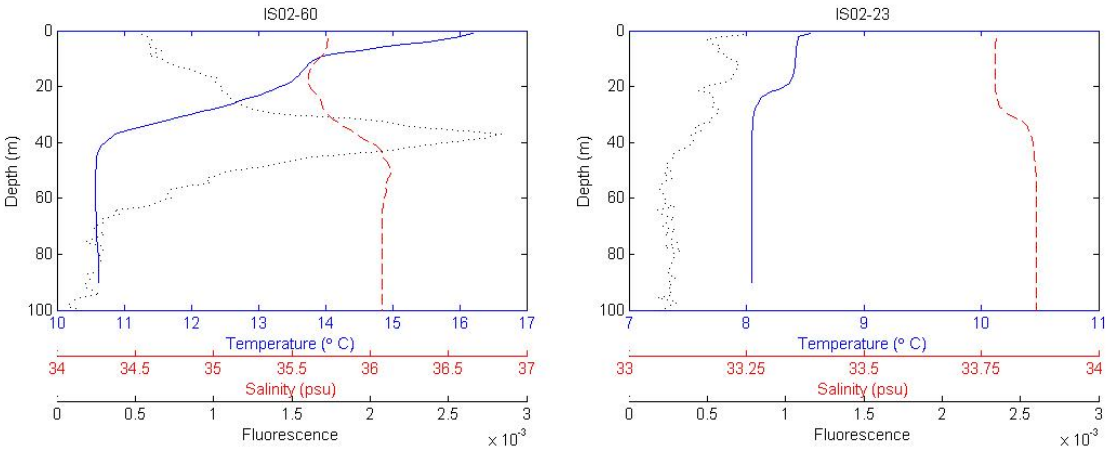

Figure 4.3. Profiles of salinity (red dashed line), temperature in degrees C (blue solid line) and fluorescence (dotted black line) from 2 stations taken in April 2002 and July 2002. Profiles correspond to a station taken on the gyre southwest of Isle of Man (left) and to a station taken in the Celtic Sea (right). Strong tidal mixing induces a well mixed water column.

4.3 Data acquisition.

The dataset was collected and processed by Dr McKee and specifications on the sampling protocols and data processing were provided by him. For this thesis, a comprehensive quality control process was initiated that resulted in acceptance of 70 stations with a complete dataset (IOP's, radiometry and constituents) from a total of 120. In this study, only sub-surface data were analyzed.

Operation of the AC-9

A 25-cm path length WET Labs AC-9 was used to measure the absorption coefficient and beam attenuation coefficient of materials other than water at nine wavelengths (10 nm FWHM) across the visible spectrum. Optical blanks for the AC-9 were regularly measured using ultrapure Millipore water treated with ultraviolet light, and calibration of the two optical channels remained within the manufacturer's specifications of ±0.005 m^{-1}. Absorption and attenuation signals were corrected for temperature and salinity dependent water absorption (Pegau et al., 1997) and data were averaged over 1 m depth intervals. Total absorption, a, and attenuation, c, coefficients were obtained by adding partial coefficients for pure water obtained from the literature using Pope and Fry (1997) for absorption and Smith and Baker (1981) for scattering. Procedures for the correction of in situ reflecting tube absorption measurements for scattering artefacts were applied. The scattering correction of Zaneveld (1994) was used in the dataset, but it may not fully account for the effects of wavelength dependent scattering phase functions in shelf seas (McKee and Cunningham, 2005; McKee et al., 2003; McKee et al., 2008).

Hydroscat

Total backscattering, b_b, at 470 and 676 nm was derived from Hydroscat-2 (HOBI Labs) measurements using the manufacturer conversion factors to b_b and correction factors for path

length absorption effects. Particulate backscattering, b_{bp}, was obtained by subtracting values for pure water backscattering derived from the measurements of Smith and Baker (1981). The 676 nm backscattering channel has a 20 nm FWHM filter to permit dual use as a chlorophyll fluorometer and therefore there is potential for fluorescence contamination in this channel. Given the limited range of chlorophyll concentration encountered in this data set, it is suggested that backscattering signals at 676 nm may be slightly overestimated for some stations (McKee and Cunningham, 2006).

Filter pad measurements

Filter pad absorption was measured using a custom-built spectrophotometer with a blank filter used as a reference to give the absorbance of all particulate material retained on the filter. Algal pigments were extracted by soaking the filters in 90% (neutralised) acetone overnight. Detrital absorbance was measured by remeasuring the absorption of material on the filter pad after pigment extraction. Phytoplankton absorption was obtained by subtracting detrital absorption from total particulate absorption.

Absorption coefficients were obtained by converting absorbance to natural logarithms (a = (2.303*absorbance*V)/A) and applying a β correction factor (β = 2, Roesler 1998) to correct for amplified light absorption effects in glass fibre filters. Algal absorption at 750 nm was assumed to be zero.

Pigment measurements

Pigment concentration was obtained using the Jeffery and Humphrey (1975) spectrophotometric method. Two different methods were applied to retrieve Chlorophyll *a* and phaeopigments. All samples were measured in triplicate.

The absorbance of pigments extracted in 90% (neutralised) acetone was measured in a 1 cm cuvette in a custom-built spectrophotometer. The trichromatic equations were used to calculate

chlorophyll concentrations. The concentration of phaeopigments was measured by acidifying the pigment extract with a few drops of 1 % hydrochloric acid and measuring the absorbance of the acidified extract. The Jeffery and Humphrey equations were used to determine concentrations of both Chlorophyll a and phaeo-pigment.

The protocol for this method suggests using a 10 cm cuvette and 15 ml acidified pigment extraction. In this dataset, for practical reasons, 8 ml of extraction were used and a 1 cm cuvette, due to unavailability of a 10 cm versions. Using a smaller cuvette and shorter path length, worsens the measurement (x10 worse) by reducing the signal to noise. However by using half the pigment extraction suggested in the protocol the quality of the measurement was improved by a factor of two in signal to noise. Overall accuracy is likely to be five times lower than suggested in the protocol (3% error).

Coloured dissolved organic material (CDOM) samples were filtered through 0.2-μm membrane filters, with the filtrate being collected in acid-rinsed glass bottles with nalgene caps and stored under refrigeration. Absorption by CDOM was measured in a custom-built spectrophotometer using 10 cm cuvettes and UV treated ultrapure water as a reference. Absorption values of CDOM at 715 nm were assumed to be zero. This offset was subtracted from the whole spectrum.

The requirements of this work led us to a quality reassessment of the data. Some data obtained with filter pad measurements were removed from the original dataset, where the acetone bleaching extraction method for pigments was not complete, and uncertainty would be added to the phytoplankton absorption signal and the non-algal particle (NAP) absorption signal. Samples where chlorophyll absorption spectra were negative or the spectral values of the NAP were contaminated by incomplete pigment extraction were removed. Previously published works have shown this type of problem on the NAP absorption signal (Babin et al., 2003) that was resolved by fitting the exponential expression of the NAP absorption to the spectrum region not affected by pigment absorption. Since the aim of this work is to characterise uncertainty

estimates in optical modelling, these data were removed to avoid added sources of uncertainty. A final quality controlled dataset of 70 stations was used in this work.

Constituents

Total suspended solids (TSS) samples were obtained by filtering 5 litres of seawater through pre-weighed 90-mm GF/F filters and rinsing with 50 ml of distilled water. Samples were stored frozen until returned to the laboratory where they were dried in an oven at 100 ˚C for 3 hours and reweighed. The concentration of mineral suspended solids (MSS) was obtained by re-weighing samples after they had been placed in a furnace at 500 ˚C for 3 hours, at which point it was assumed that all organic materials had been combusted.

4.4 Distribution of constituents

Figure 4.4 shows Total Suspended Sediments (TSS) content, which appeared to be highly variable across all stations sampled. Higher levels of mineral suspended sediment (MSS) were found off the north coast of Anglesey, and along the north coast of Wales, as well as in shallow stations (McKee and Cunningham, 2006).

Some stations sampled in this region during July 2002 and November 2001 that showed very high concentrations of TSS were removed to maintain consistency of the data. The absorption coefficient associated with suspended particulate matter (SPM) is expressed as an exponential form and assumes absorption is zero at 750nm. It was previously discussed in chapter 3 that this assumption might lead to a significant source of error in highly loaded filter pad samples, where SPM absorption in the near-IR is not negligible. That is why for data quality purposes, data from these stations were removed.

Chlorophyll content in the region appeared to be fairly low, with an average value of 1.16 mg m^{-3} and a maximum of 3 mg m^{-3} even during spring and summer, when phytoplankton is

expected to be more abundant. Previous chlorophyll studies in the region have shown high concentrations in the Liverpool Bay area (Gowen et al., 2000) in spring and summer and in the front region in the NW of the Irish Sea (Gowen et al., 1995). It might be possible that high chlorophyll waters were undersampled, but it is also possible that productivity in this area is not as high as in other shelf seas.

Absorption values of CDOM at 440 nm for this dataset were relatively low. Maximum values of a_{cdom} 440 were 0.25 m^{-1}, even though a number of samples were taken close to outflows of rivers (e.g., in Conwy Bay). These values were low compared to some other UK coastal waters, particularly the fjord systems of the Scottish west coast (McKee et al., 2002).

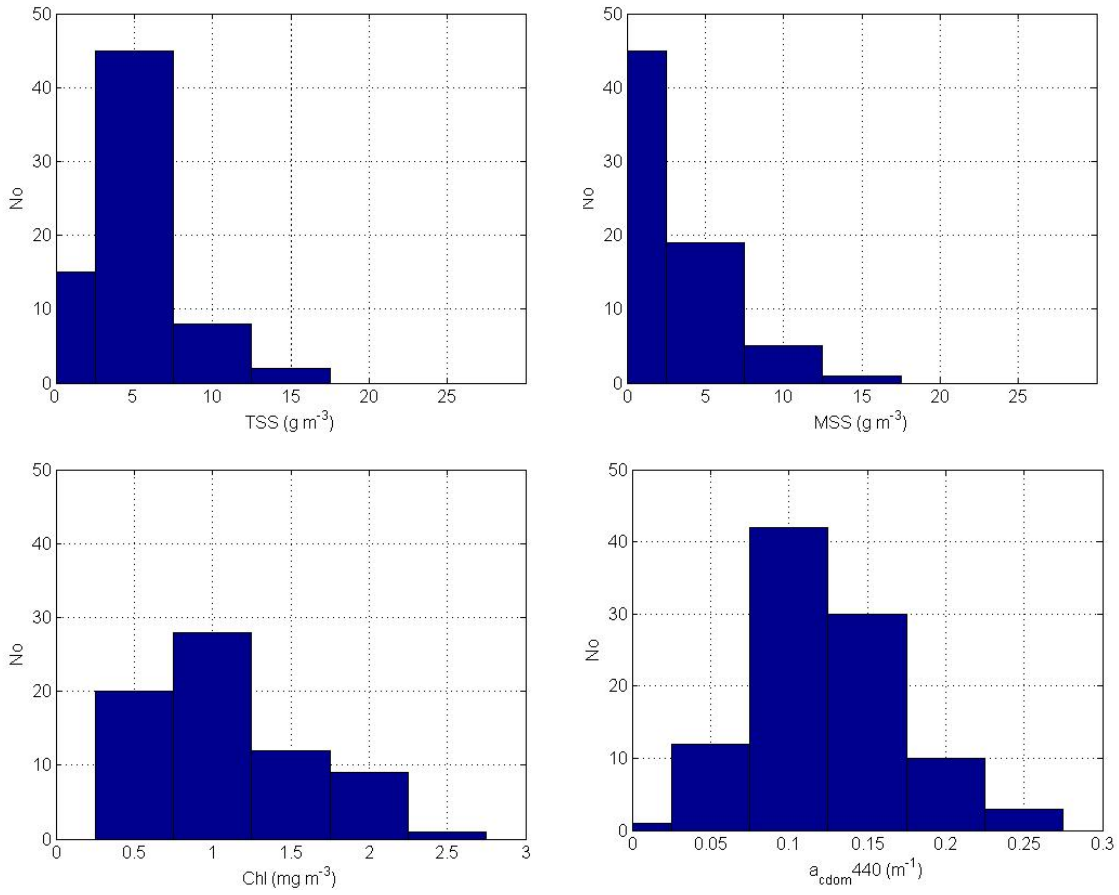

Figure 4.4. Histograms of the concentrations of seawater constituents (TSS, MSS, Chl and CDOM) for surface samples.

4.5 IOP distributions and optical water types

To study IOP's in this region, filter pad data were used for particle absorption coefficients because of the hyperspectral sampling they provide. Particle scattering and backscattering coefficients were retrieved from AC-9 and Hydroscat-2 respectively.

Figure 4.5 shows the total absorption coefficient from filter pad measurements for this subsurface dataset, and the particle backscattering coefficient, b_{bp}, at 676 nm. Both total absorption and backscattering coefficients presented a range of variability. The absorption coefficient appears to be divided into two well defined groups of stations with two different spectral shapes. One of the patterns seems to correspond to stations with a predominant content of particulate matter and CDOM, presenting a well defined decreasing exponential pattern, but with a clear feature at around 670 nm corresponding with the second absorption peak of chlorophyll. A second group of stations appear to be dominated by phytoplankton whose spectral shape governs the total absorption coefficient.

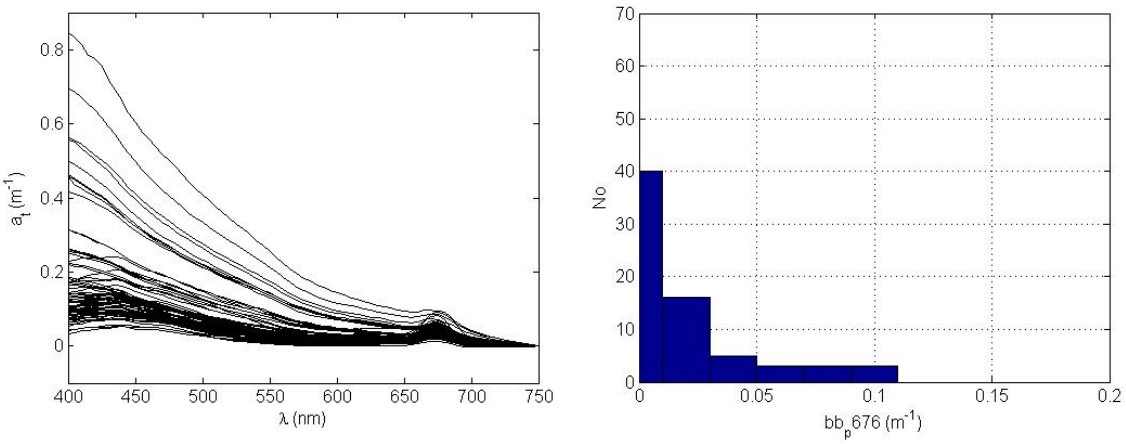

Figure 4.5. Total absorption spectra for dataset and frequency values of $b_{bp}470$.

The total absorption coefficient ranged from 0.05 m^{-1} to 0.6 m^{-1} at 440 nm, spanning one order of magnitude with an average of 0.16 m^{-1}. Stations with a clear exponential pattern for the total absorption coefficient presented a wider variability in the blue region than those with an

absorption coefficient dominated by phytoplankton. Total absorption at 676 nm was always below 0.1 m^{-1} for all samples in different seasons, which indicates a fairly low presence of phytoplankton in this region.

Particle backscattering at 676 nm was below 0.025 m^{-1} for a significant group of stations. Values from 0.025 m^{-1} to 0.1 m^{-1} are uniformly distributed between different stations.

Particulate backscattering ratio (b_b/b) at 470 nm (not shown here) varied by an order of magnitude, from 0.005 – 0.05 with an average value of 0.025. At 676 nm, highest backscattering ratios (b_b/b = 0.33) were found in the north coast of Anglesey, where the highest concentrations of mineral particles were found. Lowest b_b/b were observed during the April 2002 cruise in the north-west of the Irish Sea, with values of b_b/b = 0.005 in the cyclonic gyre. Waters in this region appeared relatively clear at that time of the year, with low chlorophyll content as well as few mineral particles. Spectral dependence of b_b/b has been observed in a recent study in this region (McKee et al., 2009, *in press*), and therefore the use of this parameter in bio-optical modelling could have major implications in the output of the model.

The two distinctive spectral patterns for the absorption coefficient might be indicative of two different optical water types within the overall region. The wide range of variability of the absorption coefficient together with the wide variation of b_b/b could also be indicative of different water types in this region.

To examine this hypothesis, particle absorption at 676 nm is plotted against particle absorption at 440 nm (figure 4.6). These wavelengths correspond to the two absorption peaks of chlorophyll. In the near red region of the spectrum, the most significant OAC are phytoplankton and water itself. In contrast, mineral absorption can be significant in the blue, decreasing exponentially with wavelength. Therefore, low a_p440/a_p676 ratios will correspond to a total absorption coefficient dominated by phytoplankton, whereas high a_p440/a_p676 ratios will correspond to an absorption coefficient dominated by particles.

By using this ratio the dataset appears to be divided into two clusters. Samples in Group A show higher values of a_p440/a_p676 ratio, whereas samples in Group B presents lower values of

a_p440/a_p676. The same sample partitioning is present on the b_{bp}676/a_p676 scatter plots (McKee and Cunningham, 2006). Group A, with higher b_{bp}676/a_p676 ratios, could be identified as waters with predominant mineral content coming from sediments resuspension and river inputs. Group B with lower b_{bp}676/a_p676 ratios are attributable to waters with predominant phytoplankton content.

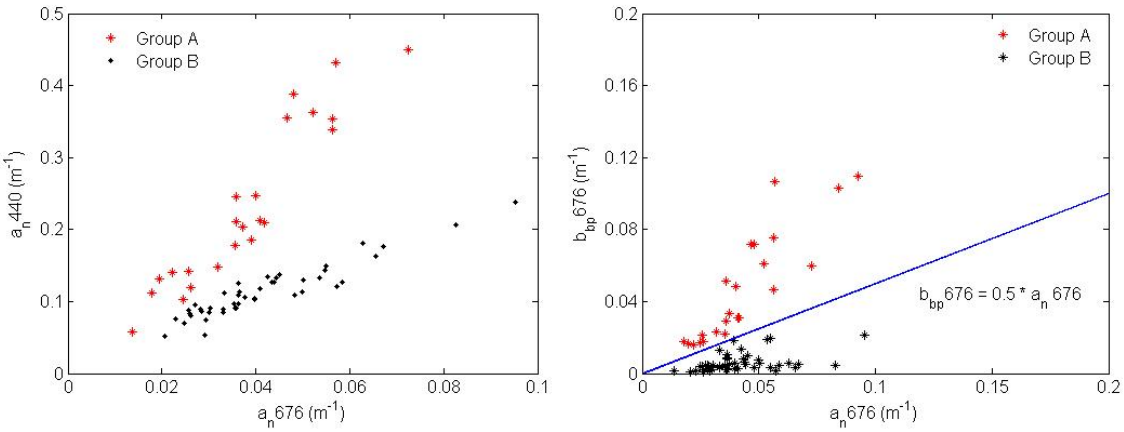

Figure 4.6. Total absorption at 676 nm vs total absorption at 440 nm. Total absorption at 676 nm vs backscattering at 676 nm.

Group A waters were mainly found in the Liverpool Bay area (figure 4.7) which presents a significant terrigenous content. Stations in this area were relatively shallow, with average depths of 30 m and presented a well mixed temperature-salinity profile. Group B waters were found in St George's channel, along the western boundary of the Irish Sea and on the cyclonic gyre located SW of the Isle of Man. These stations were deeper than group A stations and waters were generally stratified, with the exception of St George's channel, strongly influenced by tidal mixing. The classification adopted here is completely based on the ratio of b_{bp}676/a_p676 and could be dubious when high chlorophyll and minerals are found in a particular region as occurs for some group A stations located in the cyclonic gyre.

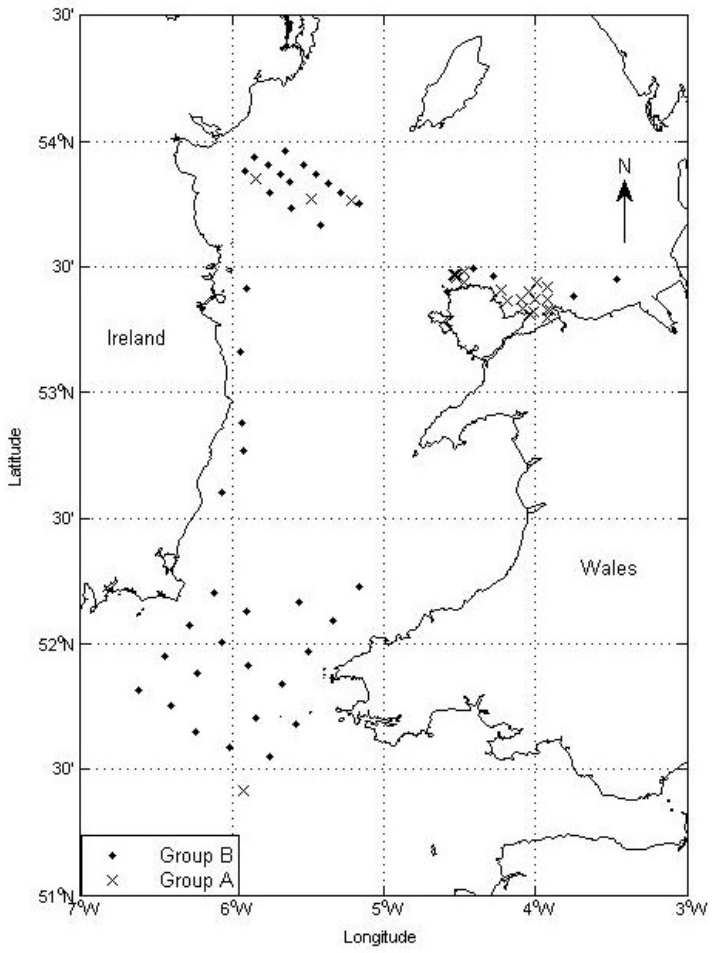

Figure 4.7. Location of Group A stations, mineral dominated, and Group B stations phytoplankton dominated.

4.6 Constituent IOP's.

Minerals and detritus

Further analysis was applied to these data in order to identify the constituent composition of each water type. Figure 4.8 shows the relationship between MSS and chlorophyll for all samples. The two groups, group A predominantly mineral and group B predominantly chlorophyll, are clearly separated. Group A, along with mainly high mineral concentrations, also contains some fairly high chlorophyll concentrations, but their ratio still indicates a

predominant mineral content in these waters but with some phytoplankton content as well. Group B waters correspond to phytoplankton dominated water even though a small mineral fraction could be observed. *Skeletonema, Chaetoceros* or *Thalassiosira* are genera of phytoplankton diatoms commonly observed in the Irish Sea, which contain a small mineral biogenic fraction (McKinney et al., 1997).

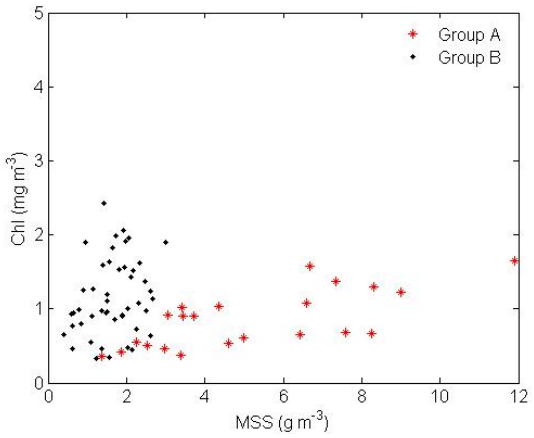

Figure 4.8. MSS vs chlorophyll for Group A and Group B.

Figure 4.9 (upper panels) plots the detrital absorption coefficient at 440 nm vs MSS content for group A, presenting a determination coefficient of 0.97 between them, which confirms that the detrital fraction is mineral for Group A waters. Similar values of mineral absorption have been found for clay samples with ochre coloration (Babin and Stramski, 2004), featuring spectral shoulders correspondent to the variable mineral composition of the sample. From now on, the detrital absorption coefficient in Group A waters will be named mineral absorption coefficient, a_{mss}. Mean a_{mss} spectral coefficient is also presented in figure 4.9. In group B waters, the detrital fraction is poorly correlated with both chlorophyll and MSS content (figure 4.9, lower panels).

The absorption coefficient associated with detritus includes any remaining unpigmented organic material with absorbing properties as well as the effect of intracellular material of living phytoplankton cells. Regression analysis between detritus and chlorophyll is clearly low, since samples have been bleached to eliminate any remaining pigment. A low slope regression value will also affect the correlation coefficient. However this is largely a result of limited signal

ranges in both X and Y variables and significant trends can be discerned. For these Group B waters it can reasonably be concluded that the detrital absorption signal is generally associated with the algal population though there is scope for contributions from other particle types too.

The range of variability for the detrital absorption coefficient at 440 nm for Group B is very low, with an average of 0.0367 m^{-1}. The very small range of variation in detrital absorption can also indicate a phytoplankton related detrital fraction.

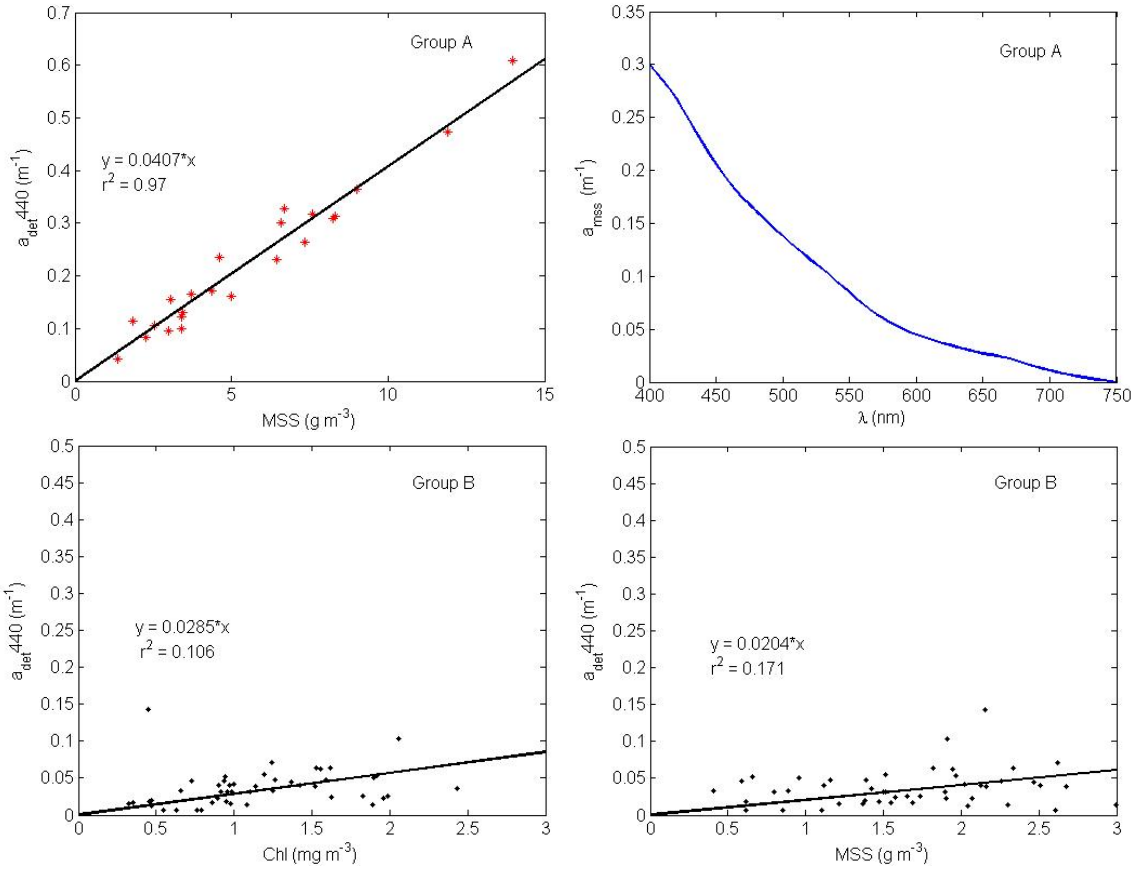

Figure 4.9. (upper panels) Detrital absorption vs. MSS for Group A and mean a_{mss} spectra. (lower panels) Detrital absorption vs. chlorophyll for Group B and detrital absorption vs. MSS for Group B.

To explore in further depth the source of the detrital fraction in Group B, figure 4.10 presents the average Group B specific detrital absorption coefficient, a_{det}* based on mineral

concentration, a_{det}/MSS, and based on chlorophyll concentration, a_{det}/Chl. In the case of a_{det}/MSS, the spectral values are significantly lower than for a_{mss} in Group A (figure 4.9, upper right panel) and the spectral shape smoothly decreases, in contrast to the a_{mss} spectra in figure 4.9 with marked slope changes in the spectrum. Changes in slope have been observed in a_{mss} spectra corresponding to a variable mineral composition (Babin and Stramski, 2004). Hence, we can conclude that the detrital fraction in Group B is chlorophyll related. Similar values for the a_{mss} coefficient to those presented here were also reported by Babin and Stramski (2004) for clay samples.

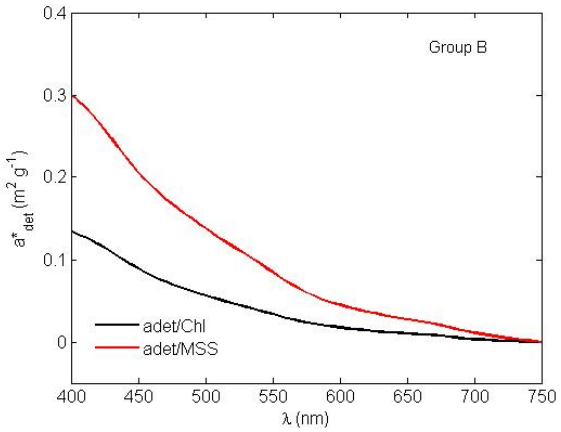

Figure 4.10. Specific detrital absorption coefficient calculated from MSS and Chl.

The detrital absorption coefficient is explicitly not related to total SPM, distinguishing our approach from that of other studies (Babin et al 2003; Bowers et al 1996), since to do so would separately include mineral biogenic content and organic content even though they possibly come from the same source, and therefore would double count the real phytoplanktonic pool.

Phytoplankton

Phytoplankton absorption spectra were obtained using the filter pad technique for the whole dataset. In figure 4.11 (upper left panel) phytoplankton absorption spectra and mean phytoplankton absorption spectrum (red line) are presented.

In this region, pigment concentration was generally low compared with previous studies in the region even though three of the four cruises were performed in spring and summer. Phytoplankton absorption values were, in contrast, found higher than other studies that suggest a ratio for the phytoplankton absorption to the chlorophyll concentration of 0.02 (Mitchell and Kiefer, 1988; Stramski and Morel, 1990). These higher values found in this study might be due to: (1) problems with the chlorophyll retrieval method, (2) in low irradiance, coastal, oligotrophic wasters a higher efficiency of phytoplankton and higher absorption curves have been observed (Sosik and Mitchell, 1995) or (3) choice of β factor for scattering effects. Variability on the phytoplankton absorption spectra in general was low, presenting variability in the blue of 2.5 times the mean value (Figure 4.11).

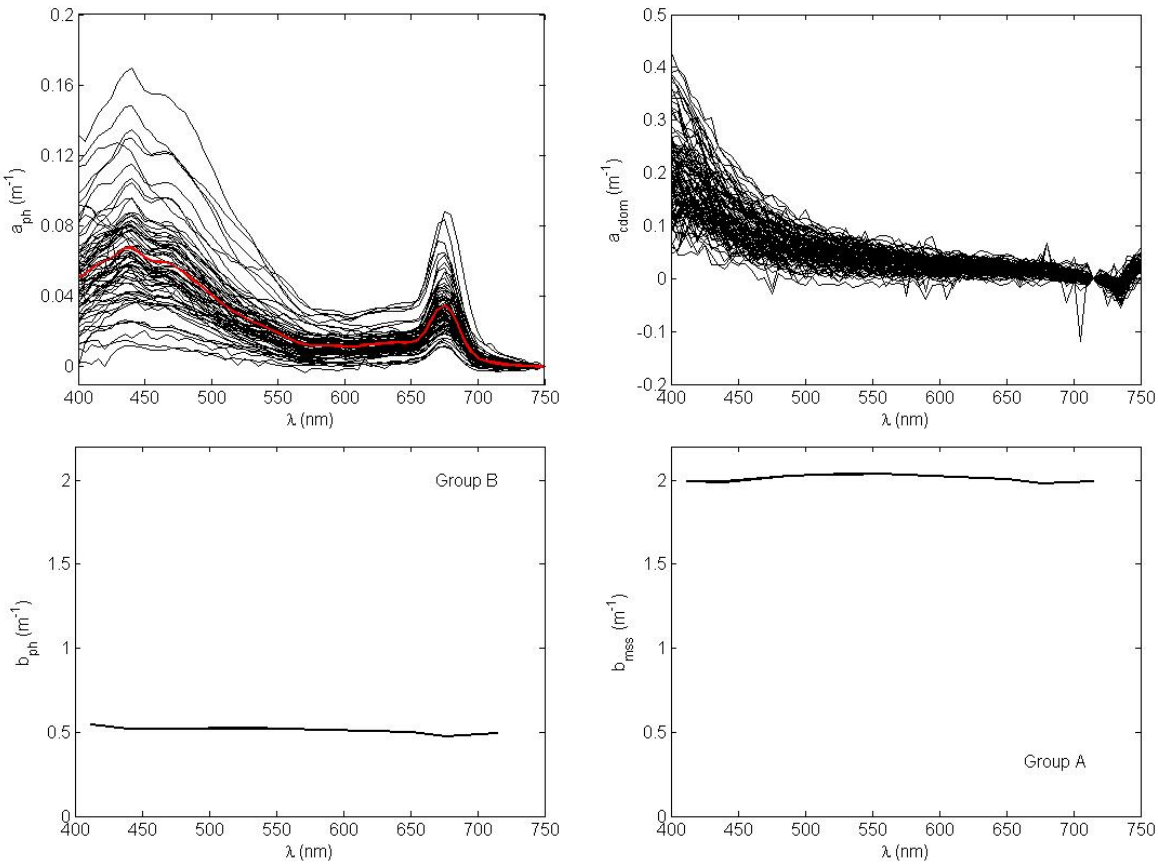

Figure 4.11. Phytoplankton absorption spectra, CDOM absorption spectra, mean phytoplankton scattering spectrum, mean MSS scattering spectrum.

CDOM

Absorption by CDOM was also found to be generally lower compared with previous studies in the region (McKee et al., 2002; Tilstone et al., 2005). As figure 4.11 shows (upper right panel), the a_{cdom} values varied over a reasonably small range even though three cruises were carried out in spring and summer and close to river outflows. Typical a_{cdom} values at 440 nm have been reported from 0.01 to 0.1 m^{-1} in oceanic waters and from 0.04 to 20.0 m^{-1} in coastal, estuarine and inland waters (Kirk, 1994) whereas $a_{cdom}(440)$ was 0.06 m^{-1} in this dataset. In this region however it has also been documented that there is low CDOM contribution to total absorption signals (Bowers and Mitchelson-Jacob, 1996). For comparison purposes with other studies a_{cdom} spectra were fitted to the exponential parameterization. During the COASTlOOC experiment for coastal sampling around Europe, average slope coefficient of a_{cdom} was 0.0176 nm^{-1} with a standard deviation of 0.002 nm^{-1} (Babin et al., 2003) whereas in this dataset it was significantly lower, 0.0129 $m^{-1}nm^{-1}$.

A dependence of a_{cdom} on temperature and salinity has been reported at 740 nm (Sullivan et al., 2006), but this effect has not been corrected for in this dataset. CDOM absorption data were not fitted to an exponential expression for data smoothing in order to avoid added uncertainty at the extremities of the visible spectrum of the measured data.

Phytoplankton and MSS scattering coefficients were obtained after classification by applying optical water type criteria for distinguishing Group A and Group B waters. Thus, in a singular location the scattering coefficient is assigned either to phytoplankton or MSS. Figure 4.11 (lower panels) shows mean spectra of b_{ph} and b_{mss} presenting wavelength independency. This will have profound implications when deriving and applying particulate backscattering ratios for bio-optical modelling.

4.7 A four component model for the Irish Sea

Using a similar expression to that proposed by other authors (Babin et al., 2003; Carder et al., 1991; Prieur and Sathyendranath, 1981; Roesler et al., 1989), we can express the complex absorption and scattering properties of the Irish Sea as a four component model:

$$\begin{aligned} a &= a_w + (a^*_{chl} + a^*_{\det}) \cdot Chl + a^*_{mss} \cdot MSS + a_{cdom} \\ b &= b_w + b^*_{chl} \cdot Chl + b^*_{mss} \cdot MSS \end{aligned} \tag{4.1}$$

where every specific IOP is related with its constituent concentration. Decomposing the absorption coefficient for the two water types identified in sections 4.5 and 4.6, it can expressed as:

Group A $$a = a_w + a^*_{chl} \cdot Chl + a^*_{mss} MSS + a_{cdom}$$

Group B $$a = a_w + a^*_{chl} \cdot Chl + a^*_{\det} \cdot Chl + a_{cdom}$$

By setting up this model, the Irish Sea has been optically characterized based upon constituents and specific IOP's. Even in complex waters such as the Irish Sea and without taxonomical information for phytoplankton species, different optical water types can be envisaged, depending on its composition and differentiation between biogenic and non-biogenic sources and using basic relationships between constituents and IOP's. An explicit characterization of constituent IOP's is crucial to evaluate variability in IOP's caused by variations in constituents or optical uncertainties. From that we gain the capability to estimate uncertainty in bio-optical modeling.

Using biogenic and non-biogenic partitioning also has important consequences in ecosystem modeling: the use of different water types allows a precise characterization of constituents and

hence of the optical properties. For a given region from Group A waters, as defined above, its optically active constituents are mineral sediments, phytoplankton and colored dissolved organic matter and hence the underwater light field can be calculated based upon them (Fuji et al., 2007). Similarly for a region with Group B waters that are phytoplankton dominated. Furthermore, the partitioning into biogenic and non-biogenic sources allows the possibility for ecosystem models to establish pools and sources of detritus or particulate carbon from phytoplankton or other sources, and mineral particles as by-products of phytoplankton or mineral sediment from resuspended materials.

This chapter has described the data used and defined the IOP's present in the dataset. Furthermore it has shown that by using simple optical ratios, the biogeochemical source of IOP's can be defined, when no other compositional information is available. By using this partitioning analysis, it has been possible to establish an optical model for the Irish Sea. This model can be used to define total absorption and scattering for different water types in a forward optical model according to their biogeochemical composition.

Chapter 5

Uncertainties on constituent IOPs:

A new approach to reduce uncertainties in optical data.

5.1 Introduction

Optical parameters defining the properties of sea water and its content are used for assimilation in radiative transfer modelling and so an accurate characterization of them is necessary when using numerical optical models to compute the underwater light field. Variability in optical measurements can be attributed to changes in the concentration and composition of OACs. However, some of the observed variability will also be attributable to measurement uncertainties, a fact that has often been overlooked in previous studies.

Some of this variability arises from random uncertainties in data; instrument noise, changing illumination conditions, etc. Some is caused by systematic uncertainties in the acquisition process and data processing. Correction factors applied in measuring absorption coefficients, such as the AC9 scattering correction factor and the path length amplification factor when using the filter pad method (chapter 3), are likely to introduce substantial error to the measurement of the optical properties. Furthermore, when optical data from different sources are combined to derive other optical parameters, uncertainties can potentially be amplified greatly.

Uncertainties in IOPs have been reported to be one of the major problems when attempting to perform closure exercises, i.e. computing water leaving radiance from IOPs using numerical modelling and comparing with in-situ radiometry (Bulgarelli et al., 2003). Chang et al. (2003), reported that some of the problems associated with closure exercises might arise from faulty scattering corrections applied to AC-9 data. Other sources of uncertainty in IOPs have been attributed to model assumptions for the chlorophyll fluorescence quantum yield and the spectral

chlorophyll-specific absorption coefficient for the red wavelength (discussed here in chapter 3), as well as radiance measurements inaccuracies (Gordon and Ding, 1992; Leathers and Downes, 2001).

The goal of this chapter is to quantify the uncertainties of IOPs and constituents, and how these two propagate when deriving specific IOPs (SIOPs). Here different statistical approaches are compared with a view to obtaining a clearer understanding of natural variability in SIOPs taking account of measurement uncertainties. For this, constituent IOPs are introduced in 5.2, leading to an analysis and discussion of the constituent SIOPs for the Irish Sea dataset, and their associated variability. In 5.3 we analyze separately the variability in IOP data and in the constituent measurements, followed in 5.4 by considering how the uncertainties of both IOPs and constituents are combined and may be amplified in the constituent SIOP errors. Finally in 5.5 an alternative statistical approach is introduced to retrieve constituent SIOPs in a way that reduces SIOP variability arising from measurement uncertainty, and it is compared with traditional calculations of constituent SIOPs.

5.2 Variability of constituent IOPs

The importance of the variability of measured IOPs is the uncertainty which that variability creates for the output of optical models that use those IOPs. IOPs are the initialization variables of the optical model, which describe a specific water mass with particular concentrations of OACs. When IOP data are available, these can be introduced in the optical model. However, it is common to generalise this approach by the use of IOPs normalized by the mass of the constituent so they can be used as optical descriptors for a particular region independently of its OAC concentration. The IOP signature across the spectrum depends on the constituent type and concentration:

$$IOP_{const} = f([constituent-type],[constituent-concentration],\lambda) \qquad (5.1)$$

This is generally simplified by assuming that the spectral shape of the constituent, which we can write as $S_{const}(\lambda)$ is determined by the type of constituent, while its magnitude depends on the absolute concentration of the constituent, C_{const}. Thus:

$$IOP_{const} = f(C_{const}, S_{const}(\lambda)) \tag{5.2}$$

This function is often further simplified as a simple product of the concentration and the spectral shape function, now assumed to be invariant with the constituent concentration and which is then referred to as the specific IOP or SIOP. Then

$$IOP_{const} = C_{const} \cdot SIOP(\lambda) \tag{5.3}$$

In principle this approach should simplify the way of estimating constituent IOPs for use in bio-optical models. If C_{const} is known (for example by measurement or as a prediction from within an ecosystem model) then as long as the SIOP is known as a function of wavelength for that constituent, equation 5.3 provides the estimated IOP_{const}.

However, this requires knowledge of the SIOP, which must be derived empirically. The SIOP cannot be directly measured, but is derived from a set of paired measurements of IOP_{const} and C_{const}. Such measurements include the range of variability identified in chapter 4. Thus, although the reported variability in constituent SIOPs is mostly attributed to natural variability, it may also be a result of measurement uncertainty in both C_{const} and IOP_{const} and also the way in which the SIOP is derived from those measurements. This chapter focuses on the variability in SIOPs which is introduced by measurement uncertainties, and is therefore potentially capable of reduction, with the ultimate goal of improving the performance of bio-optical models when such SIOPs are applied.

SIOPs are usually derived in a point-by-point approach as the optical cross section of an optically active constituent, OAC, divided by its corresponding constituent mass per unit water volume concentration:

$$SIOP = \frac{IOP_m}{[const_m]} \tag{5.4}$$

SIOPs cannot be directly measured and are always obtained through direct measurements of measured IOPs (IOP_m) and measured constituent concentration ($[const_m]$).

Figure 5.1 presents an ensemble of the specific absorption coefficients of chlorophyll, detrital particles, mineral suspended sediments, and coloured dissolved organic matter, as derived from individual sampling stations. Specific scattering coefficients of chlorophyll and MSS are presented as well. All SIOPs were normalized by the corresponding OAC mass concentration measured at the same sampling station. Phytoplankton specific absorption coefficient, a_{ph}*, is called phytoplankton specific absorption coefficient by chlorophyll from now on, a_{chl}*, since the optical cross section of phytoplankton is related only with Chl *a* content. Chl *a* is the most optically significant component, but not the only one (chapter 4) and although most studies would approximate a_{chl}* to a_{ph}* here it will not be done to preserve rigour in the data presentation. In the case of a_{cdom}*, $a_{cdom}440$ was used as a proxy for CDOM concentration.

In this dataset, the mean observed values of a_{chl}* 676 were 0.0356 m^2(mg Chl *a*)$^{-1}$, with a range of 0.0165-0.0822 m^2(mg Chl *a*)$^{-1}$. As previously discussed in chapter 4, these values appear to be slightly higher than others found in the literature, but within similar ranges. Cota et al., (1994) reported a value of a_{chl}* of 0.023 ± 0.011 m^2 (mg Chl *a*)$^{-1}$ and Moisan and Mitchell (1999), observed a range of variation for a_{chl}* of 0.012-0.030 m^2(mg Chl *a*)$^{-1}$ for lab cultures. The results presented here were obtained from in situ samples which usually have a lower a_{chl}*. However, higher phytoplankton efficiency absorption in coastal waters has also been reported (Sosik and Mitchell, 1995) comparable with this dataset. These high values could also be the result of the protocol used for Chl *a* measurement (chapter 4) or the path length correction amplification factor selected (β = 2). McKee and Cunningham (2006), presented AC-9 and a_{cdom}

values for this dataset whose combined result to obtain particulate absorption was still lower than those obtained here for particulate absorption from filter pad measurements. It is believed that the choice of path length amplification factor could be responsible for the high a_{chl}* values (see chapter 3).

Detrital absorption in this region is due mostly to phytoplankton by-products, organic material from different sources as well as a small mineral fraction possibly biogenic (diatoms). a_{det}* was obtained by normalizing the SPM fraction from Group B waters to Chl *a* concentration (as justified in chapter 4). Mean observed values of a_{det}* at 440 nm were 0.033 $m^2 mg^{-1}$ with a range of variation of 0.040 - 0.112 $m^2 mg^{-1}$. a_{det}* spectra were not fitted to any exponential expression, as is often done in the literature, in order to avoid added uncertainty in further analysis. For comparison purposes, exponentially fitted spectra were examined and the average slope coefficient was 0.0124 which is within literature observed values. Studies from a well defined detrital fraction from organic origin are difficult to find. Most of them include absorption effects from mineral particles since separating absorption signatures of organic and inorganic pool is only possible in lab experiments. Babin et al., (2003) observed a slope coefficient for the detrital faction of 0.0123 nm^{-1} which reportedly includes effects from mineral particles. Bowers et al., (1996) reported similar slope values for mineral particles in the Irish Sea. Field studies for the absorption coefficient of detrital fraction are ambiguous in terms of their chemical origin, which is key to interpret their optical properties.

Specific absorption coefficient of mineral suspended sediments, a_{mss}*, was obtained by normalizing the detrital fraction from Group A, mineral dominated (chapter 4) with MSS concentration, since regression analysis showed a determination coefficient of 1 with MSS content. Mean a_{mss}* at 440 nm was 0.0405 $m^2 g^{-1}$ with a range of 0.0296-0.0617 $m^2 g^{-1}$. Babin and Stramski, (2004) found similar values in coastal mineral water samples of clay extracts with characteristic ochre coloration and for iron oxides samples with less than 5% POC content. For clay samples, those with highest Fe content presented highest a_{mss}* values and Fe appeared to dominate the a_{mss}* signal. Also, changes in the spectral slope of clay samples were evident as in our data, a result of the variable composition on the mineral fraction.

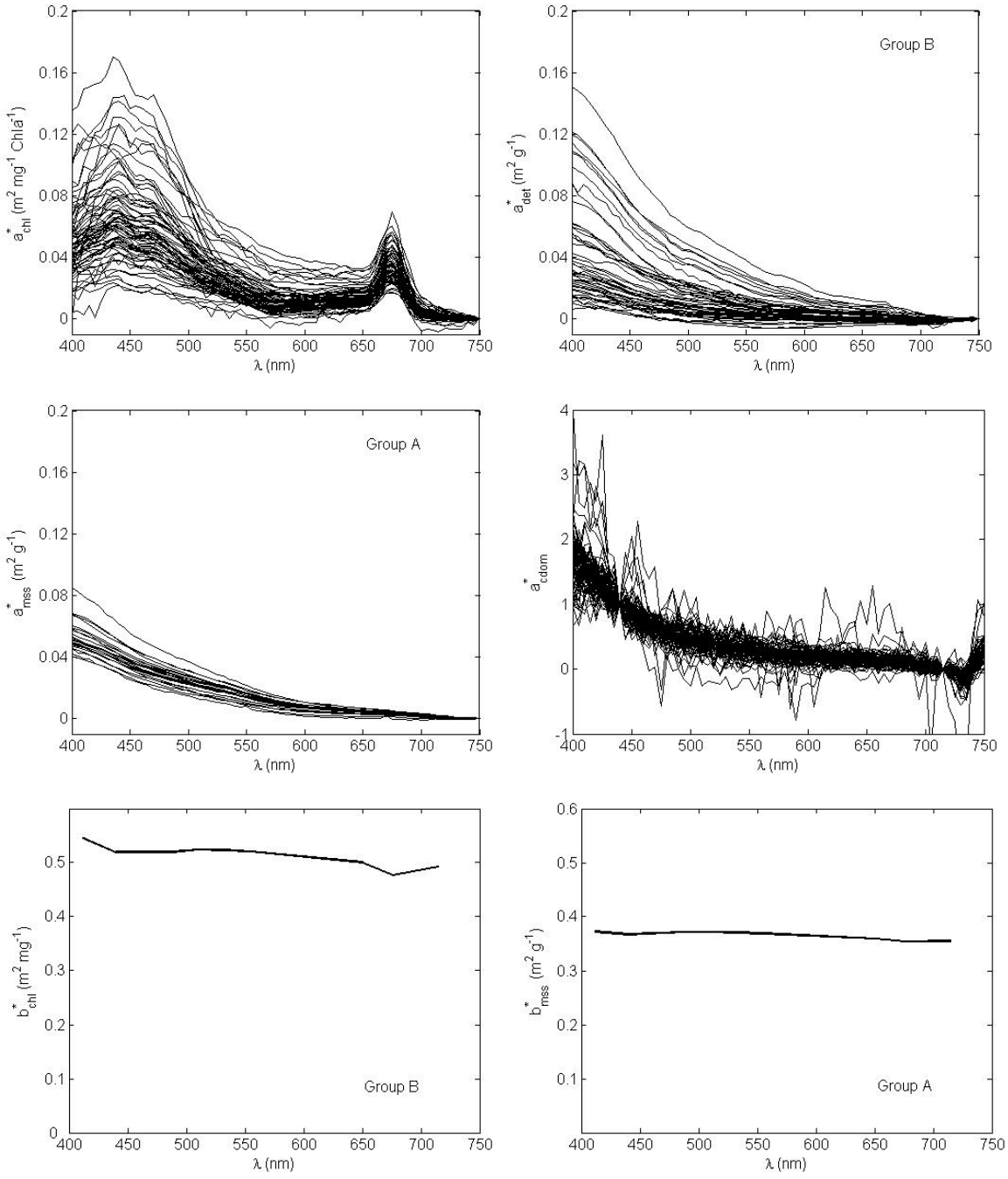

Figure 5.1. Specific absorption coefficients of chlorophyll (upper left), detritus (upper right), MSS (middle left) and CDOM (middle right). Mean specific scattering coefficient of chlorophyll (bottom left) and MSS (bottom right).

Specific absorption spectra by CDOM, a_{cdom}*, were also not fitted to an exponential expression to avoid added uncertainty by the data smoothing procedure. Low variability can be observed in this data even though samples were taken in different regions and seasons in the Irish Sea (chapter 4). The a_{cdom}* data appears noisier than filter pad absorption data as the filter pads had effective path lengths of the order of 1-2 m, while a_{cdom} was measured with a 0.1 m cuvette. a_{cdom} data have therefore got poorer signal to noise.

Specific scattering coefficients were obtained from individual measurements of scattering coefficients, applying optical water type criteria (chapter 4) and then divided by the appropriate constituent concentration. For scaling reasons we have presented mean chlorophyll specific scattering coefficient b_{chl}* and mean MSS specific scattering coefficient b_{mss}* so their spectral features can be observed.

b_{chl}* and b_{mss}* presented low spectral dependency with minimum values at 440 and 660 nm corresponding with the blue and red chlorophyll absorption. b_{chl}* spectrum can be explained as a result of the intracellular chlorophyll concentration, cell diameter and Q_b, scattering efficiency factor (Ahn et al., 1992), where the efficiency factor is defined as the ratio of attenuated energy scattered by this mean cell to the energy impinging on its geometric cross section. The chlorophyll minimum also present in b_{mss}* shows that the water type criteria partitioning applied to the scattering coefficient might not be very precise since a fraction of phytoplankton can be clearly observed in b_{mss}*.

5.3 Quantifying uncertainties

The constituent SIOPs shown and discussed above were calculated in a "point-by-point" approach as shown in equation 5.4, where every IOP measured value is referenced against its constituent concentration measured value. Both of these measurements, IOP and constituent concentration, present variability. Some of it can be attributable to natural variability, but part of this variability will be also due to measurement uncertainty.

$$SIOP \pm \varepsilon = \frac{IOP_m + \varepsilon_{IOP}}{[const_m] + \varepsilon_{const}} \quad (5.5)$$

Some authors have identified the problems related with IOP measurement uncertainty (Prieur and Sathyendranath, 1981) and their impact on derived parameters such as SIOP precisely due to this calculation method (Bricaud et al., 1995). Therefore it is important to distinguish between natural variability and variability due to uncertainty. SIOPs are also used as optical descriptors for a given area in optical modelling, and often are used to obtain theoretical constituent IOPs (IOP_t), reconstructing IOPs from SIOPs based on the above approach as:

$$IOP_t = (SIOP \pm \varepsilon) \cdot ([const] + \varepsilon_{const}) \quad (5.6)$$

Figure 5.2 presents as an example $a_{ph}440$ values vs Chl *a* concentration for this dataset. As shown, data are homogeneously distributed along a prediction line for $a_{ph}440$ vs Chl *a* values. By using SIOPs derived in point-by-point, a theoretical IOP (IOP_t) can be obtained from the SIOPs based on equation 5.6. With this approach, uncertainties on calculated SIOP will propagate and increase when retrieving IOP_t.

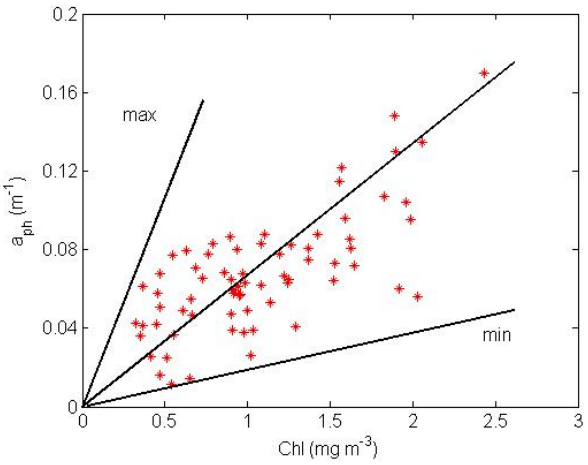

Figure 5.2. a_{ph} 440 measured vs Chla concentration measured. Max/min ranges of a_{ph} theoretical.

In this case, a_{ph} theoretically can be obtained from a_{chl}* given the Chl *a* concentration range introduced in equation 5.4. Using this approach, the IOP_t values obtained will include variability from SIOP uncertainty and constituent uncertainty whose combined uncertainty results in an IOP_t range given by the maximum and minimum value observations for the dataset (figure 5.2). Part of the apparent variability introduced in IOP_t will be due to measurement uncertainty.

To estimate uncertainty associated with SIOPs the individual contributions to the total uncertainty in SIOPs have to be identified, coming both from IOP measurements and from constituent concentration measurements.

For constituent IOP uncertainty, consecutive wavelengths have been taken for regression analysis. Assuming a slow variation on the IOP signal, the variability between 2 consecutive wavelengths is attributed to noise in the measurement. For phytoplankton absorption, detrital absorption, MSS absorption and CDOM absorption, regressions have been applied for 500 and 505 nm (figure 5.3). The signal generally decreases with wavelength in this spectral range. Geometric mean regression analysis is applied to model observations. Modelled values minus observed values will provide the range of variability attributable to uncertainty, since true variation in the signal is assumed to be adequately accounted for by the linear regressions.

Geometric mean regression

To ensure regression data are given equal weighting, a geometric mean regression (GMR) technique has been applied to the study of consecutive wavelengths. The slope of the GMR is the geometric mean of the two slopes determined by regressing Y on X and X on Y. As opposite to the ordinary least squares regression, which assumes no error on the independent variable x, the GMR (or reduced major axis regression) minimizes the horizontal residuals as well as the verticals. The slope and the intercept of the GMR can be expressed as:

$$b_{GMR} = \frac{b_{OLS}}{|r|},\ a_{GMR} = \bar{y} - b_{GMR}\bar{x} \tag{5.7}$$

where b_{GMR} and b_{OLS} are the slopes of the geometric mean regression and the ordinary least squares regression, r is the correlation coefficient and x and y are the average of data.

IOP uncertainty

In figure 5.3 is presented GMR studies for a_{ph}, a_{det}, a_{mss}, and a_{cdom} together with error estimates from modelled constituent IOPs minus observed constituent IOPs.

The method provides excellent agreement at consecutive wavelengths for a_{ph}, a_{det} and a_{MSS}, which proves the consistency of the method. For a_{ph}, a_{det} and a_{mss}, correlation coefficients are 0.997, 0.999 and 1 respectively and measurement uncertainties are 0.004 m^{-1} for a_{ph} and 0.002 m^{-1} for a_{det} and a_{mss}. All three measures for these coefficients come from filter pad measurements and from the same sample and we can observe a consistent random uncertainty in the measurement. In the case of a_{ph}, the slightly higher variability could be associated with natural variability from sample to sample. In general we can say that absorption measurements with filter pad present a random uncertainty in the measurement of ± 0.002 m^{-1}.

For a_{cdom} measurements (figure 5.4), GMR regression is worse than for those from filter pad measurements with a correlation coefficient of 0.893. a_{cdom} measurements have a path length an order of magnitude lower than filter pad measurements, and therefore an order of magnitude worse signal to noise (± 0.02 m^{-1} compared to ±0.002 m^{-1} random uncertainty ranges).

GMR for phytoplankton scattering and MSS scattering is excellent, with a correlation coefficient of 0.99. It was previously stated that these coefficients have low spectral dependency. The linear fitting provides a slope value close to 1 which explains the spectral variability between these two wavelengths. AC-9 specifications provide an instrument accuracy of 0.01 m^{-1} and the measurement uncertainty observed in this analysis is very closely related, 0.02 m^{-1}.

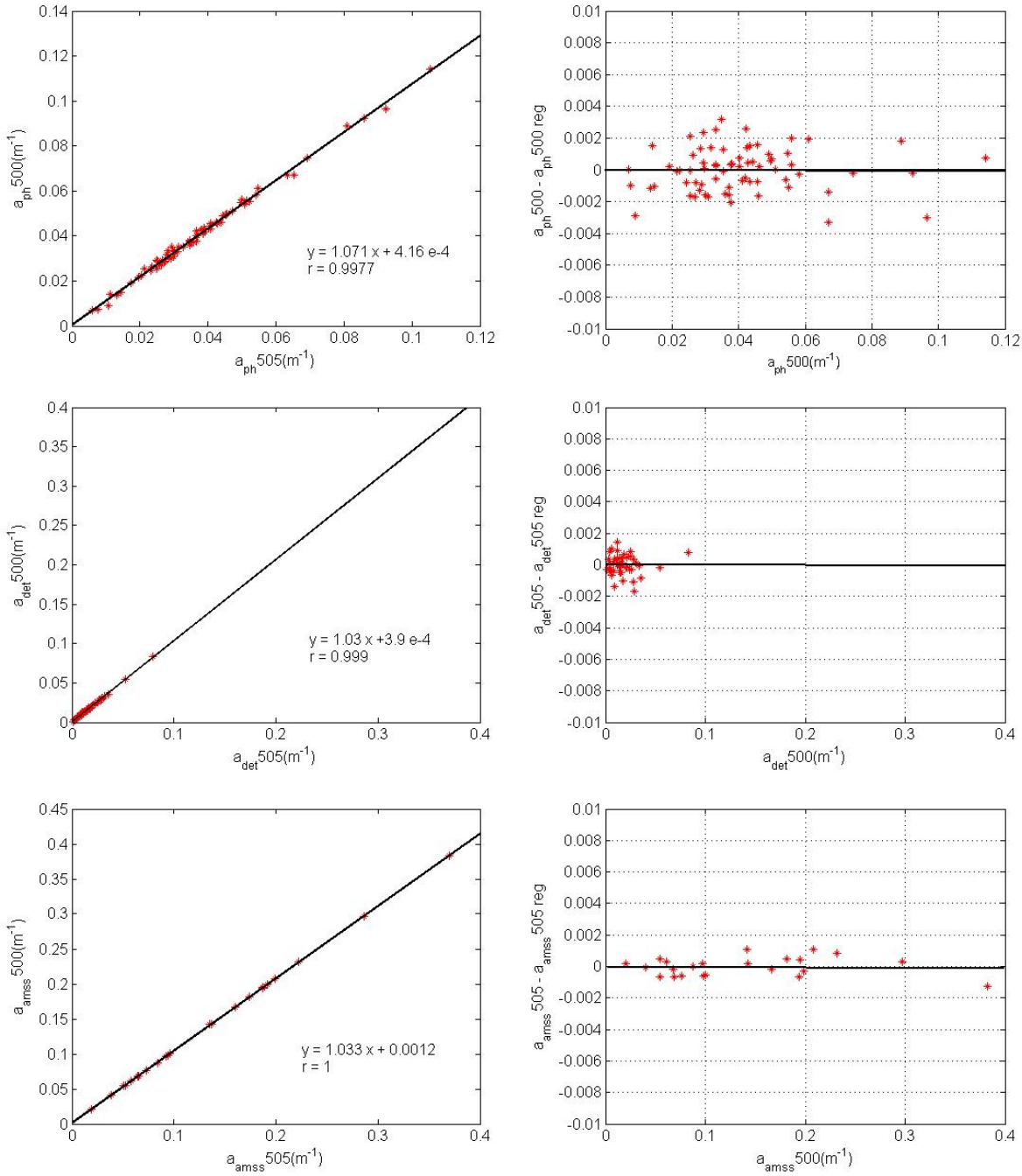

Figure 5.3. GMR analysis at consecutive wavelengths for phytoplankton absorption, detrital absorption and MSS absorption (left panels). Error estimates from predicted values by regression minus observations for phytoplankton absorption, detrital absorption and MSS absorption (right panels).

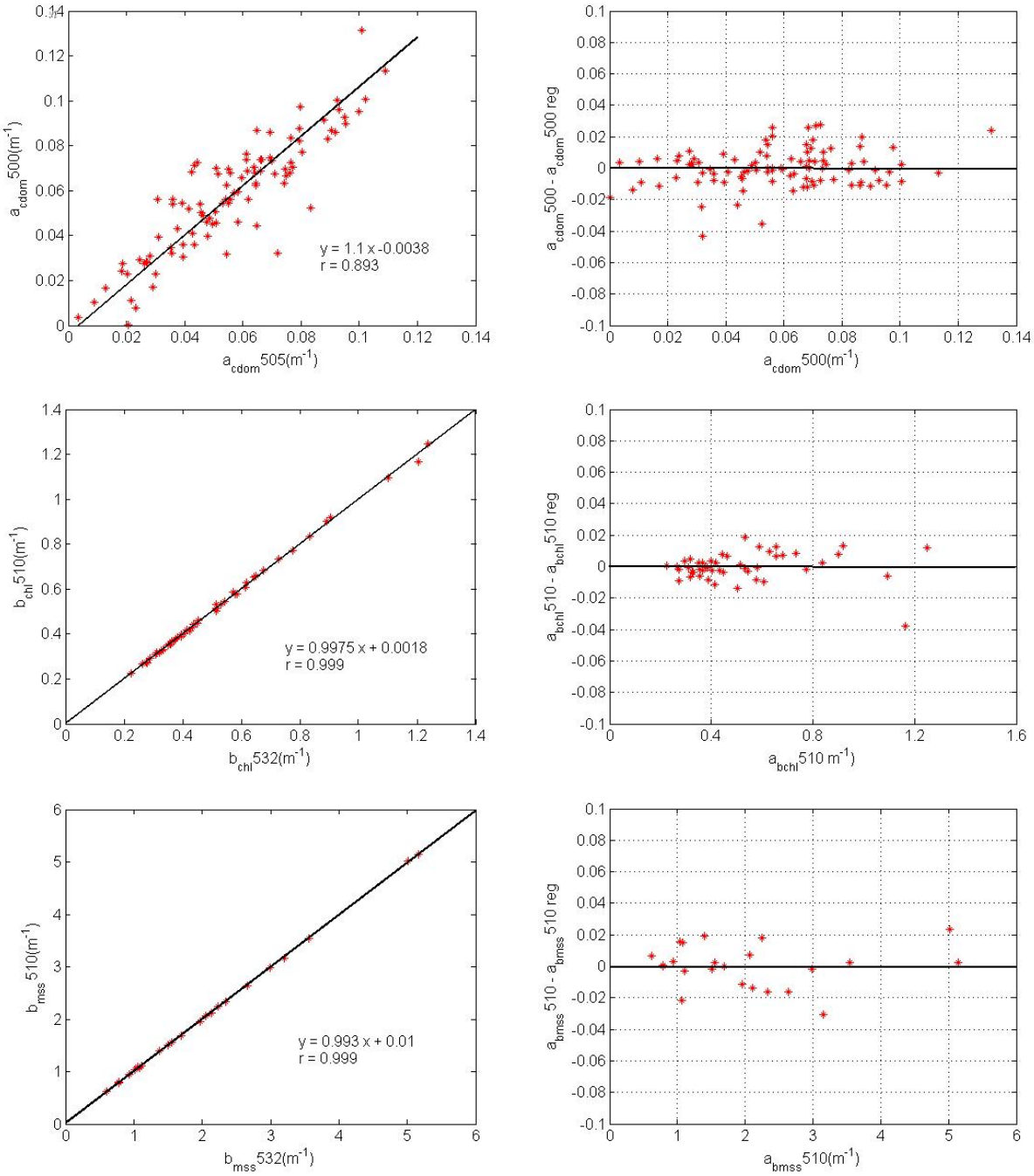

Figure 5.4. GMR analysis at consecutive wavelengths for CDOM absorption, phytoplankton scattering and MSS scattering (left panels). Error estimates from predicted values by regression minus observations for CDOM absorption, , phytoplankton scattering and MSS scattering (right panels).

Constituent uncertainty

The same statistical approach was used to measure uncertainties in constituent concentration in figure 5.5. Since SIOPs are the result of the optical measurement and the constituent concentration, error uncertainties on constituents are necessary for an adequate characterization of total error uncertainties on SIOPs. For our constituents measurements, only chlorophyll was obtained by 2 different methods, which were compared for error estimates on the chlorophyll concentration. $a_{cdom}440$ was used as a proxy for CDOM concentration since it has been used to normalize a_{cdom} spectral values throughout this study.

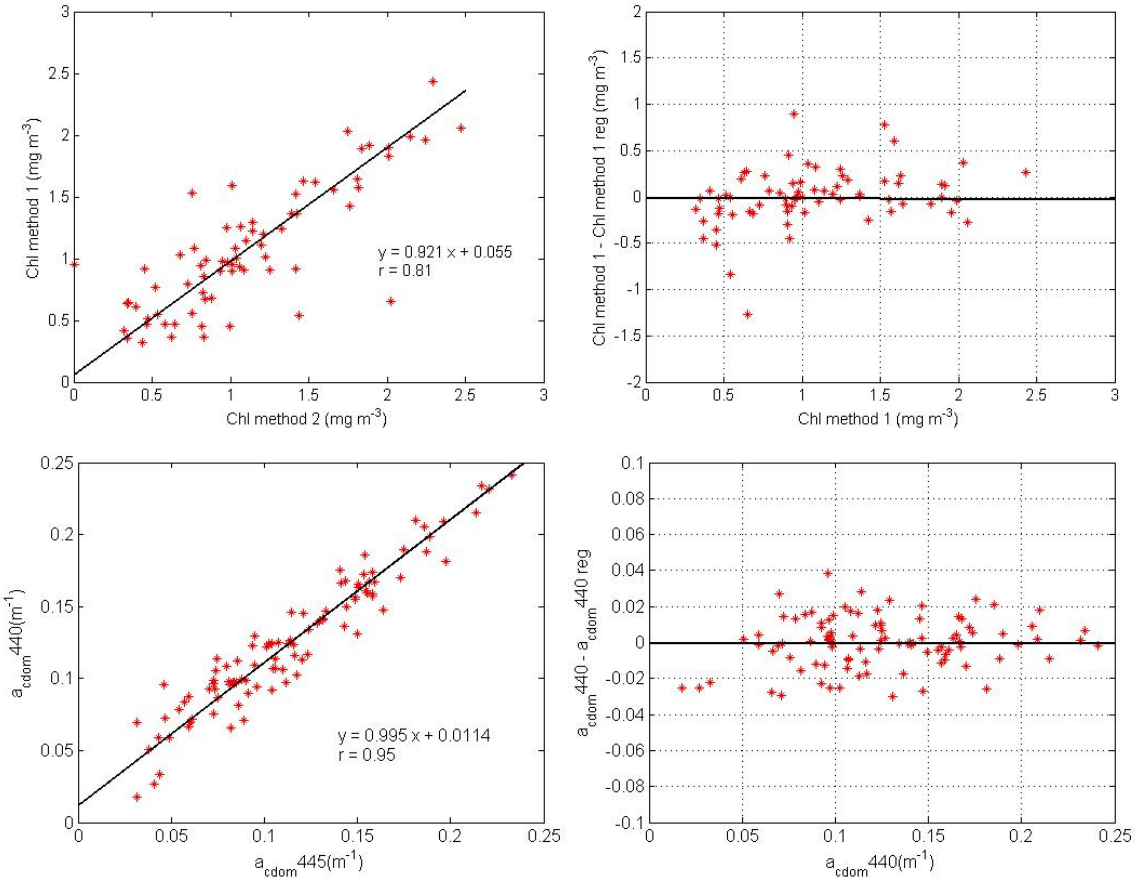

Figure 5.5. GMR analysis for 2 different methods for chlorophyll a concentration retrieval and for $a_{cdom}440$ (left panels). Error estimates from predicted values by regression minus observations for chlorophyll a concentration, and for $a_{cdom}440$ (right panels).

Chlorophyll concentrations were obtained with the Jeffrey and Humphrey method, where Chl *a* concentration is retrieved from spectrophotometric measurements. Sample absorbance is measured before and after extraction with 90% acetone (chapter 3 and 4). Two different sets of equations were used to estimate Chl *a* concentration, the trichromatic equations and the equations to simultaneously calculate phaeopigment concentration after acidification with dilute Hydrochloric acid.

GMR regressions are shown in figure 5.5 for the comparison of the 2 retrieval methods of chlorophyll a. The agreement between the two methods is reasonably good, with 81% of the observed variability accounted for by the GMR. The two methods present an r = 0.91 of agreement. Error estimates indicates a mean bias of 0.5 mg m^{-3} chlorophyll between methods. This systematic uncertainty can be due to:

- Protocol for chlorophyll a retrieval: a modification to the standard protocol proposed by Jeffrey and Humphrey was used on this dataset which could have led to reduced accuracy in the method (chapter 4).
- Equations for chlorophyll a retrievals: from the two sets of equations for sample absorbance, the first one was optimal for chlorophyll a retrievals whereas the second one provided chlorophyll a concentration as complementary information to phaeophytin concentration (chapter 4).
- Choice of β path length amplification factor.

a_{cdom} 440 variability was evaluated using GMR with a neighboring wavelength, in this case applying GMR for a_{cdom} 440 and a_{cdom}445. Its measurement uncertainty is within the same range observed at 500 nm, which predicts a constant uncertainty measurement throughout the spectrum.

5.4 Variability accounted by measurement uncertainty

The errors in SIOPs are the result of calculations from measurements, and contain errors as expressed in equation 5.5 (repeated below). These SIOP errors can also be expressed as the combined uncertainty of IOP uncertainty and constituent uncertainty:

$$SIOP = SIOP_c \pm \varepsilon = \frac{IOP_m + \varepsilon_{IOP}}{[const_m] + \varepsilon_{const}} \qquad \text{(5.5 repeated)}$$

In this expression, IOPs and constituent concentration errors are expressed as a constant value. This was demonstrated in figures 5.3 and 5.4, where the measurement uncertainty was approximated as a constant value to express variability on the measurement. The fact that the measurement uncertainty in each signal is constant rather than proportional to the signal is very significant when the apparent variability in SIOPs is assessed. In this case, when errors in IOPs and constituent concentrations are small, $SIOP_m$ will tend towards the true SIOP value but when errors are significant, $SIOP_m$ may significantly deviate from the true SIOP value. Furthermore this will be particularly important at low signal values where most of the signal would be due to uncertainty.

In figure 5.6, uncertainty retrieved in IOP measurements is combined with systematic uncertainty obtained in constituent measurement. Best fit relation was taken from the GMR best-fit slope at a particular wavelength (440 nm in this case) between the IOP and its constituent, shown in solid line, and added uncertainties from IOPs and constituents, shown in dashed line.

The spread of data points can be confined by the added uncertainty, previously observed both in constituent IOPs and concentration. For a_{chl}*, an uncertainty was observed of 0.004 m^{-1} on the optical measurement and 0.5 mg m^{-3} for Chl *a* concentrations which defines the spread of data points. Similarly, this procedure was applied for a_{det}*, with an uncertainty of 0.002 m^{-1} on a_{det} and 0.5 mg m^{-3} for Chl *a*. The a_{mss}* data spread could be confined with an uncertainty of 0.002 m^{-1} on a_{mss} and 1g^{-1} m^2 for MSS concentrations.

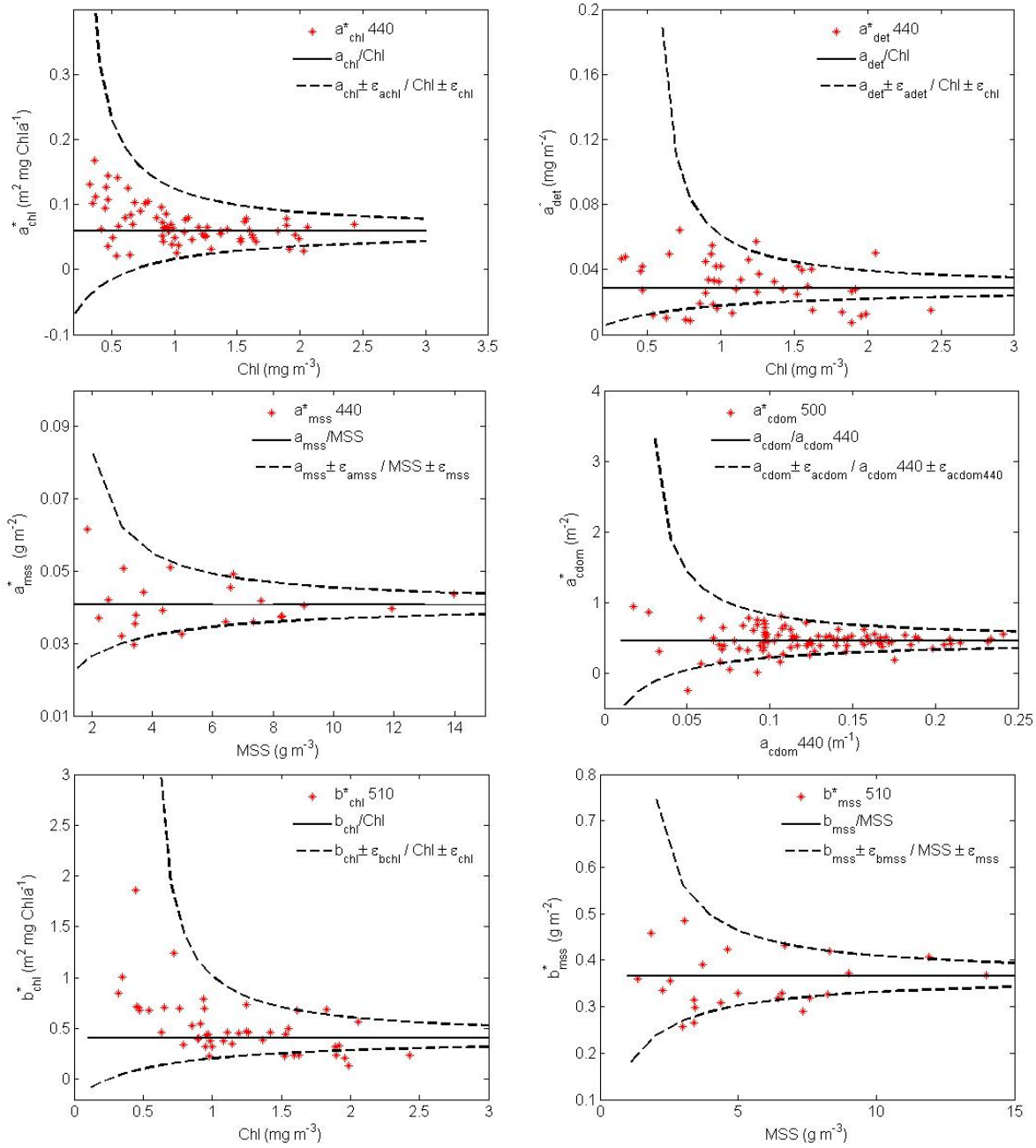

Figure 5.6. Combined uncertainty on IOP and constituent concentration for a_{chl}*, a_{det}*, a_{mss}*, a_{cdom}*, b_{chl}* and b_{mss}*.

The a_{cdom}* combined uncertainty had a single source of measurement, and the 0.02 m^{-1} uncertainty observed on the a_{cdom} measurement was sufficient to define the data spread. The b_{chl}* data were constrained by the combined uncertainty in Chl *a* measurement (0.5 mg m^{-3}) and the uncertainty on the b_{ph} signal (0.02 m^{-1}). Doing the same for b_{mss}* gave a combined uncertainty of $1g^{-1}$ m^2 for MSS and 0.02 m^{-1} for b_{mss}. These plots show the effect of constant (as opposed to fractional) measurement uncertainty ranges, and its significance at small signal values.

5.5 An alternative approach: regression SIOPs

In 5.3 it was stressed that SIOPs calculated in a point-by-point approach could significantly enlarge the range of variability of SIOPs as per equation 5.5. Figure 5.7, presents a_{ph} 440 (IOP) vs. chlorophyll concentration (constituent). Both of them are naturally distributed along a prediction line. Using a point-by-point calculation on SIOP could enlarge artificially the range of possible values for reconstructed IOPs to the maximum and minimum values.

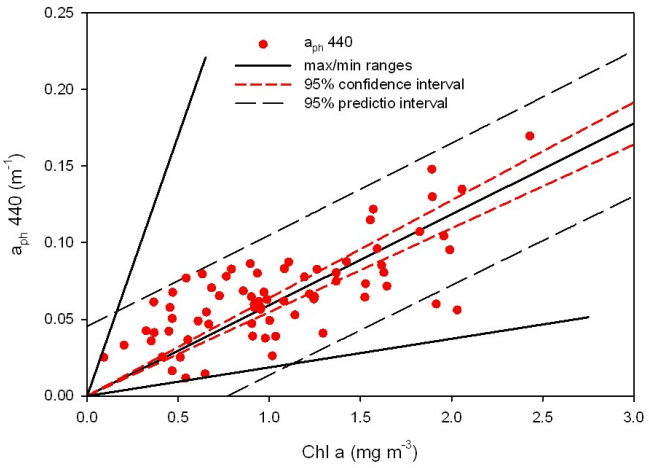

Figure 5.7. Regression analysis with confidence interval and prediction interval for a_{ph}440 and Chl *a* concentrations. The maximum and minimum ranges for point-by-point approach are also shown.

Given the distribution of data, SIOPs could be obtained by linear regression analysis as in figure 5.7. The slope value of the GMR applied for a constituent IOP and constituent concentration will be the constituent SIOP and any significant offset could indicate a potential systematic measurement error. Data distribution would define the mathematical function that associates an IOP with its constituent. In this case, simple linear regression provides the best fit, but other functions could be applied (cubic, exponential as per Chl *a* absorption saturation curve, etc...).

In this approach, data are treated as an ensemble. All constituent IOP values observed at a particular wavelength are related with the observed constituent concentrations that generates the constituent SIOPs. A 95% confidence interval is given to explain natural variability on constituent SIOPs. The SIOPs obtained in regression analysis will be the SIOP descriptors for the dataset used. Regression analysis works on the data range and is less affected by signal to noise issues than the point-by-point approach, as is the case for Chl *a* retrievals.

SIOPs obtained in point-by-point and regression approaches have been compared hyperspectrally in figure 5.8. For regression SIOPs, a linear regression is applied at every wavelength with 95% confidence interval. For point-by-point SIOPs, mean SIOPs are presented as well as maximum and minimum ranges, where any value lying between this range could be representative of an SIOP as we have been showing through this chapter. It can be observed that regression SIOPs have similar spectral shapes and magnitudes as mean SIOPs obtained from the point-by-point approach.

Analyzing in detail the variability range between both approaches (figure 5.8.), a_{chl}* with regression ± confidence intervals gives an 8.85% variation on average over the entire spectra for a_{chl}*, whereas a_{chl}* with point-by-point analysis has a 14.3% variation on the mean spectra and 270% variability range to the mean a_{chl}* spectrum. Table 5.1 summarizes the variability ranges in SIOPs comparing both calculation methods and appendix A provides full SIOPs values.

The a_{det}* in the point-by-point approach shows also a variability of up to 10 times the mean value in the blue region of the spectrum, whereas the regression approach show a variability of 40%. On the other hand, a_{mss}* does present a smaller variability compared with a_{chl}* and a_{det}*, where most of the variability was induced by the uncertainty in the Chl *a* measurement.

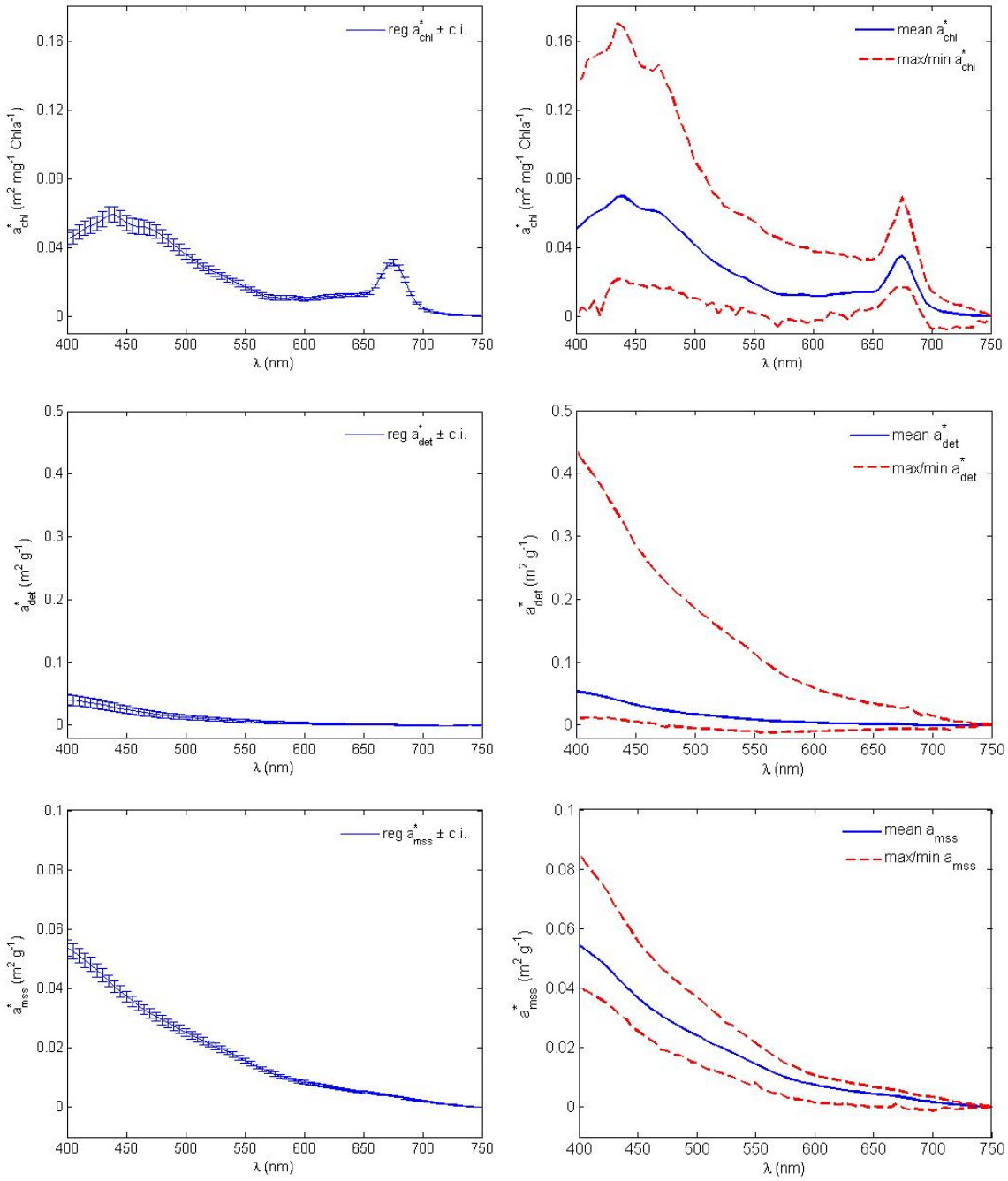

Figure 5.8. a_{chl}*, a_{det}* and a_{mss}* calculated in regression approach (left panels). a_{chl}*, a_{det}* and a_{mss}* calculated in point –by-point approach (right panels).

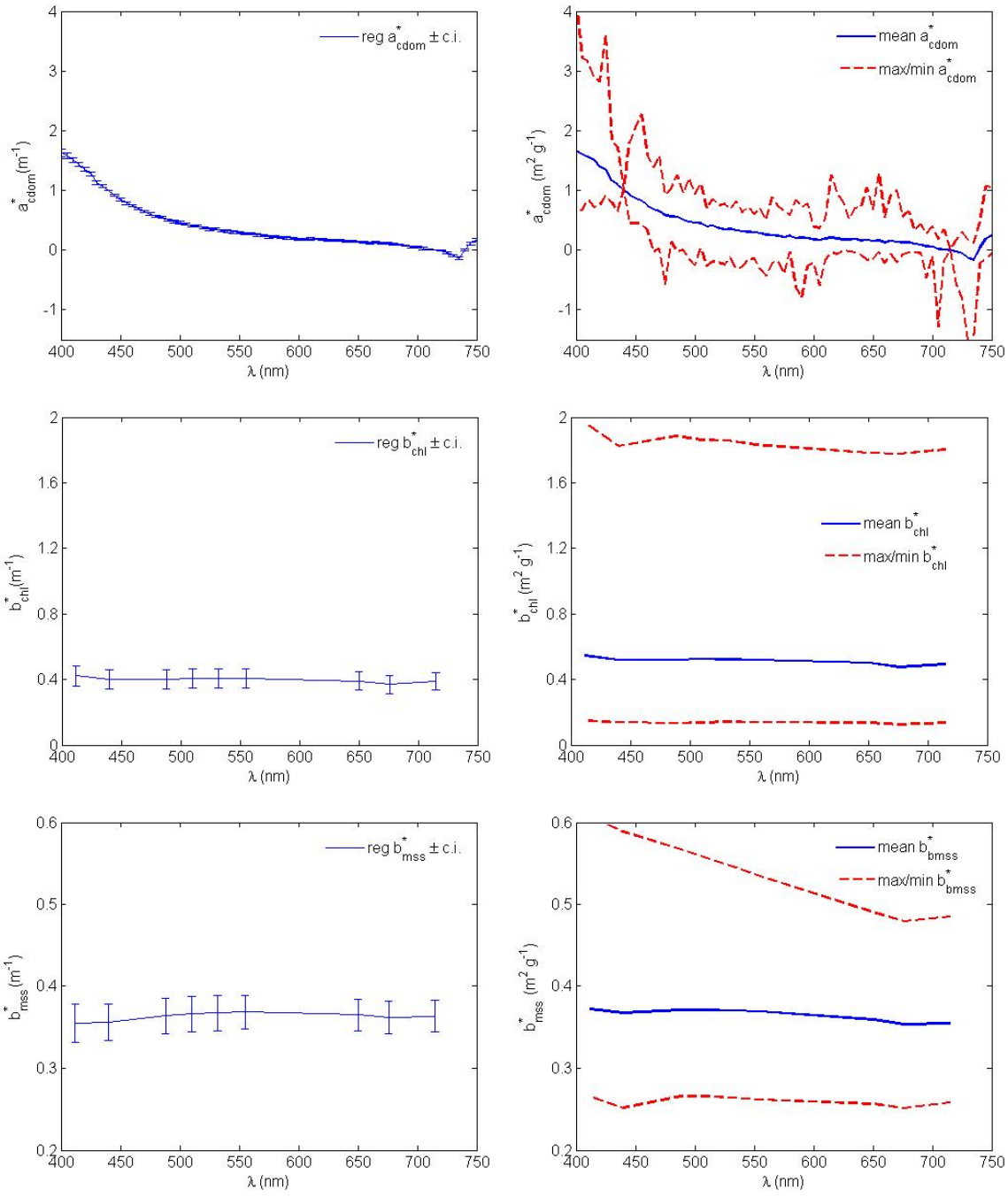

Figure 5.9. b_{chl}* and b_{mss}* calculated in regression approach (left panels). b_{chl}* and b_{mss}* calculated in point-by-point approach (right panels).

The range of variability of a_{cdom}* in the point-by-point approach is also very large; up to 5 times the average spectrum whereas the regression approach was about 25% for the regression SIOP spectrum.

Specific scattering coefficients of chlorophyll and MSS, b_{chl}* and b_{mss}*, were calculated by the GMR and point-by point approaches from b_{ph} and b_{mss}, obtained after water type partitioning applied to particle scattering data as in chapter 4. Variability in specific scattering data is naturally large because of the nature of the measurement itself (figure 5.9), but calculation of the specific scattering coefficient in the point-by-point approach enormously increases its apparent variability. Also, possible errors introduced into the scattering calculation after applying the AC-9 scattering correction could enlarge the variability range in the scattering coefficient (chapter 3).

Table 5.1. Variation of SIOPs calculated in point-by-point (pbp) or regression (reg) analysis.

	Range pbp (m^{-1})	**Range reg (m^{-1})**	**Δ% pbp**	**Δ% reg**
a_{chl}*	0.02-0.16 (440 mn)	0.05-0.06 (440 mn)	273.4	28.5
a_{det}*	0.007-0.32 (440 mn)	0.02-0.03 (440 mn)	882	40.2
a_{mss}*	0.03-0.06 (440 mn)	0.03-0.04 (440 mn)	142	13.6
a_{cdom}*	-	-	449	25
b_{chl}*	1.83-0.14 (555 mn)	0.34-0.46 (555 mn)	332	28.7
b_{mss}*	0.26-0.53 (555 mn)	0.34-0.38 (555 mn)	76	11.6
bb/b_{chl}	0.001-0.08 (676 nm)	0.009-0.01 (676 nm)	698	53.9
bb/b_{mss}	0.001-0.04 (676 nm)	0.021-0.025 (676 nm)	358	15

The backscattering ratio presented in table 5.1 was obtained applying regression and point-by-point analysis to both the b_b and b coefficients. b_{bph} and b_{bmss} were also obtained after water type partitioning applied to particle backscattering data. In this case, variations in bb/b_{chl} and bb/b_{mss} were given by varying b_{chl}* and b_{mss}* respectively, both in regression analysis ± confidence intervals and point-by-point analysis, with mean, maximum and minimum. The two calculation methods differ enormously on the results they provide for bb/b_{chl} and bb/b_{mss}.

5.6 Summary

Throughout this chapter it has been emphasised how important SIOP are as optical descriptors of a water mass and their relevance when used in forward optical modelling. In the light of these results, some conclusions can be drawn about the use of field measurements to provide appropriate SIOPs for optical models:

- Optical measurements have errors associated with the data acquisition process and data processing (correction factors in AC9, β factor in filter pad data, etc...).
- Optical variables such as SIOPs, derived from optical measurements, will propagate and enlarge errors associated with the measurement.
- Uncertainty in optical measurements must be quantified in order to provide an accuracy range for the measurements.
- Uncertainty in optical measurements have constant ranges (i.e. do not scale with signal, e.g. $\pm 0.02 m^{-1}$ rather than 2%) and this will be relevant when optical signals are low.
- The point-by-point calculation to derive SIOPs significantly enlarges and propagates variability due to uncertainty.
- Regression calculations minimizes error propagation in SIOPs by distributing uncertainties through the data ensemble.

It has been demonstrated that point-by-point calculation of SIOPs significantly enlarges their apparent variability. Part of this variability is due to uncertainties in the measurement. Deriving any optical quantity from optical measurements can potentially increase the apparent variability of the derived optical variables and the calculation method is crucial for the magnitude of these errors. This is particularly important when optical variables are used in optical modelling, because of the potential impact it could have on the model output, to be examined in the next chapter.

Here it has been presented a statistical approach using linear regressions that provides equal weighting to the data and hence minimizes error propagation, although other mathematical functions could also be applied to define the relationship between two optical variables. This statistical method reduces variability on derived parameters, most of which can be attributed to measurement uncertainty. SIOPs obtained in the literature are typically calculated as in the 'point-by-point' approach, which can introduce significant error simply by its calculation method although published results rarely provide confidence ranges for the derived SIOPs. These SIOPs can be further applied in optical modelling propagating SIOPs errors. By applying this analysis not only provides reliable derived parameters, but also provides accuracy range. This is extremely important when these are used in optical modelling, so confidence intervals are given for the model outcome.

Chapter 6

Impact of SIOPs and water types in radiance field

6.1 Introduction

When using forward bio-optical modelling, SIOPs are the initialization variables employed for the forcing of the model and their accuracy is crucial for the output of the model. Furthermore, when using a coupled bio-optical/ecosystem model these will be the optical descriptors of the state variables from the ecosystem model and an adequate characterization is needed in order to have well defined state variables in the ecosystem model and to represent accurately light-dependent biogeochemical cycles. Chapter 5 studied in detail SIOP variability and examined the variability in SIOPs due to measurement uncertainty. Chapter 4 studied the optical properties of the Irish Sea and defined two different optical water types according to their OAC.

This chapter studies the combined effect of SIOP variability and water types in optical modelling. SIOPs and constituent concentrations define the initialization stage in optical modelling. The contribution of the variation of these two factors towards uncertainty in the total IOPs (absorption, scattering and backscattering ratio) and the radiance field will be analyzed, studying the impact both in magnitude and spectral shape. This will be achieved by defining a number of hypothetical scenarios with a range of OACs broadly covering the range of optical water types such as the Case II waters found in the Irish Sea data set and (1) looking at variability of SIOPs calculated by different methods (as per chapter 5), and (2) varying constituent concentrations to determine which SIOPs provide the most sensitivity for radiance signals under different conditions. HYDROLIGHT (Sequoia, Inc), a radiative transfer model will be used for the radiance modelling simulations.

The sensitivity of radiance values obtained from radiative transfer simulations to each SIOP will depend on: (1) variability of each SIOP, (2) the relative concentration of each OAC given by

different case scenarios and (3) wavelength, as the fractional contribution of each constituent IOP to the total IOP varies with wavelength. The chapter finishes with an appraisal of the significance of the results and what they reveal about the potential impact of different OACs on the light field.

6.2 SIOPs to define the underwater light field:

Regression SIOPs vs point-by-point SIOPs

Previously in chapter 5, the traditional calculation method to retrieve constituent SIOPs (point-by-point analysis) was compared against a regression analysis that can significantly reduce any variability in SIOPs due to measurement uncertainty. It was shown that SIOPs calculated in a point-by-point approach can have a large variability range due to error propagation in the calculation method, (chapter 5, figure 5.6) which will result in a wide maximum and minimum range of SIOP values.

SIOPs are used as optical descriptors of the water mass and these are used to reconstruct IOPs given the concentration of the OAC in the water. When SIOPs are used in optical modelling, they can potentially introduce added uncertainty (chapter 5). In this chapter the potential impact of SIOPs on the underwater radiance field is tested and compared for SIOPs calculated using both the point-by-point approach and the regression approach.

To obtain radiometric values both in the water column and above surface, a radiative transfer model, HYDROLIGHT version 4.1 (Sequoia, Inc) has been used. HYDROLIGHT (Mobley, 1994), computes radiance distributions and related quantities (irradiances, reflectances, diffuse attenuation functions, etc.) in the ocean. The user can specify the water absorption and scattering properties, the sky conditions, and the bottom boundary conditions in various ways: by selection of built-in defaults, by reading in user-supplied data (such as WETLabs® AC-9 data), or by providing their own subroutines to define their input. HYDROLIGHT then computes the in-water light field and other quantities of interest to optical oceanography, such

as water-leaving radiance and remote-sensing reflectance. Within the set-up modes to run HYDROLIGHT, the "case 2 water" model was chosen for this study. This is a four component model where the OAC are water, phytoplankton and derived products, minerals and CDOM and the SIOPs can be either supplied by the user, as in here, or taken from previous literature. The optical model for the Irish Sea obtained in chapter 4 was used to define absorption and scattering coefficients as:

$$\begin{aligned} a &= a_w + (a^*_{ph} + a^*_{\det}) \cdot Chl + a^*_{mss} \cdot MSS + a_{cdom} \\ b &= b_w + b^*_{chl} \cdot Chl + b^*_{mss} \cdot MSS \end{aligned} \tag{6.1}$$

Runs were set to compute radiance distributions from 400 to 750 nm in 5 nm intervals, in a 20 m deep water column infinitely deep, with outputs in 1 m steps. The incoming irradiance was obtained with RADTRAN (Gregg and Carder, 1990) using a 30° solar zenith angle and 0.75 m s^{-1} of wind for the surface conditions. For this analysis it was always used radiance reflectance (Lu/Ed) just below the surface as the principal output product. Using the subsurface reflectance at zero depth instead of the above-water reflectance will avoid the added dependence on variables that have an effect on the interphase change, such as wind roughness, albedo, etc…

The impact of SIOP variability on radiometry was tested by using SIOPs calculated using the point-by-point approach and the regression approach. For the point-by-point approach, mean, maximum and minimum calculated SIOPs were used for every OAC, so the entire range of possible SIOPs values retrieved in a point-by-point calculation is tested (chapter 5 and appendix A). For the regression approach, regression values ± 95 % confidence intervals were used, where the confidence interval allows natural variability for every OAC (chapter 5 and appendix A).

For an initial test, a baseline case scenario was set, representing fairly typical Case II water conditions, where the concentrations of the OAC were 1 mg m^{-3} for chlorophyll, 1 mg m^{-3} for MSS and 0.15 mg m^{-3} for CDOM concentration. In each run, one SIOP was varied at a time.

For SIOPs obtained by the regression approach, runs were done for regression SIOP, regression SIOP + 95% confidence interval and regression SIOP - 95% confidence interval. For SIOPs obtained in the point-by-point approach, runs were done with mean SIOP, max SIOP and min SIOP.

Figures 6.1 and 6.2 presents model outputs of radiance reflectance using SIOPs calculated in both the point-by-point and regression approach.

In Figure 6.1 radiance reflectance from specific absorption coefficients of every OAC is shown. Effects of variation in a_{chl}*, a_{det}*, a_{mss}* and a_{cdom}* are separately presented. Regardless of the SIOP calculation method, higher absorption values generate lower reflectance signals and vice-versa.

In this figure, specific absorption coefficients calculated in the point-by-point approach generate a significantly wider variability in the reflectance spectra than those calculated by regression approach. The difference between radiance reflectance from the two SIOP calculation methods is of more than an order of magnitude, compared with which the variability range generated by regression SIOPs is very small. It must be noted that radiance reflectance spectrum from the point-by-point mean SIOPs are almost identical to those from regression SIOPs. It was previously observed in chapter 5 that regardless of the calculation method, regression SIOPs and mean point-by-point SIOPs were similar (appendix A) effectively showing that the two methods 'normalize' SIOPs with similar results but that the variability introduced due to error propagation is much less for the regression analysis.

Radiance reflectance from the extremes of the point-by-point SIOPs present ranges that are not balanced either side of the mean. This is most likely due to the fact that max/min SIOPs are highly sensitive to outliers in the distribution, and are likely therefore to be skewed in this manner. This result highlights the potential danger of using individual spectra with individual concentrations of OAC to calculate SIOPs for use in radiative transfer simulations.

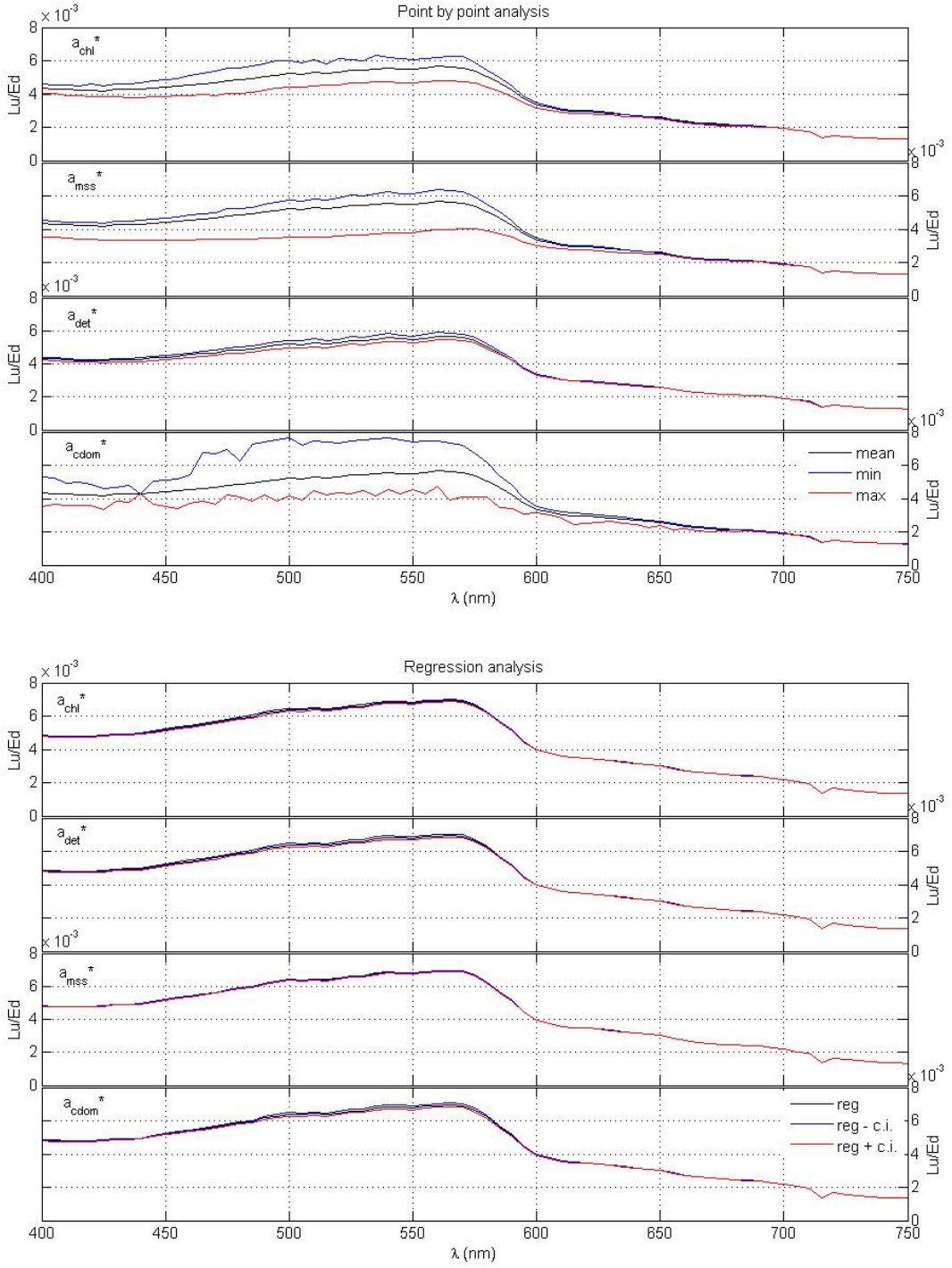

Figure 6.1. Radiance reflectance spectra evaluated individually from a_{chl}*, a_{det}*, a_{mss}* and a_{cdom}* calculated by point-by-point analysis (upper panel) and by regression analysis (lower panel).

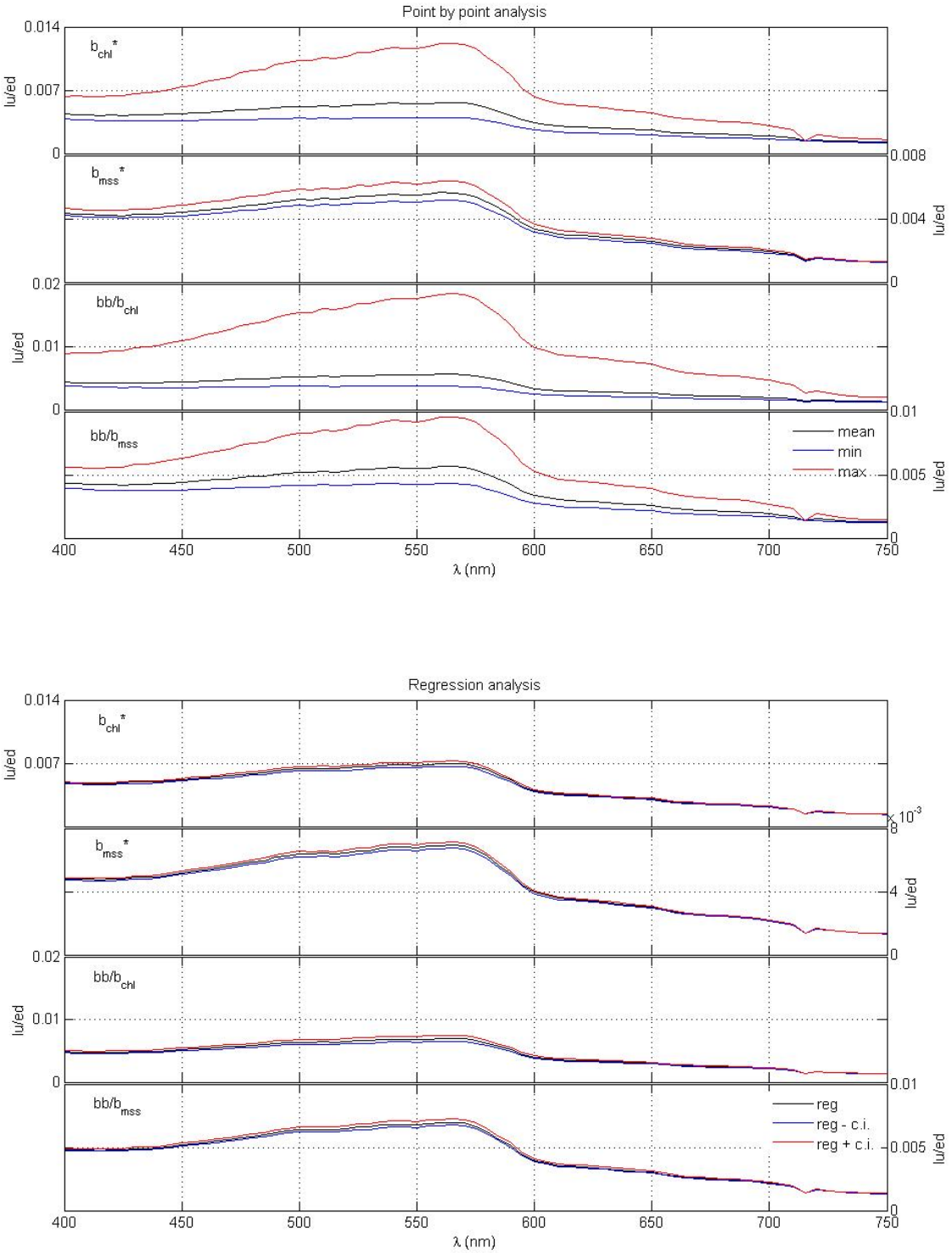

Figure 6.2. Radiance reflectance spectra evaluated individually from b_{chl}*, b_{mss}*, bb/b_{chl} and bb/b_{mss} calculated by point-by-point analysis (upper panel) and by regression analysis (lower panel).

Using the standard deviation on the point-by-point calculation method would generate more balanced distributions than using individual SIOPs or max/min of the distribution, but traditional studies use any SIOPs calculated in point-by-point method between max and min ranges as representative of that water type. Note that the 95% confidence intervals are inherently balanced around the regression slope.

In figure 6.2, scattering related quantities used to obtain radiance reflectance also show a wide range of variability particularly b_{chl}* and bb/b_{chl}, which have the highest variability range for these concentrations and this set of SIOPs. Scattering and backscattering ratio appear to have a strong effect on radiance reflectance and can determine the magnitude of the spectra. When running HYDROLIGHT, the backscattering ratio is assumed to be a constant value both spectrally and through the water depth. Given the large impact that the backscattering ratio appears to have in the radiance field, these assumptions could lead to significant errors when introduced in an optical model. It was also mentioned in chapter 3 that recent studies question the spectral independence of the backscattering ratio (McKee et al., *in press*).

To analyze in finer detail the effect of every SIOP calculated by point-by-point and regression analysis, figure 6.3 presents the percentage of variation of reflectance spectra for every SIOP calculated by the two methods. Percentage of variation was calculated using reflectance from each regression SIOP as a baseline. The percentage of variation on radiance reflectance is always significantly higher using SIOPs from point-by-point analysis than those from regression analysis. Among the specific absorption coefficients and for this set of OAC concentrations, a_{cdom}* variability generates the highest variability in radiance reflectance and in particular in the region of 440 – 600 nm. This is precisely within the range used to fit exponential expressions to CDOM for data smoothing.

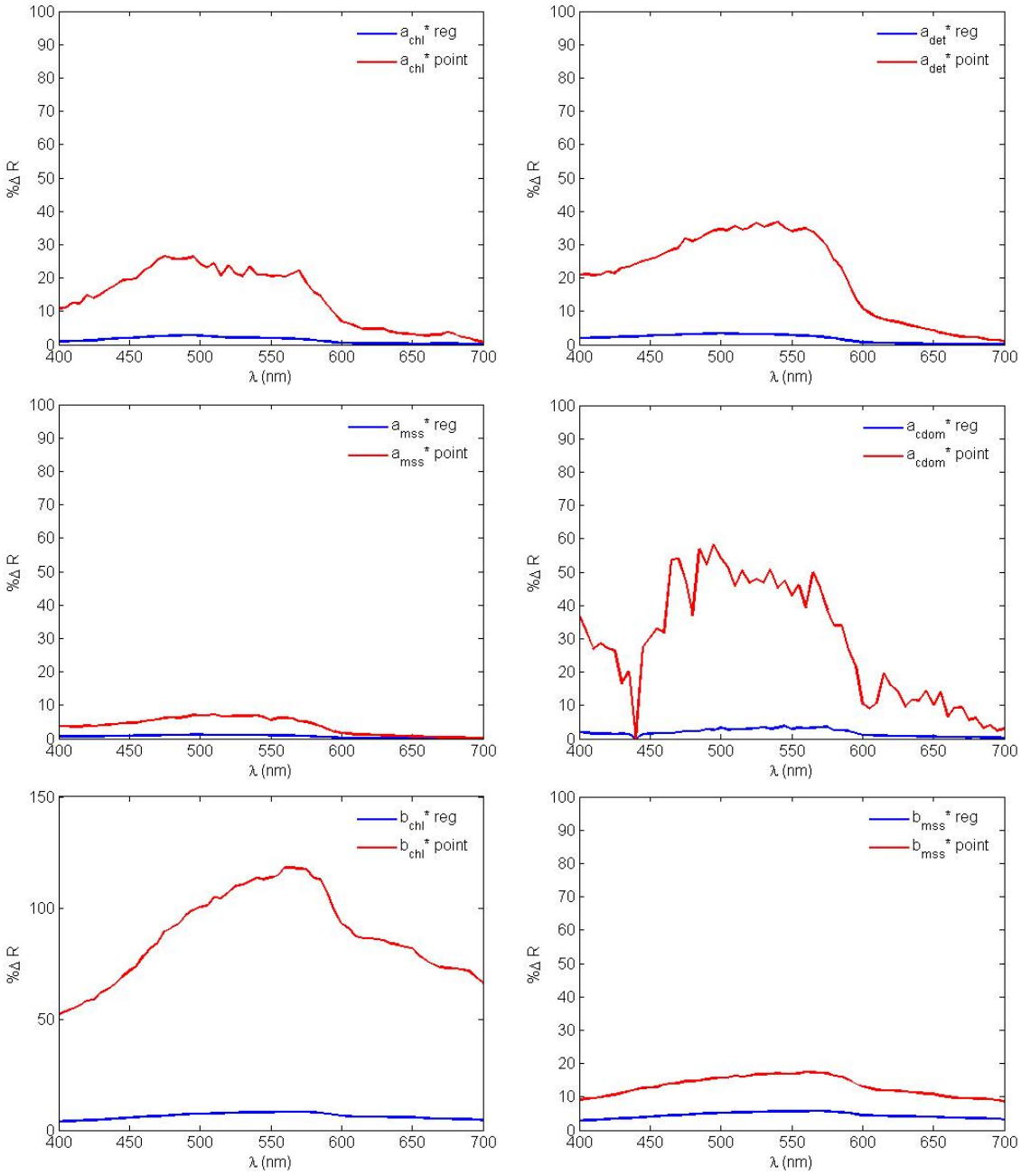

Figure 6.3. Percentage of variation on radiance reflectance for a_{chl}*, a_{det}*, a_{mss}*, a_{cdom}*, b_{chl}* and b_{mss}*, all them in point-by-point approach and regression approach.

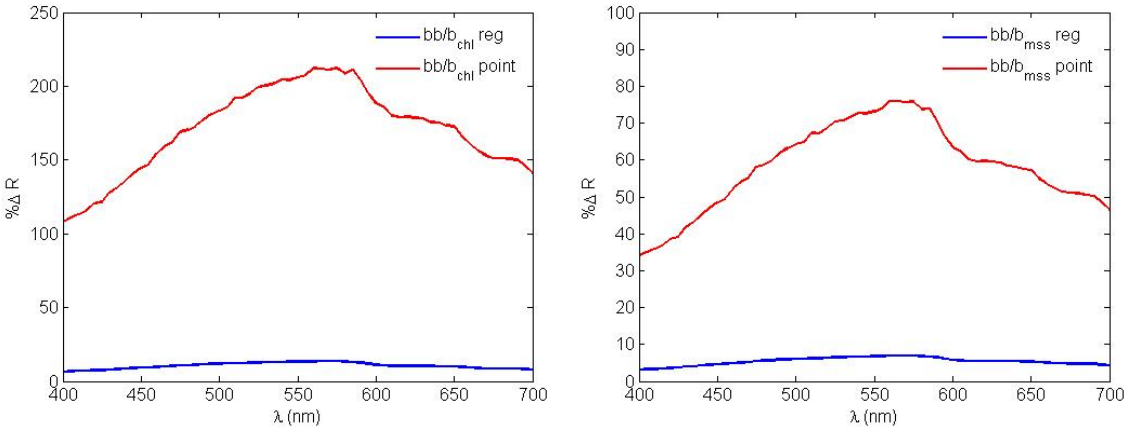

Figure 6.3. (cont.) Percentage of variation on radiance reflectance for bb/b_{chl} and bb/b_{mss} in point-by-point approach and regression approach.

As explained in chapter 4, a_{cdom} was not fitted to any exponential expression as is always done in the literature (Bricaud et al., 1981; Carder et al., 1989), since this procedure could be an added source of uncertainty on the data. Here it can be observed that the 440-600 nm region can potentially generate variability of up to 60% in the radiance reflectance from point-by-point SIOPs, and part of this variability could also be due to uncertainty in the exponential fitting of a_{cdom} for data smoothing. This is particularly relevant since a_{cdom} can significantly attenuate available radiance for biogeochemical processes in coastal environments (Kirk, 1994). Similar reasoning applied to a_{cdom}* can be applied to a_{det}*. It should be recalled that a_{det} and a_{mss} were obtained upon optical partitioning of the absorption coefficient by non-algal particles (chapter 4). The a_{det} coefficient is also usually fitted to an exponential expression (Babin et al., 2003; Roesler et al., 1989) and it is obtained after chemical extraction of phytoplanktonic pigments (chapter 3). When the pigment extraction method is incomplete, remaining absorption peaks of chlorophyll can easily be observed in the a_{det} spectra (Babin et al., 2003). In these plots can be observed a significantly wide percentage of variability on radiance reflectance from a_{det}* in the spectral region of 480-600 nm, which lies within the range used for exponential fitting expressions on a_{det}* (480-620 nm, following (Babin et al., 2003)). There are potential artefacts

from incomplete pigment extraction that can appear in a_{det} data and applying an exponential fitting may further contribute to inaccuracy at certain wavelengths.

a_{mss}* variability presents the lowest impact on radiance reflectance for this dataset in both calculation methods. It was observed in chapter 4, that the correlation between absorption by non-algal particles, a_{nap}, and MSS for Group A waters was excellent, with an R=0.977. Therefore the smaller variability of MSS related quantities, a_{mss}* and b_{mss}* could be due to the highly well defined MSS fraction belonging to a reduced number of types of sediments conforming the MSS fraction (Babin and Stramski, 2004). In general, radiance reflectance from regression specific absorption coefficients presents variability of less than 5%, whereas for point-by-point calculations it is up to 25% for a_{chl}*, 35% for a_{det}*, 8% for a_{mss}* and up to 60% for a_{cdom}*.

For specific scattering coefficients, the potential effect of variability of b_{chl}* in radiance reflectance can be up to 118%, whereas the regression b_{chl}* generates a maximum variability of 8% at 550 nm. Radiance reflectance variability from b_{mss}* is significantly smaller than it is for a_{mss}*; 5% for regression b_{mss}* and 17% for point-by-point b_{mss}*. It can be observed that scattering values dramatically define the spectral shape and magnitude of the radiance reflectance spectrum.

The significantly wider variability of radiance reflectance from point-by-point SIOPs effectively shows the impact of error propagation in optical modelling. Previously chapter 5 showed the variability range of SIOP in table 5.1 (see also appendix A), where among the specific absorption coefficients a_{cdom}* presented the widest variability in this dataset, followed by a_{det}*, a_{chl}* and a_{mss}*. When introduced in Hydrolight, a_{cdom}* still presents the widest variability towards radiance reflectance, with an average of 25% variability over the spectrum, followed by a_{det}*, a_{chl}* and a_{mss}*. For the scattering related properties, bb/b_{chl} and b_{chl}* have the widest variability impact towards radiance reflectance, followed by bb/b_{mss} and b_{mss}*. Table 6.1 summarizes the variability range in radiance reflectance from different SIOPs.

Figure 6.4 presents together the potential variability contributed by each SIOP and backscattering ratio towards the radiance reflectance for both calculation methods in this particular case scenario. It is clear that bb/b_{chl} and b_{chl}* present the highest variations, followed by mineral backscattering ratio. This identifies the significant effect of light scattering on the radiance field. It must also be noted that this optical model has been set up with SIOPs obtained from coastal and Case II waters. Even though the case scenario defined does not attempt to reproduce precisely the observations obtained in the Irish Sea, it aims to reproduce a realistic case scenario in coastal environments as represented by equation 6.1. In this type of environment, phytoplankton and detritus are not as relevant as CDOM towards the absorption signal. However, here phytoplankton scattering appears to dominate the variability in the optical signal.

Table 6.1. Variability range of radiance reflectance from SIOPs in point-by-point and regression analysis at a reference wavelength. Percent of variation of radiance reflectance on the entire spectra

	Δ Lu/Ed pbp SIOP	Δ Lu/Ed reg SIOP		Mean % Δ Lu/Ed pbp SIOP	Mean % Δ Lu/Ed reg SIOP
a_{chl}* 440	0.0049-0.0050	0.0038-0.0047	a_{chl}*	12.12	1.16
a_{det}* 440	0.0033-0.0045	0.0049-0.050	a_{det}*	17.6	1.5
a_{mss}* 440	0.0042-0.0044	0.0049-0.0050	a_{mss}*	3.2	0.5
a_{cdom}* 440	-	-	a_{cdom}*	24.9	1.5
b_{chl}* 555	0.0039-0.0138	0.0066-0.0071	b_{chl}*	79.94	5.73
b_{mss}* 555	0.0051-0.0063	0.0067-0.0071	b_{mss}*	12	4
bb/b_{chl} 555	0.0037-0.179	0.0065-0.0074	bb/b_{chl}	158.6	9.7
bb/b_{mss} 555	0.0043-0.0094	0.0067-0.0071	bb/b_{mss}	53.4	4.9

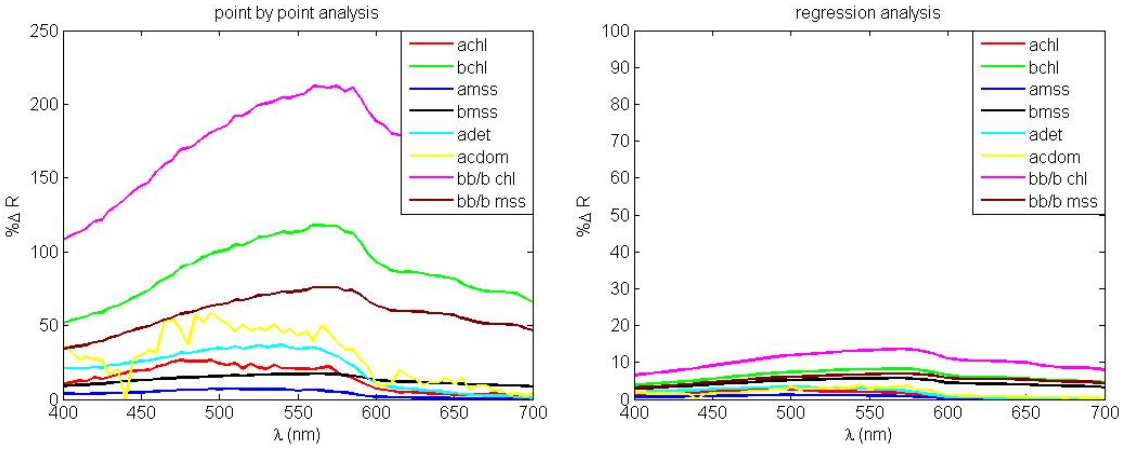

Figure 6.4. Percentage of variation in radiance reflectance from SIOPs and backscattering ratios calculated in point-by-point analysis and regression analysis.

Using a fairly typical Case II water type, it has been noted that variability in the SIOP calculation method introduces very large potential variation on the radiance field based on the calculation method. The significance of every SIOP in both methods is conserved; however the range of variation is massively enlarged for the SIOP obtained in point-by-point analysis. This demonstrates that SIOPs from point-by-point calculations can have a dramatical impact when used in bio-optical modelling.

SIOPs derived from point-by-point analysis can obscure other important sources of variation in the light field such as different water types. Therefore in the subsequent analyses described in this chapter, only the SIOPs from regression analysis will be used.

6.3 Case Scenarios. Impact of SIOPs in different water types

The optical characteristics of a particular water body are defined by their SIOPs and their OAC concentrations. Having previously studied the potential effect of variation in SIOPs towards the radiance field in a general Case II waters scenario, we now consider the effect of different water types, where the concentrations of OAC are variable combined with SIOP natural variability.

For this, four different case scenarios are set up to test the combined effect of SIOP variability and OAC concentration. In the previous section it was concluded that SIOPs obtained from point-by-point calculations can introduce an enormous variability which a significant part of it will be due to error propagation within the optical model. Here, only SIOP for regression analysis will be used.

Table 6.2. Case scenarios generated for HYDROLIGHT runs and constituent concentrations in each scenario.

	[Chlorophyll] (mg m^{-3})	[MSS] (g m^{-3})	[CDOM] (mg m^{-3})
CASE 1: Baseline scenario	1	1	0.15
CASE 2: High MSS	1	10	0.15
CASE 3: High Chl	5	1	0.15
CASE 4: High CDOM	1	1	1

The baseline case scenario that was previously introduced defines a water type with low concentrations of OAC. These new case scenarios are designed to cover extreme conditions found in the dataset used here, although even more variability could be encountered in other natural systems.

Case 2 represents a scenario with high concentration of mineral particles that could be observed in a Case II water environment with high terrestrial inputs or resuspension of sediments. Bloom conditions are defined in case 3 with high chlorophyll concentration. Case 4 represents a high CDOM scenario with significant terrestrial freshwater inputs, such as have been observed in Scottish coastal waters (McKee at el., 2003).

These case scenarios are not intended to reproduce conditions observed in the Irish Sea, although most of these conditions and OAC concentrations can be observed at different areas and times in the Irish Sea. Scattering defined for these runs, b_{chl}* and b_{mss}*, was obtained by

regressing total particulate scattering against OAC concentrations as there was no effective means available to partition the particulate scattering into constituent components (see chapter 4). There is a risk that using them together in this manner may lead to a general overestimation of scattering compared to real values.

The contribution of variability in each SIOP to the total IOP case scenario will be studied. Only when the contribution of the SIOP towards reflectance is significant (more than 5% variation) full radiative transfer simulations will be performed for the radiance sensitivity studies in section 6.4.

Figure 6.5 presents the results. In each of the four upper panels the different spectra reveal variability of the total absorption coefficient, a, across the four case scenarios. Each panel shows the results from varying a single SIOP ± confidence intervals is tested in each case scenario. The variability introduced in total absorption can only be observed when a SIOP is tested in a case scenario high in its constituent concentration. As an example, variability in a total from a_{chl}*, (figure 6.5, upper panel left) is only noticeable in case 3 scenario with high chlorophyll concentration. For the other case scenarios, variability in a_{chl}* ± confidence intervals is indistinguishable; total absorption from regression a_{chl}* ± confidence intervals are almost superimposed. Similar results are obtained for a_{det}*, where variability is only observed in case 3 with high chlorophyll concentration. a_{mss}* and a_{cdom}* variation is only observed in case 2 and case 4 respectively, with high MSS and high CDOM. For a_{chl}*, a_{det}* and a_{mss}*, variation towards total absorption is noticeable up to 600 nm. From 600 nm onwards, water absorption dominates the total absorption signal and the variation of a_{chl}*, a_{det}* and a_{mss}* in any case scenario is indistinguishable. In the case of a_{cdom}* this does not happen, and the impact of the SIOP variability towards total absorption is conserved throughout the entire spectrum.

The lower four panels show the percentage of variability on total a resulting from variation of a particular SIOP in each case scenario. Again, percentage of variation in total absorption from Δa_{chl}* is only relevant in case 3 scenario with high chlorophyll and case 1, baseline case scenario. Similarly for a_{det}*, a_{mss}* and a_{cdom}*.

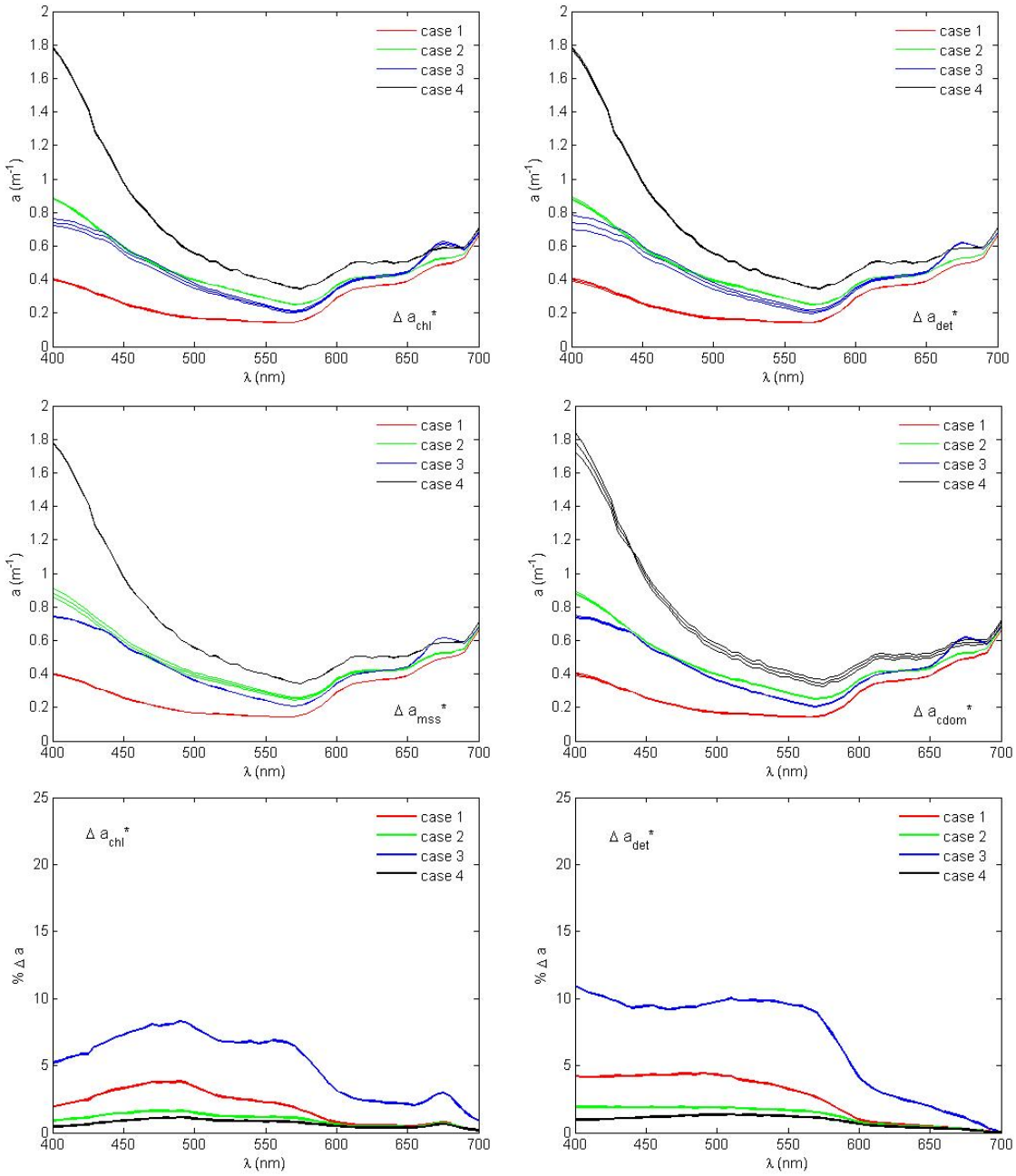

Figure 6.5. Four top panels: Each panel represents the total absorption spectra for the 4 different case scenarios (shown in different colours) with upper and lower limits showing any significant response to the variability of the SIOP named in the panel. Two lower panels: Each panel shows percentage change to the total absorption in 4 different case scenarios, caused by varying the named SIOP by its standard deviation.

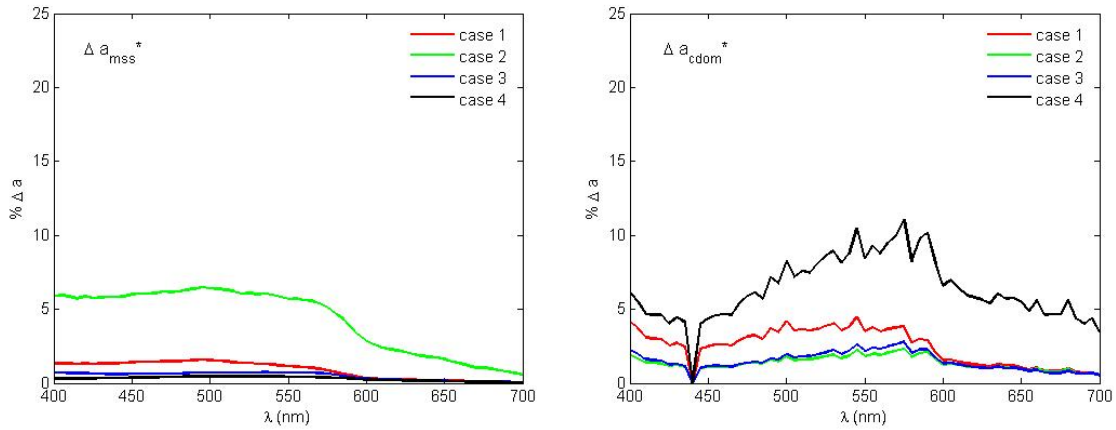

Figure 6.5. cont : Each panel shows percentage change to the total absorption in 4 different case scenarios, caused by varying the named SIOP by its standard deviation.

Again, for a_{mss}* and a_{cdom}* variation is relevant in case 2 and case 4 respectively. Among all specific absorption coefficients, a_{det}* is the one that generates the widest variability in a total within a high chlorophyll case scenario. Figure 6.6 shows the percentage of variability on total a for each specific absorption coefficient within its most sensitive case scenario. The highest contributions are given by a_{det}* (5.8%) and a_{cdom}* (5.5%), followed by a_{chl}* (4.4%) and a_{mss}* (3.7%) across the spectrum.

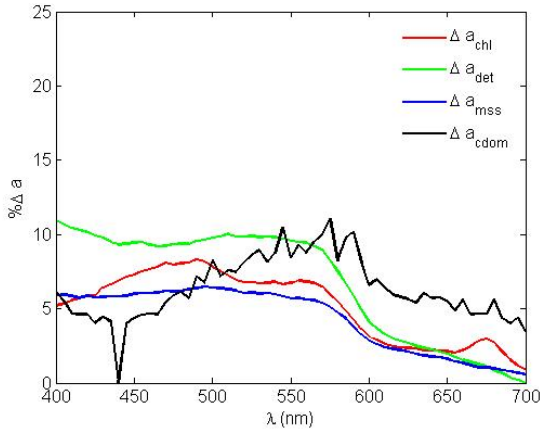

Figure 6.6. Percentage of variability in total absorption from SIOP variation in its particular case scenario.

Scattering variability from b_{chl}* and b_{mss}* is presented in figure 6.7. As in previous plots, a significant variability in total scattering from variation in b_{chl}* is mainly observed in case 3, high chlorophyll concentration and also in case 1. b_{mss}* variation is relevant mainly in case 2, high MSS and in case 1. Scattering coefficients appear flatter as a result of plot scaling.

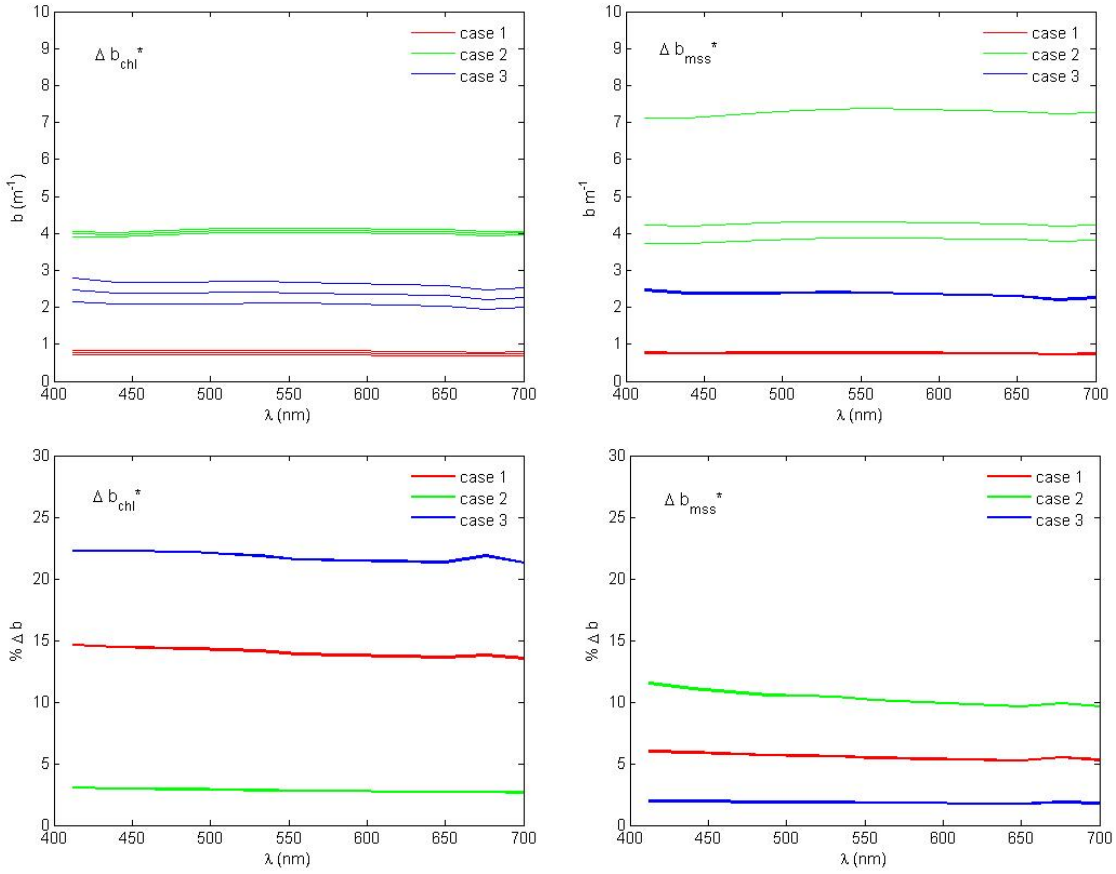

Figure 6.7. Top row: Variability in total scattering from SIOP variation in 3 different case scenarios shown in different colours. Left panel shows the upper and lower limits due to variability in b_{chl}*. Right panel shows upper and lower limits due to changes in b_{mss}*. Bottom row: Percentage of variability in total scattering in 3 different case scenarios (shown in different colours) from SIOP variation. Left panel is the response to variability in b_{chl}*. Right panel is response to variability in b_{mss}*.

6.4 Significance of SIOPs in the radiance field

To complete this chapter, figure 6.8 presents the impact of variability of each SIOP on the radiance reflectance within the case scenario for which it has high constituent concentration. Among specific absorption coefficients, a_{mss}* presents the maximum significance in reflectance, b_{mss}* for specific scattering coefficients and bb/b_{chl} for backscattering ratios. Table 6.3 also summarizes the percentage variability observed in each regression SIOP, and the resulting percentage variability it causes for total a and b and for the radiance reflectance.

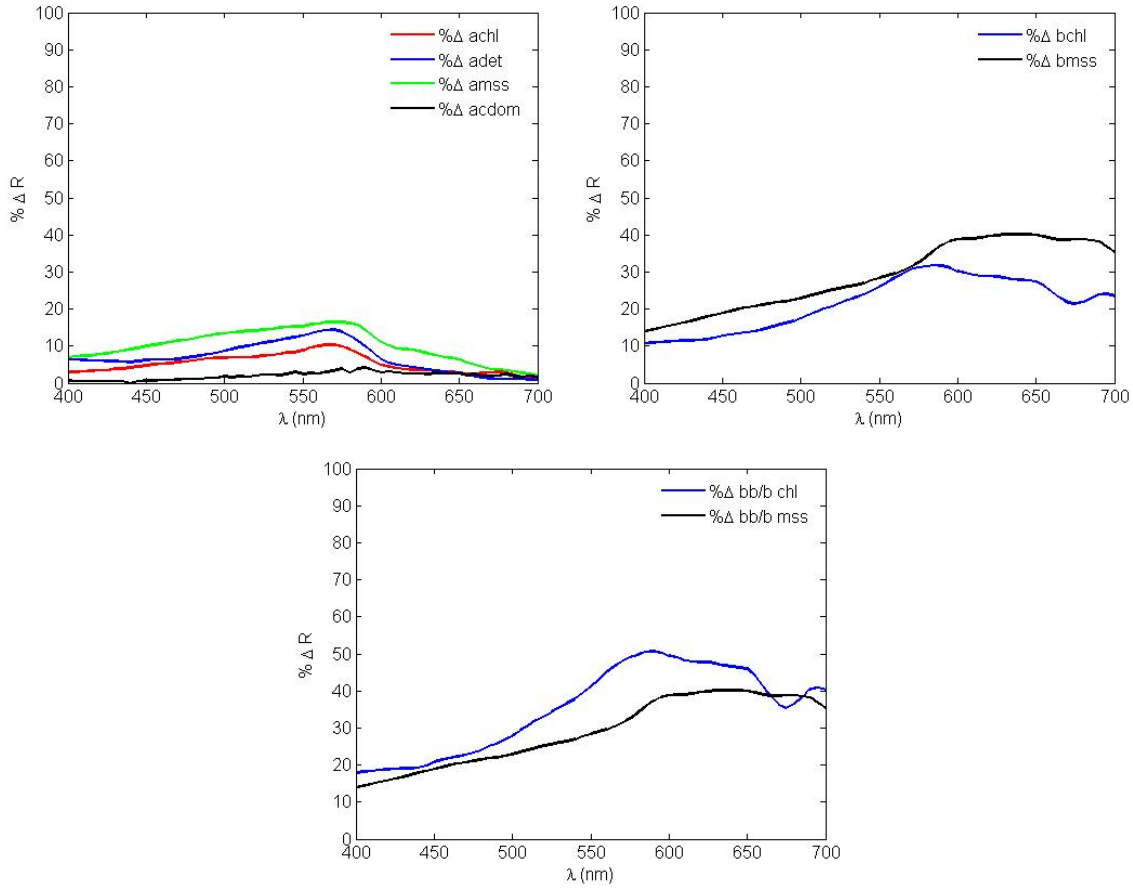

Figure 6.8. Impact of variation of specific absorption, specific scattering and backscattering ratio in radiance reflectance.

Table 6.3. Variability of SIOPs, variation on total *a* and *b* and variation on radiance reflectance.

	% Δ	%Δ in *a*	%Δ in R
Δ a_{chl}*	28.5	4.4	4.5
Δ a_{det}*	40.2	5.8	5.9
Δ a_{mss}*	13.6	3.7	8.8
Δ a_{cdom}*	25	5.5	1.7
		%Δ in *b*	%Δ in R
Δ b_{chl}*	28.7	21	20
Δ b_{mss}*	11.6	10	27
		%Δ in *bb/b*	%Δ in R
Δ bb/b_{chl}*			33
Δ bb/b_{mss}*			27

Some conclusions can be drawn from this. The variability of an SIOP towards total *a* and *b* is not closely related to the potential variability it can introduce into the reflectance. Impact on reflectance depends on variability of the constituent IOP, given by the SIOP and the constituent concentration and it is a fractional contribution to the total IOP. The results obtained here are dependent on the case scenarios set and the constituent concentrations given.

Δa_{mss}* is the SIOP that presents lowest variability and hence lowest variation in total *a*. However it has a strong optical signature and among the absorption parameters contributes the most to reflectance. The situation is similar for Δb_{mss}*, whose variability is smaller but introduces a large variability in reflectance. It is clear from Table 6.3 that the backscattering ratios define the potential magnitude and spectral shape of radiance reflectance. These results are critical, since the backscattering ratio is often assumed to be spectrally flat. This assumption could introduce significant errors when further applied in bio-optical modelling. Most

importantly, the use of a constant backscattering ratio can completely modify the spectral shape of the radiance reflectance.

This analysis demonstrates that the sensitivity of the radiance field to SIOP modelling depends on the variability of each SIOP, the fractional contribution of each constituent IOP and the variability throughout the spectrum.

Chapter 7

The use of IOPs from the published literature

7.1 Introduction

The initialization of a bio-optical model requires the specification of constituent IOPs or, alternatively, constituent SIOPs and the corresponding concentrations of OACs. Ideally these parameters should be measured for the location or region to which the model refers, but in practice this is often unfeasible. When running a forward optical model, the availability of real time optical measurements is almost impossible and hence recourse must be made to IOP data or parameterizations reported in the scientific literature.

Some optical studies provide parameterizations of SIOPs for the region of study of the dataset in an attempt to model the optical properties of a particular water body. These can be applied in forward optical modelling to define the individual constituent SIOPs and constituent concentration, in order to specify absorption and scattering coefficients used in the radiative transfer equation (see chapter 2).

The previous chapters have discussed the importance of an adequate characterization of constituent IOPs (chapter 4), the potential error propagation from constituent IOPs when used in forward optical modelling (chapter 5 and 6), and the importance of particular SIOPs in different water types (chapter 6).

The appropriate characterization of constituent SIOPs is a very active topic in bio-optical modelling in natural waters (IOCCG, 2006). In the past, various SIOPs reported in scientific papers (hereafter referred to as “literature SIOPs”) have been proposed for use in published bio-optical models (Garver and Siegel, 1997; Lee et al., 2002) or as input to radiative transfer models such as Hydrolight. One of the main problems when applying literature SIOPs in

general optical modelling is the scarce availability of them and their limitations when, despite being retrieved from a regional or local analysis, they are applied to models in a general context. A good example of this approach can be found in the important recent study by Fuji et al. (2007), who presented a coupled optical-ecosystem model in which a particular set of SIOPs was selected to describe the absorption and scattering properties of the OAC within the ecosystem model. Ultimately these SIOPs are used as input in radiative transfer modelling to define the radiance field within the ecosystem model and their light dependent processes.

To complete the research objectives of this thesis, this chapter addresses the question of whether there is adequate information already available about SIOPs to support the needs of optical models, especially in the context of linking them to ecosystem models. The utility of different SIOPs reported in the literature will be analyzed and compared with values obtained in the Irish Sea based on the regression calculation. The impact of literature SIOPs in different case scenarios (as per chapter 6) will be studied by determining the sensitivity of the modelled reflectance to those SIOPs. When SIOPs are used as optical descriptors of the OACs used as variables within an ecosystem model, a rigorous examination of each constituent IOP and its relation to type and concentration of constituent is necessary. This chapter aims to provide a critical assessment of how each literature SIOP is defined and matched to the compositional content of a model. Their adaptability for different water types and especially their suitability for case II waters scenarios is discussed.

7.2 Phytoplankton absorption coefficient

Phytoplankton is the determinant for the available radiation in Case I waters, where phytoplankton is the main OAC and its contribution to the absorption coefficient accounts for 73 % and 27% for non-algal particles (NAP) (Bricaud and Stramski, 1990). In Case II waters phytoplankton is still the largest absorption signal (43%) but the relative contribution to total a is significantly lower than for Case I, with 25% by a_{nap} and 20% by a_{cdom} (Tilstone et al., 2005). Hence, an adequate characterization of a_{ph} coefficient is extremely important. The following

subsections consider three of the a_{ph} parameterizations presented in the literature and often used in bio-optical modelling.

Prieur and Sathyendranath, (1981)

The Prieur and Sathyendranath (1981) parameterization of a_{chl}* has been widely used in bio-optical modelling (Garver and Siegel, 1997; Mobley, 1994), and as the base line for further developments aimed at improving a_{chl}* parameterization (Bricaud et al., 1995; Morel, 1988). This study presented an optical model for coastal and oceanic waters based on the spectral shape of specific absorption coefficient of phytoplankton, non-chlorophyllous particles and CDOM. Scattering was also based on Chl *a* concentration and the model was developed for potential retrievals of reflectance. Here only a_{chl}* will be examined for its value as a literature SIOP. In their approach, absorption values were deduced from radiometric measurements using the expression by Morel and Prieur (1977):

$$a(\lambda) = \frac{K_d(\lambda)[1 - R(\lambda)]\cos j}{0.6 + [0.47 + 2.5R(\lambda)]\cos j} \tag{7.1}$$

Where K_d is downwelling attenuation coefficient, R is irradiance reflectance and j expresses the solar zenith angle. Assuming a four component model for the absorption coefficient, it is expressed as:

$$a(\lambda) - a_w(\lambda) = C \cdot a_c^*(\lambda) + P \cdot a_P^*(\lambda) + Y \cdot a_y^*(\lambda) \tag{7.2}$$

$a_c^*(\lambda)$, $a_p^*(\lambda)$ and $a_y^*(\lambda)$ are the specific absorption coefficients of phytoplankton, non-chlorophyllous particles and yellow substance or CDOM and C, P and Y represent their concentrations. The absorption by water alone, $a_w(\lambda)$, and $a_y^*(\lambda)$ are known parameters. Each of the characteristic specific absorption curves was normalized to its respective value at 440 nm:

$$a_i(\lambda) = C_i' \cdot a_c^{*\prime}(\lambda) + P_i' \cdot a_P^{*\prime}(\lambda) + Y_i' \cdot a_y^{*\prime}(\lambda) \tag{7.3}$$

and

$$a_i(440) = C_i^{'} + P_i^{'} + Y_i^{'} \tag{7.4}$$

$a_c^{*\prime}(\lambda)$ and $a_p^{*\prime}(\lambda)$ were calculated with an iterative method based on predefined spectral shapes. $a_y^{*\prime}(\lambda)$ was predefined for the study. Results of the analysis for $a_c^{*\prime}(\lambda)$, $a_p^{*\prime}(\lambda)$ and $a_y^{*\prime}(\lambda)$ are presented in table 2 of Prieur and Sathyendranath (1981).

The coefficients $C_i' + P_i' + Y_i'$ were obtained by ridge regression (Jones, 1972) giving:

$$C' = 0.06[C]^{0.602} \tag{7.5}$$

C' being in m^{-1} and C in mg m^{-3}. The ridge regression was a result of possible correlation between independent variables with least squares analysis.

Then phytoplankton absorption was expressed as:

$$a_{ph}(\lambda) = a_{chl}^{*}{}'(\lambda) \cdot 0.06 \cdot [C]^{0.602} \tag{7.6}$$

Reliability of these parameterizations ($C_i' + P_i' + Y_i'$) was only assured from 400-570 nm. Higher wavelength values were omitted because of the significant increase of water absorption above 570 nm inducing errors in the radiometric measurements.

Bricaud et al., (1995)

The Bricaud et al. (1995) parameterization of a_{chl}^* has been proposed as standard a_{chl}^* parameterization in bio-optical modelling (IOCCG, 2006) and for IOP inversion in neural networks (Schiller and Doeffer, 1999). The study by Bricaud measured the variability in the phytoplankton absorption coefficient with a large dataset of 815 samples comprising eutrophic, oligotrophic and mesotrophic waters around coastal Europe.

In the protocols, phytoplankton absorption coefficient was obtained as in Kishino et al. (1985). Chl *a* specific absorption coefficients of phytoplankton were obtained by dividing $a_{ph}(\lambda)$ (m^{-1}) by the Chl *a* concentration (mg m^{-3}) in a point-by-point approach, where Chl *a* concentration included dvinyl chl a and pheophytin. Pigment concentrations were determined using HPLC, broadband fluorometry, spectrofluorometry and spectrophotometry. Spectrofluorometric measurements were steadily higher than HPLC values for which a correction factor was applied

using HPLC as a reference baseline. Pigment concentrations in the study ranged from 0.03 to 24.5 mg m^{-3}. In the present study in case II waters, pigment concentration ranged from 0.2-2.7 mg m^{-3}, significantly lower than those of Bricaud's study. However, the Bricaud phytoplankton absorption model is widely used and claimed to be also representative of coastal and case II waters and so must be considered in this study.

From examination of a_{ph}* versus Chl *a* concentration a power law was found to relate both quantities Therefore a_{ph}* was fitted to a power function of chlorophyll concentration for every wavelength as:

$$a^*_{chl}(\lambda) = A(\lambda)[chl]^{-B(\lambda)} \tag{7.7}$$

where coefficients *A* and *B* were determined at each wavelength (Bricaud et al., 1995, table 2). This parameterization reproduces properly the "flattening" of the absorption spectra with increasing Chl *a* concentration, resulting both from the package effect and from the decrease in the relative concentrations of accessory pigments. The same study points out the potential effect of errors both in a_{ph} and Chl *a* concentration when obtaining a_{chl}* (as considered in chapter 5).

Ciotti et al., (2002)

The Ciotti et al. (2002) parameterization was chosen for consideration because it is among the SIOPs employed in the study by Fuji et al. (2007) to define IOPs in a coupled optical-ecosystem model. In their study, the photoadaptative state of phytoplankton and the carbon-to-chlorophyll ratios are included for an accurate definition of the photosynthetic processes within the ecosystem model. Here, the analysis will be centred solely on the parameterization proposed by Ciotti. The photoadaptative state is given by the ecosystem dynamics which are out of the scope of this research.

This parameterization was obtained using a dataset obtained in the Bering Sea and the Bedford Basin. Phytoplankton absorption spectra were normalized using the mean absorption as:

$$\left\langle a_{ph} \right\rangle = \frac{1}{301} \sum_{\lambda=400}^{700} a_{ph}(\lambda) \cdot \Delta\lambda \tag{7.8}$$

with the spectral resolution $\Delta\lambda$ = 1 nm. To account for natural variability among spectra, a size factor was introduced which classified the spectra into those from picoplankton and those from microplankton. The total variability in phytoplankton spectra was expressed as a combination of both:

$$\hat{a}_{ph}(\lambda) = [S_f \cdot \overline{a}_{pico}(\lambda)] + [(1 - S_f) \cdot \overline{a}_{micro}(\lambda)] \tag{7.9}$$

where $\overline{a}_{pico}(\lambda)$ and $\overline{a}_{micro}(\lambda)$ are the basis vectors corresponding to the normalized absorption spectra for the smallest and largest cells (Ciotti et al., 2002, table 3), and S_f is the size factor given for different phytoplanktonic species (Ciotti et al., 2002, table 4).

Skeletonema Costatum and *Chaetoceros* are the main phytoplankton groups present in a case II environment such as the Irish Sea (McKinney et al., 1997). For comparison purposes with likely phytoplankton composition, an average a_{ph} parameterization has been selected based on values given for *Skeletonema Costatum* and *Chaetoceros*, provided by the size factor S_f. Average S_f factor used for these groups was 0.262.

Figure 7.1 presents these a_{chl}* parameterizations compared with the values obtained for the Irish Sea form the local observations. On the left panel, a_{chl}* obtained in this dataset by regression analysis is compared against the parameterizations given by Prieur (1981), Bricaud (1995) and Ciotti (2002). Among all of them, the Prieur (1981) is closest to the a_{chl}* values obtained in the Irish Sea. On the right panel, these parameterizations are tested in different case scenarios as in chapter 6. Here case 1, the baseline scenario with Chl = 1 mg m^{-3} and case 3, the high chlorophyll scenario, Chl = 5 mg m^{-3} are used to evaluate their adaptability to different water types.

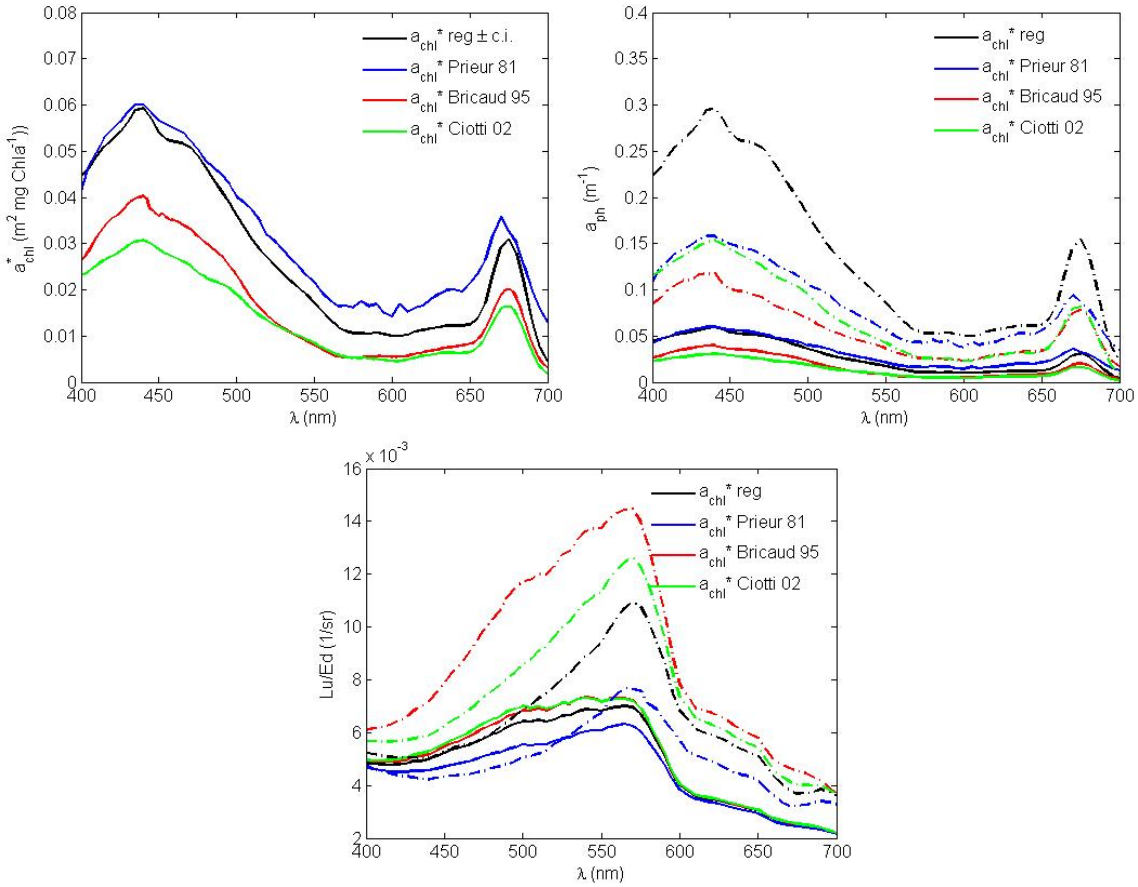

Figure 7.1. Left panel: a_{chl}* parameterizations of Prieur 81, Bricaud 95 and Ciotti 02 with a_{chl}* from this dataset. Right panel:. a_{ph} from Prieur 81, Bricaud 95, Ciotti 02 and Irish Sea dataset using case 1 (solid lines) and case 3 scenario (dashed lines). Bottom panel: Impact of a_{ph} from Prieur 81, Bricaud 95, Ciotti 02 and Irish Sea dataset in radiance reflectance, using case 1 (solid line) and case 3 (dashed line) scenarios.

For the high chlorophyll scenario, all a_{chl}* parameterizations are smaller than the a_{chl}* values for this dataset. The Prieur (1981) and Bricaud (1995) parameterizations introduce an exponential expression that relates phytoplankton absorption with chlorophyll concentration. In this example, the Prieur parameterization is closest to the a_{chl}* obtained from this dataset. It was previously stated that the retrieved values in this dataset are higher than typical observations of a_{chl}* (chapter 4) and uncertainties in the retrieval method and calculation might have affected the result (chapter 5). The best-fit relationship for a_{ph} and chlorophyll concentration used in the

present study was linear, applying regression analysis between these two parameters. However it was noted in chapter 5 that the regression analysis could be applied with other fitting functions. The literature parameterizations used here propose a variable dependence of chlorophyll concentration on the a_{ph} spectra which might be a better representation of the a_{ph} coefficient measured in natural waters.

Sensitivity of radiance reflectance to these parameterizations is presented in figure 7.1 bottom panel for the two case scenarios tested. The Prieur parameterization introduces less variability in reflectance, 20 % variation across spectrum between the two scenarios tested, whereas the regression a_{chl}* from this dataset was 35 % variation. The Bricaud and Ciotti parameterizations had a 75 % and 49 % of variation respectively between case scenarios. The parameterization proposed by Ciotti, where specific phytoplankton groups were introduced, appears to have a closer response to the dataset used here.

7.3 MSS absorption coefficient

Absorption by mineral particles can be a significant contribution to the total absorption coefficient in case II waters. In bio-optical modelling in case II waters, terrigenous contributions in coastal areas and mineral resuspension in turbulent regions will have an impact on the radiance field and an adequate characterization of them is needed. Individual measurements of mineral particles (Babin and Stramski, 2004) are rare to find, as are parameterizations of the a_{mss} coefficient. Separating the individual contributions in the unpigmented particle fraction from filter pad measurements is difficult unless measurements are made from lab samples (chapter 3), and therefore clear descriptions of the composition of the unpigmented particle fraction is very uncommon. As previously discussed in chapter 3, an unclear definition of the unpigmented particle fraction prevents establishing a robust link between the bio-optical model and the OAC in the ecosystem model, since the constituents generating the IOP are not adequately defined. At

the time of this study, only one parameterization of the a_{mss}* was found, which relaters the unpigmented fraction related with MSS content.

Bowers et al., (1996)

A relevant study for this work was performed by Bowers et al., (1996) based in the Menai strait region, in the eastern boundary of the Irish Sea, whose waters are covered within the dataset used in this study. To obtain measurements solely from the mineral fraction, samples were filtered in Whatman GF/F filters and rinsed to eliminate any salt. Samples were furnaced at 500 ˚C to remove any organic particles including phytoplankton. Even for combusted mineral particles, a CDOM-like spectrum was observed that was fitted to an exponential function. This procedure might hide particular features of the spectra (chapter 4) that are often present in the mineral absorption spectra (Babin, 2004). Based on 121 samples, were obtained the following statistics:

- Mean slope: -0.011nm^{-1}
- Standard error of slope: 0.0021 nm^{-1}
- Mean correlation coefficient (r^2): 0.95

From these results, a good correlation was observed between absorption and mineral suspended sediment at any wavelength. Choosing 440 nm as reference wavelength and applying lineal regression analysis between filter absorption data and MSS with null intercept the following relationship was reported:

$$a_f 440 = 0.097[MSS] \tag{7.10}$$

Combining equation 7.10 with the wavelength dependence gives an equation for a_{mss} as:

$$a_f(\lambda) = 0.097[MSS]\exp(-0.011(\lambda - 440)) \tag{7.11}$$

The regression for $a_f 440$ with MSS was corrected for path length amplification factor, $\beta = 4$ as derived in the study, dividing the slope of the regression by 4, obtaining:

$$a_{mss} 440 = 0.02425 \cdot [MSS] \quad (7.12)$$

Combining this equation with the slope value proposed by Bowers, the following expression is obtained:

$$a_{mss}(\lambda) = 0.02425 \cdot [MSS] \cdot \exp(-0.011(\lambda - 440)) \quad (7.13)$$

It is worth noting that although other studies have previously addressed the MSS absorption coefficient, the study of Bowers was probably the first one that published a parameterization for the MSS absorption coefficient. The generalization and applicability of their results is, however, limited with regard to the following points: (1) particles may have been altered by the heat treatment, and (2) the error associated with measurement of absorption was not assessed although this error may be especially high for mineral particles whose absorption-to-scattering ratio is expected to be very low.

Figure 7.2 (left panel) presents the a_{mss}* obtained from Bowers and the a_{mss}* obtained in this dataset. On initial examination of the data, a significant difference between the two coefficients was observed, which might have been caused by the chosen β path length amplification factor applied on filter pad data. The a_{mss} coefficient from this dataset had a β factor of 2 (chapter 4), whereas Bowers used a β factor of 4. Once the a_{mss}* from this dataset was corrected for β factor by multiplying by 2 (the results shown in the figure), both coefficients appear closely related, with the exception of the blue region of the spectra, which could be an artefact of the exponential fitting used by Bowers. This fitting could also obscure particular spectral features of mineral particles relevant in the UV and blue region of the spectra (Babin and Stramski, 2004).

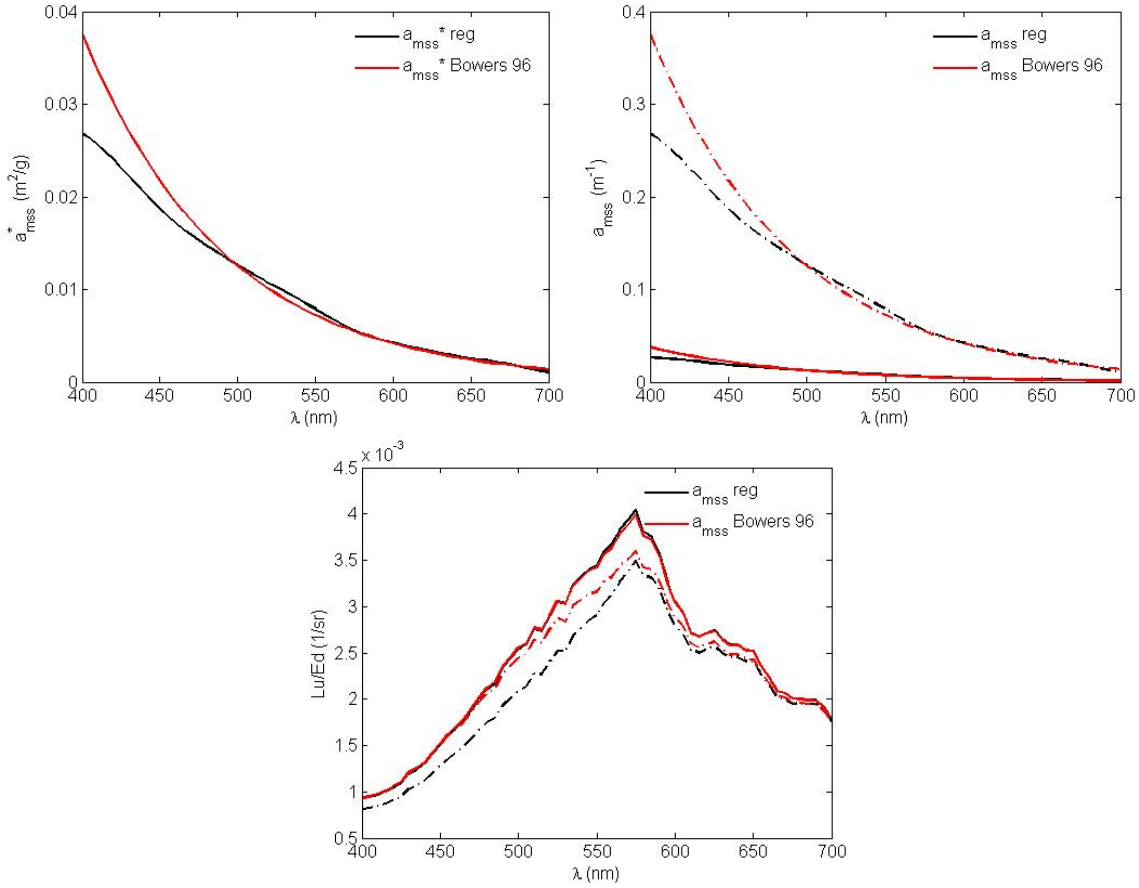

Figure 7.2. Left panel: a_{mss}* parameterizations of Bowers 96 with a_{mss}* from this dataset. Right panel: a_{mss} from Bowers 96 and Irish Sea dataset using case 1 and case 2 scenario. Bottom panel: Impact of a_{mss} from Bowers 96 and Irish Sea dataset in radiance reflectance, using case 1 (solid line) and case 2 (dashed line) scenarios.

The case 1 scenario and case 2 scenario (high MSS content, MSS = 10 g m^{-3}) were used to investigate the adaptability of the different SIOPs to different water types, as shown in the right panel. Both coefficients varied similarly with difference in the blue region. Variations in radiance reflectance were similar (bottom panel) with a variation of 11 % across the spectrum in this dataset and 4% for the a_{mss} parameterization by Bowers.

7.4 Detritus absorption coefficient

Previously it was pointed out that there is a significant contribution of a_{nap} towards the total absorption, which in case II waters can generate 25% of the signal. As with the MSS absorption coefficient, clear distinctions between absorption behaviour based on the composition of the NAP are rare. The detritus absorption coefficient, as defined in this work, is conformed of phytoplankton by-products and organic material. In practice, the NAP fraction includes these plus any other contribution of material after subtracting photosynthetic pigments. This will usually include a mineral fraction. The parameterization chosen here is widely used to define the absorption coefficient by the non-pigmented organic fraction (Fuji et al., 2007).

Babin et al., (2003)

The study published by Babin et al. (2003) presented the results of phytoplankton absorption, non-algal particle absorption (a_{nap}) and CDOM absorption from the COASTLOOC campaigns, measuring optical properties in European coastal waters. This study proposed a parameterization of a_{nap} based on the observations obtained, which covers a wide range of optical water types and concentrations of OAC. 387 samples were used in this study. The a_{nap} signal was observed to be highly correlated with suspended particulate matter, SPM, which reportedly included some mineral content.

Measurements were obtained on Whatman GF/F filters. Corrections for path length amplification factor were applied (Tassan and Ferrari, 1995). Corrections for scattering effect in the sample were made by subtracting a_{nap} at 750 nm from all the measured spectral values of a_{nap}. Residual pigment absorption from incomplete bleaching was observed in some samples. This problem was overcome by fitting an exponential function in those regions not affected by main pigment absorption; this is excluding the regions of 400-480 nm and 620-710 nm. However it is likely to have remaining pigment absorption in the region of 480-620 nm, hence

some uncertainty can be assumed in these results (chapter 3). The observed slope values from the exponential parameterizations obtained were similar to those reported in other studies in case I and case II waters regardless of its primarily mineral or phytoplanktonic content.

Applying a regression analysis for a_{nap} 443 and suspended particulate matter (SPM) resulted in:

$$a_{nap}443 = 0.036 \cdot [SPM] \tag{7.14}$$

where suspended particulate matter includes phytoplankton by-products and can contain mineral particles too. The a_{nap} was found to follow the expression:

$$a_{NAP}(\lambda) = a_{NAP}(443) \cdot 0.75 \cdot \exp(-0.0123(\lambda - 443)) \tag{7.15}$$

Combining both equations, a_{nap}* is expressed as a function of SPM concentration:

$$a^*_{NAP}(\lambda) = 0.027 \cdot [SPM] \cdot \exp(-0.0123(\lambda - 443)) \tag{7.16}$$

This parameterization from Babin has been compared with the absorption by detritus from this dataset, which was obtained after water type partitioning for those stations with predominant chlorophyll content.

For comparison purposes, detritus spectra were fitted to an exponential expression as proposed by Babin. In their study, average slope values, *S*, were 0.0123 nm^{-1} with a standard deviation of 0.0013 nm^{-1}. In the Irish Sea data, *S* was 0.0148 nm^{-1} with a standard deviation of 0.0064 nm^{-1}. Figure 7.3 left panel, presents the distribution of slope values in Babin and mean *S* obtained in this dataset, outlier for this distribution. On the right panel, it is presented regression analysis for $a_{det}440$ and SPM from this dataset, in a similar approach as the Babin study, in order to relate the detrital fraction with SPM concentration. It presents a poor correlation for these two parameters but previously in chapter 4 it also presented a low correlation of the detrital fraction with chlorophyll. It is also possible that the number of observations from Babin study will generate a higher correlation coefficient.

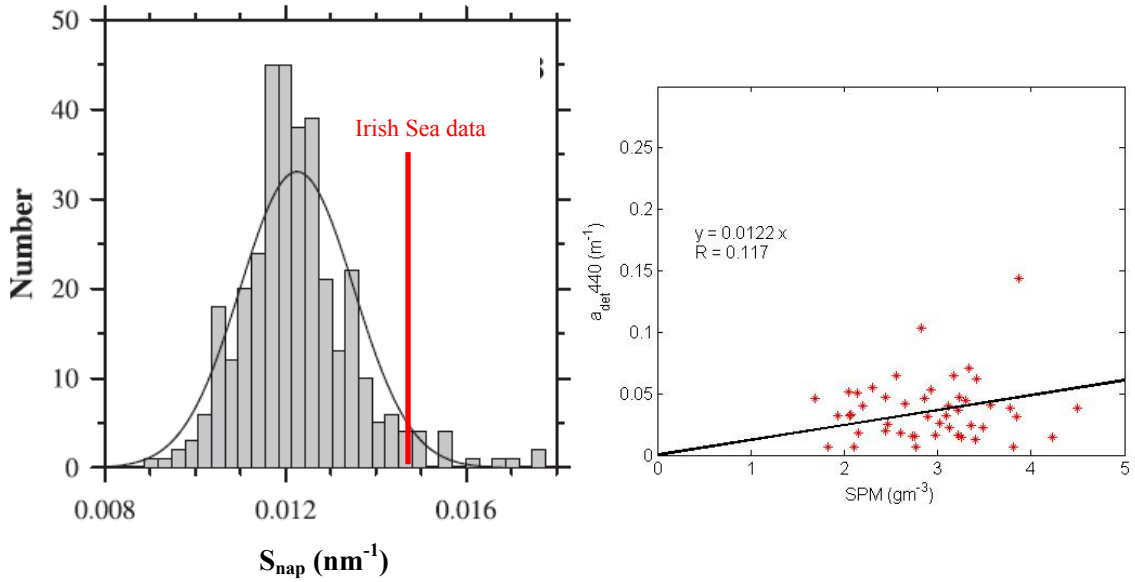

Figure 7.3. Left panel: Frequency distribution of SNAP coefficient from Babin 2003 and mean SNAP coefficient for this dataset. Right panel: a_{det} 440 vs SPM concentration for this dataset.

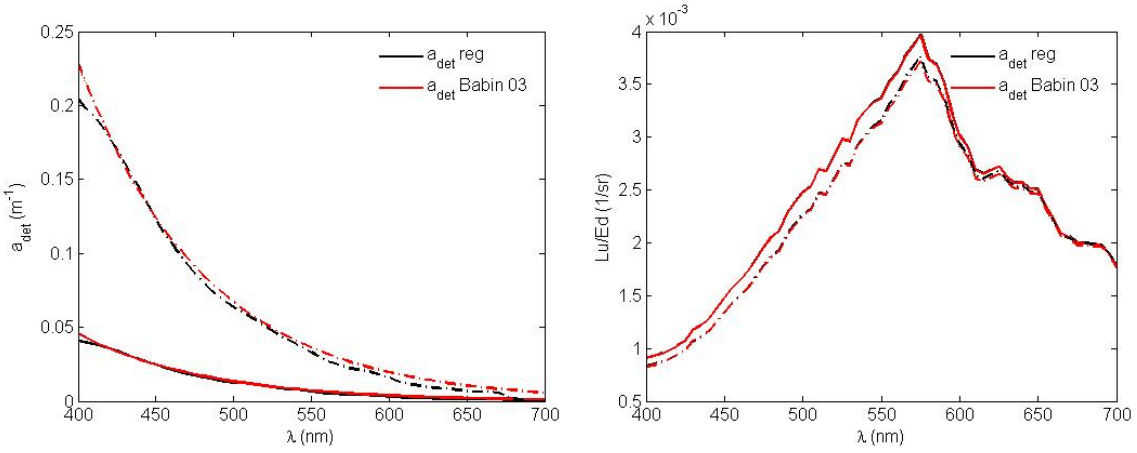

Figure 7.4. Left Panel: a_{det} from Babin 03 and Irish Sea dataset using case 1 and case 2 scenario. Right Panel: Impact of a_{det} from Babin 03 and Irish Sea dataset in radiance reflectance, using case 1 (solid line) and case 3 (dashed line) scenarios.

In figure 7.4 a_{det} has been used in two case scenarios, baseline case 1 scenario (1 mg m^{-3} chlorophyll) and case 3, high chlorophyll case scenario (5 mg m^{-3} chlorophyll). The Babin parameterization adapts well to the a_{det} coefficient derived from the Irish Sea dataset when used in different case scenarios (left panel) and when further used to retrieve reflectances from the different case scenarios (right panel). The parameterization by Babin introduced a 5.86% variation in spectral reflectance from different case scenarios, whereas the detrital fraction from the dataset had a 5.39% of spectral variation.

Although the a_{det} coefficient from the Irish Sea dataset was related only with chlorophyll content, and this parameterization relates the absorption signal by organic and inorganic material with total SPM, its effect in different case scenarios is similar, suggesting that the exponential expression could well approximate the a_{det} coefficient in case II waters modelling.

7.4 Absorption by CDOM

CDOM absorption together with MSS absorption can significantly attenuate the available radiation in case II waters (Morel and Prieur 1977) compromising photosynthetical processes. During this work it has been mentioned that a_{cdom} is always fitted to an exponential expression to correct for disturbances on the a_{cdom} spectrophotometric measurement. a_{cdom} is therefore expressed as:

$$a_{CDOM}(\lambda) = a_{CDOM}(\lambda_0)\exp[-S(\lambda - \lambda_0)] \qquad (7.17)$$

where $a_{cdom}(\lambda_0)$ and the slope coefficient S are given to describe a_{cdom} from a particular water body. Different values are provided in the literature for $a_{cdom}(\lambda_0)$ and S for a given water body. The appropriate selection of these coefficients will ultimately define the goodness of the parameterization. Comparison is made between the a_{cdom} derived in this work and one example from the literature.

Tilstone et al., (2005)

This study performed in the Irish Sea region was chosen for its representativeness of case II waters and its region of study, coincident with this dataset. Measurements were taken during spring and summer in different locations across the Irish Sea which is influenced by terrigenous inputs contributing to the dissolved organic carbon (DOC) pool. Samples were filtered through 0.2 μm Whatman nuclepore membrane filters. Absorption coefficient was measured on a Perkin-Elmer lambda-2 spectrophotometer in a 10 cm quartz cuvette from 350 to 750 nm, relative to a reference blank. The a_{cdom} was calculated from the optical density, and the cuvette path length and baseline offset were subtracted from a_{cdom}. CDOM slopes, S, were calculated using an offset exponential fit which corrects for water absorption effects above 700 nm (Sullivan et al., 2006).

The mean slope value retrieved in the study was S = 0.016 m^{-1} nm^{-1}. $a_{cdom}(\lambda_0)$ was taken from previous observations of this dataset, being 0.124 m^{-1}. The final parameterization of a_{cdom} is then expressed as:

$$a_{CDOM}(\lambda) = 0.124 \cdot \exp[-0.016 \cdot (\lambda - \lambda_0)] \qquad (7.18)$$

The parameterization is given independent of the CDOM concentration. CDOM to DOM ratios are highly variable regionally (Siegel et al., 2002) and this is one of the great challenges when relating a_{cdom} to DOM present in an ecosystem model. Here, for comparison purposes, CDOM concentration was multiplied by a_{cdom}.

The exponential fitting of a_{cdom} was compared with the a_{cdom} spectra obtained in the Irish Sea in figure 7.5, left panel, being both normalized by a_{cdom} 440. The Tilstone parameterization failed to reproduce the observed a_{cdom} spectra from 470 nm onwards. This difference is preserved when a_{cdom} is calculated for two case scenarios, case 1 baseline in solid line (0.15 mg m^{-3}) and case 4, high CDOM content in dashed line (1 mg m^{-3}) (right panel). Variability in radiance reflectance for the Tilstone parameterization and for this dataset in the two case scenarios is

given in the bottom panel. Reflectance obtained from the Tilstone parameterization is very close to that from this dataset, although some evident differences are observed in the 500-600 nm region in the high CDOM scenario. These differences could potentially be substantial when band ratio algorithms are applied. Average spectral variability in reflectance between the two scenarios was, from this dataset 22 %, and 19 % by the proposed parameterization by Tilstone.

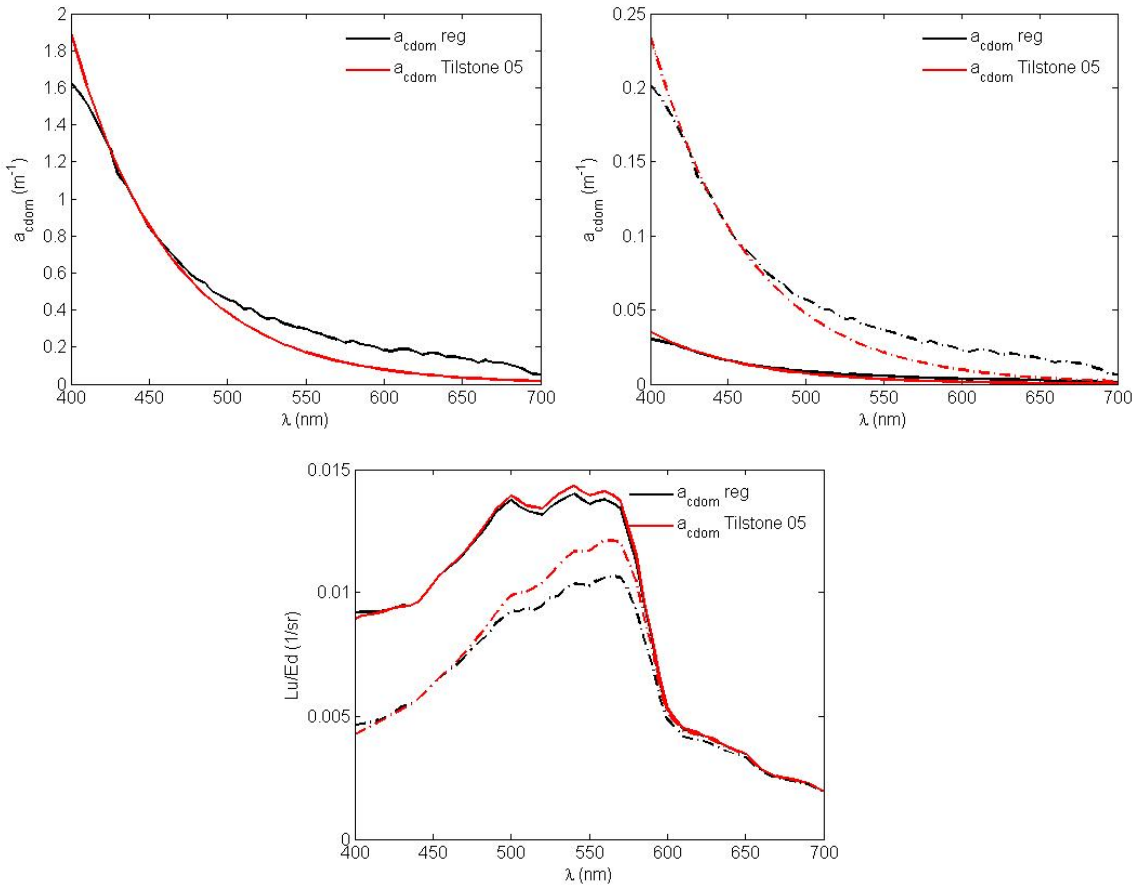

Figure 7.5 a_{cdom}* parameterization from Tilstone 05 and a_{cdom}* from this dataset (left panel). a_{cdom} from Tilstone 05 and Irish Sea dataset using case 1 and case 4 scenario (right panel). Impact of a_{cdom} from Tilstone 05 and Irish Sea dataset in radiance reflectance, using case 1 (solid line) and case 4 (dashed line) scenarios (bottom panel).

7.5 Phytoplankton scattering coefficient

It was demonstrated in the previous chapter how important the contribution of the phytoplankton scattering signal is to the radiance field in the context of this study. Phytoplankton contribution to the radiance field can be more significant than anticipated; predominant phytoplankton species in shelf seas are diatoms with a silicate structure that scatters light, while total phytoplankton absorption through the water column in turbid waters is lower due to the limited available radiation. Thus the combination of low absorption and high scattering by phytoplankton can potentially increase the radiance signal.

As in the case of particle absorption, few parameterizations are available in the literature that accounts for the individual scattering signal of each OAC. As was presented in chapter 6 for this dataset, the potential impact of scattering is significant, and therefore an adequate description of scattering signal of OAC is needed.

The particle backscattering coefficient is often related to the total chlorophyll content when assuming case I waters, because in that case there is no other source of particles contributing to the scattering signal. Two different parameterizations are considered here that introduce spectral dependency of the phytoplankton scattering coefficient as a power law function and as a linear function.

Loisel and Morel, (1998)

This parameterization proposes a revisit to the Gordon and Morel (1983) study, which relates scattering and chlorophyll as a power law function, where phytoplankton is the only scattering component in case I waters. This type of parameterization has been widely used to describe particle scattering in bio-optical models in case I and II waters (Garver and Siegel, 1997; Gordon et al., 1988). It is also used in remote sensing products to derive scattering coefficient,

and it is provided as the standard b_{ph} parameterization to define IOPs input for case II waters in radiative transfer modelling (Mobley, 1994).

In the reported study, the attenuation coefficient (c) at 660 nm was measured with a SeaTech transmissometer. Once attenuation by pure sea water was subtracted, the particle attenuation coefficient, c_p, was assumed to result only from particle scattering, b_p. To demonstrate this, the (Bricaud et al., 1995) relationship for a_{ph} was used to derive chlorophyll absorption at 660 nm:

$$a_{ph} = 0.012 \cdot (Chl)^{0.878} \tag{7.18}$$

with a $r^2 = 0.234$. For the range of chlorophyll values observed in the study, 0.02 – 4.5 mg m^{-3}, a_{ph} varied from 0.00038 m^{-1} to 0.0044 m^{-1}. These values are assumed negligible compared to those of c_p, ranging from 0.03 to 1.5 m^{-1}, and representing less that 3% of the measured values. Chlorophyll concentrations were measured with HPLC, where chlorophyll and diviniyl *a* accounted for pigment concentration. Best fit relationship was observed for a subset of near-surface chlorophyll values and c_p, named b_p by phytoplankton in the study was:

$$b_{ph}(660) = 0.407(Chl)^{0.795} \tag{7.19}$$

Then, spectral dependency was introduced by using 660 nm as a reference wavelength as in Gordon and Morel (1983):

$$b_{ph}(z,\lambda) = 0.407\left(\frac{660}{\lambda}\right)[Chl(z)]^{0.795} \tag{7.20}$$

The influence of wavelength on b_{ph} was established on the basis of two observations; 1) at low pigment concentrations (<0.1 mg m^{-3}) the scattering coefficient for ocean waters exhibits a λ^{-1} wavelength dependence; 2) at wavelengths which particles are strongly absorbing, their scattering is reduced such that their total attenuation is only weakly dependent on wavelength.

Gould et al., (1999)

Based on scattering observations with AC-9 in a variety of water types, (Gould et al., 1999) developed a model for scattering coefficient that could be applied both in case I and case II

waters. 555 nm was the reference channel selected, due to the low absorption at that wavelength in coastal waters. For each of the remaining eight wavelengths a linear function was fitted as:

$$b(\lambda) = M(\lambda) \cdot b(555) + I \tag{7.21}$$

where r^2 always exceeded 0.99. Intercepts from linear regression analysis were alluded to as errors in the measurement or instrument calibration and hence were neglected on further analysis. Then, assuming the slopes obtained, M, are linear functions of the wavelength of light:

$$M(\lambda) = m \cdot \lambda + i \tag{7.22}$$

where the coefficients were determined to be m = -0.00113, i = 1.62517 and r^2 = 0.997. Solving equation 7.21 for a reference wavelength λ_r and at any wavelength:

$$b(\lambda_r) = M(\lambda_r) \cdot b(555)\,,\; b(\lambda_r) = M(\lambda_r) \cdot b(555) \tag{7.24}$$

and combining equation 7.22 with 7.24 and solving for $b(\lambda)$:

$$b(z,\lambda) = b(\lambda_r) \cdot \left(\frac{m\lambda + i}{m\lambda_0 + i} \right). \tag{7.25}$$

The Morel (1988) model, similar to the Loisel and Morel (1998) model previously described, was introduced to relate scattering at 555 nm to chlorophyll concentration. Best fit coefficients were retrieved for measurements in case II waters, resulting in:

$$b(550) = 0.45 \cdot C^{0.62} \tag{7.26}$$

where C stands for chlorophyll concentration. Combining the spectral dependence previously obtained and chlorophyll dependence:

$$b(z,\lambda) = 0.5 \cdot \left(\frac{-0.00112 \cdot \lambda + 1.62517}{-.0..112 \cdot 550 + 1.62517} \right) \cdot C(z)^{0.62} \tag{7.23}$$

These two parameterizations express the scattering coefficient as a linear function of wavelength. They are compared with b_{chl}* obtained in this dataset in figure 7.6. On the left

panel, b_{chl}* from Loisel-Morel and from Gould are compared to b_{chl}* obtained in the Irish Sea. The specific scattering coefficient from the Irish Sea dataset has significantly less spectral variability than that introduced by these parameterizations. When applied in two different case scenarios (right panel), case 1 baseline and case 3 high chlorophyll scenario (as per chapter 6), both parameterizations fail to reproduce the range of scattering values in the case 3 scenario and both of them have decreasing scattering spectra.

.

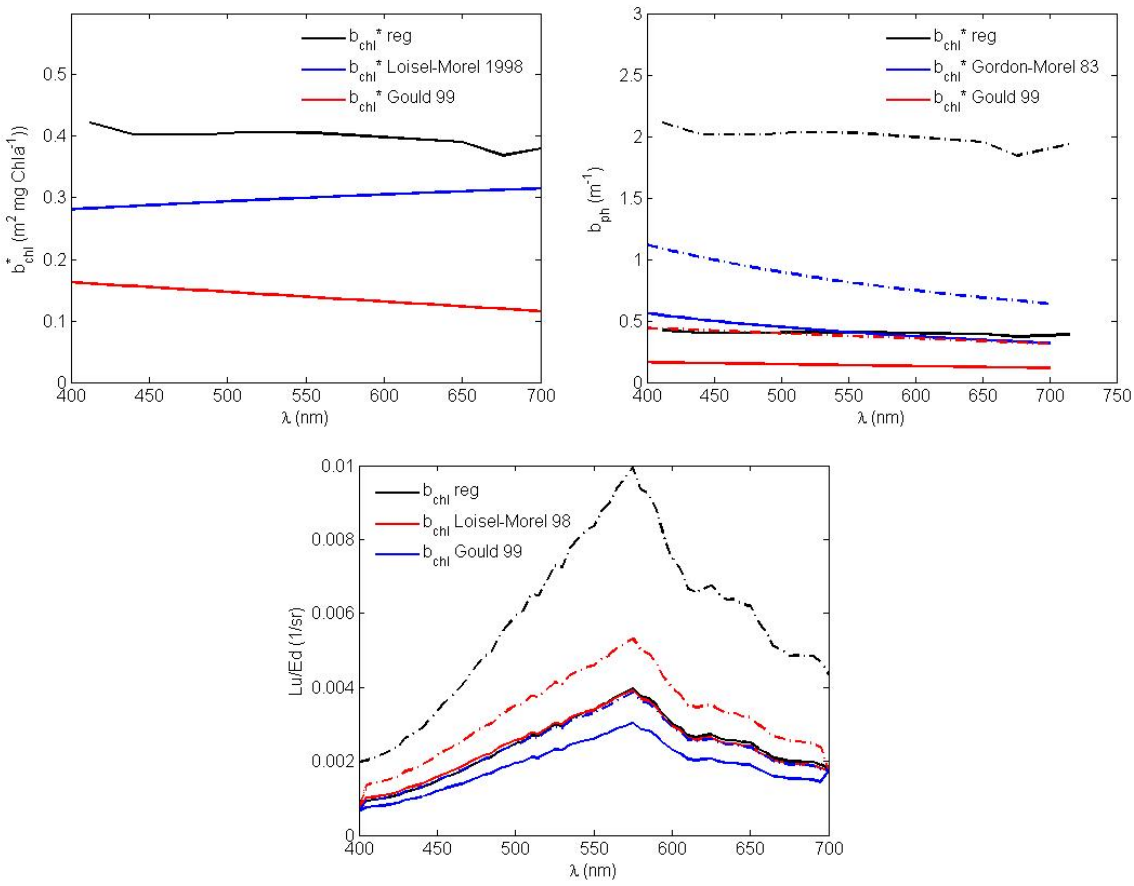

Figure 7.6. Left Panel: b_{chl}* parameterization from Loisel-Morel 98, Gould 99 and b_{chl}* from this dataset. Right panel: b_{chl} from Loisel-Morel 98, Gould 99 and Irish Sea dataset using case 1 (solid line) and case 3 (dashed line) scenario. Bottom panel: Impact of b_{chl} from Loisel-Morel 98, Gould 99 and Irish Sea dataset in radiance reflectance, using case 1 (solid line) and case 3 (dashed line) scenarios (bottom panel).

This is further demonstrated when they are applied in radiative transfer modelling. On the bottom panel of figure 7.6, the Loisel-Morel and Gould parameterizations are compared with b_{chl}* from the Irish Sea in the case 1 scenario (solid line) and case 3 scenario (dashed line). The range of spectral variability introduced from both case scenarios is significantly reduced with these reviewed parameterizations - 33% for Loisel-Morel and 19% for Gould – whereas the Irish Sea dataset has 140 % of spectral variability. The two parameterizations studied here not only introduce more spectral dependency into b_{chl}* in the form of (opposite) spectral trends than the observed SIOPs, but also fail to reproduce the spectral structure in which scattering reduces due to phytoplankton absorption at 440 nm and 660 nm. This could have significant implications when band ratio algorithms are used in inverse modelling to derive OAC

7.6 Mineral scattering coefficient

Scattering coefficient by mineral particles can be a significant contribution to radiance, controlled by the refractive index and the particle size distribution of mineral particles. However, progress in the development of high quality optical scattering measurements related to the size and mineralogy of particles has lagged behind the comparable studies of absorption related to organic material in sea water, so that stand alone measurements of scattering coefficient by mineral particles are very difficult to find. At the time this thesis was written, parameterizations of b_{mss}* that could be considered representative of mineral particles from case II waters could not be found. With the arrival of new optical sensors measuring scattering and volume scattering function, more studies have recently tackled the study of mineral scattering properties (Babin et al., 2003; Snyder et al., 2008; Stramski et al., 2001), but parameterizations or published data of b_{mss}* usable for case II water simulations still seem to be non-existent. The measurements presented here for mineral scattering were selected for the closeness of their environmental conditions to those obtained in the Irish Sea.

Stavn and Richter, 2008

The Stavn and Richter (2008) study measured scattering coefficient with an AC-9 (Wetlabs, Inc) instrument in Mobile Bay, Alabama, a highly turbid region with strong terrigenous contributions comparable to the case of some locations in the western boundary of the Irish Sea. Based on fundamental optics, the mineral scattering coefficient was defined as:

$$b_m(\lambda) = \left(\frac{\sigma_m(\lambda)}{\rho_m v_m} \right) \cdot PIM \tag{7.24}$$

where $\sigma_m(\lambda)$ is particle scatter cross section, ρ_m is the density (g m^{-3}) of the mineral particle, v_m is the volume of a single mineral particle and PIM is the mass concentration of particulate inorganic material. Thus, the spectral-mass specific scattering cross section is

$$\sigma_{PIM}(\lambda) = \frac{\sigma_m(\lambda)}{\rho_m v_m} \tag{7.25}$$

Particle scattering coefficient obtained from AC9 measurements were partitioned into specific particle organic and inorganic scattering coefficient, using least square regression or Model I, and Model II univariate regression, to obtain best estimate of regression slopes, this is, specific scattering coefficient as in the regression method presented in this thesis from field observations. Figure 7.7 presents the results of b_{mss}* from the Stavn study and from the Irish Sea data on the left panel. The b_{mss}* values from Stavn presents higher spectral dependency. These measurements were carried out in a particular location with highly turbid waters, whereas the Irish Sea data, while it can be approximated as case II water, has significant differences geographically and seasonally. Whereas b_{mss}* obtained from the Irish Sea might have contribution from other particles with less spectral dependence, the significant spectral dependence observed in Stavn study could be explained by a very well defined mineral fraction. The spectral dependence in the Stavn study remains apparent when applied to evaluate the mineral scattering IOP in different case scenarios (right panel). Following the earlier pattern, the scenarios compared are; case 1 baseline scenario (MSS = 1 g m^{-3}) and case 3, high mineral case scenario (MSS = 10 g m^{-3}). Results from radiative transfer modelling in the two case

scenarios are presented in the bottom panel, comparing the use of b_{mss}* from the Stavn study and b_{mss}* obtained in the Irish Sea. Given the significance of the b_{mss} coefficient in optical modelling (chapter 6), variations for each coefficient between cases scenarios are expectedly large. The b_{mss}* from Stavn produces a reflectance signal 125 % higher than that from this dataset.

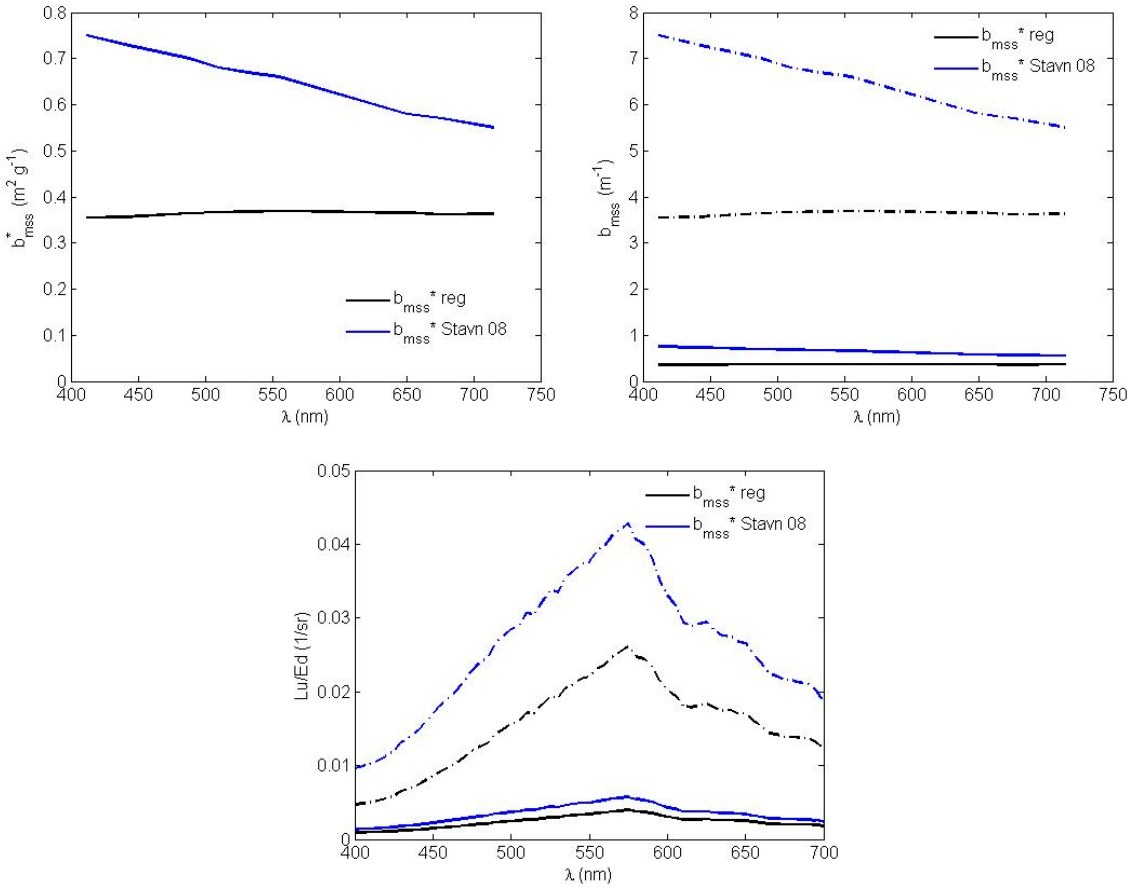

Figure 7.7 Left panel: b_{mss}* values from Stavn 08 and b_{mss}* from this dataset . Right panel: b_{mss} from Stavn 08 and Irish Sea dataset using case 1 (solid line) and case 2 (dashed line) scenario. Bottom panel: Impact of b_{chl} from Stavn 08 and Irish Sea dataset in radiance reflectance, using case 1 (solid line) and case 3 (dashed line) scenarios.

7.7 Backscattering ratio

The radiative transfer equation depends both on the absorption and angular characteristics of the medium, given by the volume scattering function, VSF, which is extremely important for deriving the radiance field. This parameter is difficult to measure and, to date, the only published study that measured VSF at a variety of angles was performed by T.J. Petzold in 1972. The VSF can also be reasonably approximated by the backscattering ratio (Mobley et al., 2002) and backscattering ratio is widely assumed to be wavelength independent if the particles are not strongly pigmented and the particle size distribution follows the commonly assumed power law distribution (Ulloa et al., 1994). Then, VSF is used to derive backscattering coefficients when such measurements are not available.

Petzold, 1972

Backscattering sensors are still relatively new and such measurements are not widely performed by the optics community. For years, the VSF data taken by Petzold were and are still being used in radiative transfer modelling, as reference values for backscattering ratio and used to derive backscattering coefficients.

Petzold's measurements were taken with a general angle scattering meter, measuring VSF at a variety of angles between 0.085˚ to 170˚ in the backward direction and centred at 470 nm with a wide acceptance angle. Experiments were taken in 3 singular locations; Bahamas, offshore southern California and San Diego harbour, which are classified as oceanic, coastal ocean and turbid waters, respectively. Backscattering ratios observed (approximated from VSF) were 0.013 for coastal ocean waters and 0.019 for turbid waters in San Diego Harbour. Average particle backscattering ratio observed in this dataset was 0.0145 which lies between those observed by Petzold for coastal ocean waters and turbid waters. An average scattering phase

function from Petzold's measurements has been used to compare with that obtained in this dataset when used in radiative transfer modelling.

Figure 7.8 shows radiance simulations for the average backscattering ratio from Irish Sea measurements and for the average backscattering ratio from Petzold. The maximum difference observed between both coefficients is 0.0002 sr^{-1} at 575 nm. This represents a maximum variation of 7% of the radiance signal. Given the importance of the backscattering signal in radiative transfer calculations, these results are quite good compared to those from mineral scattering and phytoplankton scattering parameterizations.

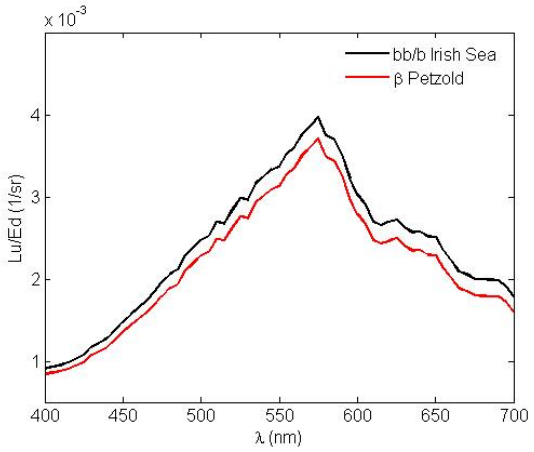

Figure 7.8 Impact of average backscattering ratio from Petzolds and Irish Sea data in radiance reflectance.

7.8 Overview

This chapter has performed a review and assessed the application of literature SIOPs capable of use in bio-optical modelling. In order to establish a bio-optical model generating constituent IOPs that will constrain the radiative transfer model, SIOP parameterizations or SIOP measured data are needed. After an extensive literature review, it is concluded that although many studies have been undertaken to measure constituent IOPs and SIOPs, it is rare that the detailed observational data are published in sufficient detail that they could be used to calculate

constituent IOPs for a given concentration of OAC. This is an obstacle to the development of optical models given that extensive databases of constituent SIOP are needed in order to adequately describe constituent IOPs for optical-ecosystem models in a particular region.

SIOPs are strongly dependent on the water mass measured, and for those values that have been published, their applicability would usually be limited to bio-optical modelling in similar scenarios. It has however been demonstrated that SIOPs measured by independent studies in the Irish Sea region have, in general, good accordance with the values measured in this dataset, which could be sufficient to describe constituent IOPs in the Irish Sea. Using literature IOPs from the region in which optical modelling is applied could well approximate their radiance field. Nevertheless, there are certain seasonal and small geographical variations that would be impossible to constrain and would compromise the sensitivity of the bio-optical model.

Finally, a rigorous description of the composition of constituent IOPs is needed to establish a robust parameterization based on constituents with similar optical characteristics. At the moment, the description of the absorption coefficient by non-algal particles (particle absorption with photosynthetic pigments removed) is mismatched with the OAC found in the ecosystem model. When the separation of the optical cross-section of each constituent is limited by methodology, regression analysis could be a useful tool to obtain constituent SIOPs (McKee and Cunningham, 2006; Stavn and Richter, 2008).

Chapter 8

Conclusions

8.1 Overview

The broad goal of the research work reported in this thesis was to explore and discuss the issues affecting the feasibility of using bio-optical models to predict the light field within ecosystem models in optically complex (case II) waters. The approach adopted has placed detailed emphasis on the description of constituent inherent optical properties, IOPs, used as inputs to the bio-optical model, basing the discussion on an observational dataset of bio-optical variables and constituents measured in the Irish Sea. From the outset it has stressed the importance of an adequate description of those optically active constituents (OACs) which control the IOP signal, that is which dominate the amplitude and spectral shape of the IOPs. At the same time the approach had to recognise the necessity of measuring constituent IOPs that correspond to OACs that can be associated with variables in the ecosystem model. A key element of the research has been to evaluate the impact of uncertainties in IOP measurements and whether that potential impact changes when introduced into bio-optical modelling of different water types. Finally, a review of state of the art constituent IOP measurements and parameterizations has been investigated, with the aim of identifying predefined constituent IOPs from literature that could be used in coupled optical-ecosystem models in case II waters.

8.2 Summary of achievements

The content of chapter 3, with an extensive description and review of what constituent IOPs are and how they are currently retrieved, already includes some points that contribute to the aim of the thesis. Certain issues were pointed out that could determine the feasibility of coupling optics

in ecosystem models. The absorption coefficient of CDOM is a parameter that is well understood and measured, but CDOM makes up only a fraction of the DOM described by the ecosystem model. Defining the optical properties of DOM as it is represented in the ecosystem model is a challenge, since ratios of DOM to CDOM are highly variable and therefore parameterizations of this ratio are difficult. Another point that has recurred throughout the thesis is how to characterise the absorption coefficient of un-pigmented SPM. This includes a diverse composition with different optical properties and hence it is very difficult to establish a universal parameterization that could be used in optical-ecosystem modelling. From the opposite perspective, an important factor that is often neglected in ecosystem modelling is mineral particles, whereas it has been demonstrated in the Irish Sea dataset that these can primarily determine the radiance field in coastal and case II waters systems. The incorporation of a term for MSS in the ecosystem model would be necessary for successful coupled optical-ecosystem modelling.

Chapter 3 also discussed the importance of correction factors applied in optical measurements, where their validity is sometimes questionable. The corrections applied to absorption data for scattering effects beyond 700 nm, assuming zero absorption in this region, is not valid for mineral particles, which have strong absorption properties that are not negligible in the near-infrared. Also, the validity of the Zaneveld et al. (1994) scattering correction factor applied in the analysis of AC9 measurements has also recently been questioned (McKee et al., 2008). This will have profound implications in the optics community given that this is the primary instrument used for in-situ absorption and attenuation measurements, and a large number of optical studies have been developed upon them. In fact, this demonstrates that our understanding of ocean optics is presently limited by our measurement capability. Optical oceanography is a constantly evolving research field and exercises to revisit the observational methodology must be performed regularly to allow progress towards more reliable optical models.

The motivation and validity of this thesis work is framed in the context of case II waters. Chapter 4 introduced the importance of defining the optical water types in which measurements

are made and introduced a bio-optical model that defines the absorption and scattering processes in the Irish Sea. Using simple scattering-to-absorption ratios two distinctive water types were isolated. This approach also resolved the problem of defining the constituents measured in the un-pigmented SPM fraction by partitioning them into detrital absorption and MSS absorption. With this approach, constituents with different optical characteristics, minerals and detritus, were assigned separately to IOPs corresponding principally to these two constituents and hence a clear relationship between the unpigmented SPM fraction and optics is established, in a way that can be related with OACs in the ecosystem model.

There are two principal elements that define IOPs measured in a particular water body; the water type in which they are measured, given by the combination of concentrations of OACs, and the SIOPs. Optical measurements are extremely variable, given the nature of light, and hence extremely sensitive to error uncertainties. However, optical measurements are rarely reported with uncertainty ranges, which is crucial when these are further used to derive other optical parameters through the use of bio-optical modelling. Chapter 5 focused on quantifying uncertainties in SIOPs which are dependent on the measurement uncertainties in IOPs and constituent concentrations. Both of these are needed to derive SIOPs. Uncertainties in these two measurements can introduce a large range of variability in SIOPs. Correction factors applied, such as β path length amplification factor in filter pad data, or the AC9 scattering correction, will introduce uncertainties in IOPs measurements. Therefore part of the reported IOP variability is artificial, and this can be further enlarged by error propagation in the SIOP calculation method. Various SIOP parameterizations and measurements from the literature have been presented in this thesis work, where the derived SIOPs are likely to have introduced uncertainty from error propagation (Bricaud et al., 1995), although generally no error estimates are reported for the data presented. Providing uncertainty ranges in bio-optical modelling is necessary before applying SIOPs so the performance of the model can be assessed. Another important outcome from chapter 5 was the demonstration of a statistical method that reduces error propagation in derived optical parameters and provides confidence intervals for the resulting SIOPs.

The propagation of these SIOP uncertainties in optical and radiative transfer modelling will determine the variability ranges of the radiance field and its sensitivity to each constituent SIOP. This is what chapter 6 aimed for; to quantify the impact of SIOP variation on the radiance field predicted by bio-optical modelling in a variety of optically complex coastal case scenarios. The variability range in SIOPs generated from the choice of SIOP calculation method had a dramatic impact on the predicted radiance reflectance: it was demonstrated that traditional SIOPs calculated from a few point-by-point derivations produced a very large variability range in radiance reflectance compared to SIOPs from regression calculations on a larger representative ensemble of IOP and AOC samples. This confirmed that quantifying error uncertainties in SIOPs and providing information of these is necessary if it is to become possible to evaluate the sensitivity and performance of a coupled optical-ecosystem model system. Another important outcome of chapter 6 was to demonstrate the relevance of mineral particles and scattering in bio-optical modelling in case II waters such as the Irish Sea. Again, the importance of including this constituent in optical-ecosystem models in case II waters is crucial to adequately define the radiance field.

The final aim of this thesis work was to study the feasibility of coupling optical models and ecosystem models. In order to have operational optical-ecosystem models, input optical data are needed to initialize the model, ideally given by real time IOP measurements. Present retrieval methods for constituent IOPs makes this unfeasible, and therefore the use of alternative input sources, such as literature values, needed to be explored. This could be a realistic approach when historic optical data or parameterizations are available for the region where the optical-ecosystem model is performed. This was the background to chapter 7 which reviewed state of the art parameterizations and IOP data that could be applied in a case II water region such as the Irish Sea. First conclusions when reviewing the existing literature were that: 1) very few studies publish in full their IOP measurements. This fact tremendously limits the possible study of coupling optics and ecosystem models. 2) Published IOP data or parameterizations often do not

provide error uncertainty ranges, which makes it difficult to perform sensitivity studies for applicability of that particular parameterization to serve as optical data in the model. 3) IOP data are not always measured in accordance to the OAC constituents present in the model (for example the case of the NAP fraction) and vice-versa (as for mineral absorption and scattering coefficients). At the present time, this point is where most effort needs to be applied by the optics community, before the results of marine optical studies can be applied usefully in wider interdisciplinary fields such as ecosystem modelling.

8.3 Alternatives to radiative transfer modelling

This thesis has explored the use of constituent IOPs embedded in radiative transfer modelling. However, approximations of the reflectance solution to the radiative transfer equation have been developed by others that link constituent IOPs with radiance as a simplified function of absorption and backscattering (chapter 2). The use of such bio-optical models can represent a significant time reduction in the computation of the radiance field, an important consideration if the optical calculations are eventually to be embedded in a three-dimensional ecosystem model of a shelf sea. The sensitivity and accuracy of such an approximate approach is worth being studied further, although such work lay beyond the planned scope of this thesis. One of the strengths of such models is the introduction of spectral variability into the backscattering coefficient. The current Hydrolight version (4.1) assumes spectral independence of the backscattering ratio, used to approximate for volume scattering function, VSF, for which the backscattering coefficient is defined as spectrally constant. Given the significance of the backscattered light in the radiance field, and the results of recent studies which contradict the assumption of spectrally insensitive backscattering (McKee et al., 2009), this could compromise the calculation of underwater radiance. On the contrary, bio-optical models with a simplified treatment of radiation transfer physics would be computationally much cheaper and could reproduce the true spectral variability in reflectance, given by absorption and backscattering coefficients.

8.4 Conclusion: The feasibility of linking optical and ecosystem models

This project set out to assess how feasible it is to link bio-optical models of the light field to ecosystem models which require accurate knowledge of how the light field is influenced by those state variables of the ecosystem model that influence the underwater optics. It has considered the subject entirely in relation to the reliability of the predictions of the light field rather than the structure of the modelling interface between optical and ecosystem processes. The achievements of the work as outlined above have identified that there are a number of weaknesses, limitations and uncertainties in the present capacity to predict the underwater light field from best estimates of the constituent optical properties. The conclusion must be drawn that as long as there are some quite large uncertainties in the bio-optical modelling of Case II waters, it would be premature to start embedding optical subsystems into ecosystem models. However, it is also clear from the radiance modelling of different case scenarios presented in chapters 6 and 7 that the models do predict significant differences in radiances for different combinations of optically active constituents. Therefore, once the modelling uncertainties can be reduced with confidence to levels that are much smaller than the modelled differences between different water types, it will be appropriate to start embedding optical models into ecosystem models in a variety of different ways that should improve the overall performance of the ecosystem model.

In order to achieve the necessary reduction in bio-optical modelling uncertainties, the following recommendations, based on the results from this thesis, are made for future bio-optical research in support of improved ecosystem modelling in Case II waters:

- Optical measurements on which the optical model relies must be corrected using state of the art correction factors, and review exercises must be undertaken for updates.

- Error uncertainties in optical measurements need to be quantified, so that derived coefficients and parameterizations used in the optical-ecosystem model have uncertainty ranges from which the internal error propagation within the model can be evaluated.
- Alternative statistical methods, such as regression analysis should be considered to reduce error propagation when deriving SIOPs from measured constituent IOPs and the concentration of the matching OACs.
- Definition of the optical water type that the optical-ecosystem model attempts to reproduce is necessary, in order to determine which OACs and SIOPs are required to represent the dominant optical processes. At the same time the selection of OACs (and matching constituent IOPs / SIOPs) for the optical model must be made with regard to the available state variables in the ecosystem model.
- For a successful description of constituent IOPs in the optical-ecosystem model previous measurements should be undertaken in the same region as that to which the model is applied.
- Exploring the use of simpler bio-optical models vs radiative transfer modelling is strongly recommended in order to reduce computational time.

These recommendations provide some insights of future directions for progress in this field. Explicit optical ecosystem modelling has been conducted by Fuji (2007) who proved that it provided a better description of the light field and therefore of light dependent processes. However this thesis has shown that there is not only scope for further improvement, but indeed an urgent necessity for further efforts to be made that will improve optical observational procedures and the retrieval of error-quantified SIOPs. The goal must be to confidently reduce the uncertainty of predicted light fields to acceptable levels that will not compromise the forecast of the ecosystem models to which they are attached.

8.5 Implications for remote sensing

The use of bio-optical models to define the radiance field does also facilitate the comparison interface of ecosystem model outputs with remote sensing data. Water leaving radiance as calculated in the optical-ecosystem model can be directly compared with remote sensing measurements, discarding the use of derived products (chlorophyll, etc...) that have low reliability in coastal and case II waters regions. This approach also permits an instantaneous assessment of the ecosystem model, readjusting OAC within the ecosystem model according to the remote sensing observations for better accuracy. Furthermore, the optical model computes the radiance field hyperspectrally which allows a full picture of the light dependent processes occurring within the ecosystem model, instead of limiting this information to single wavelengths, as remote sensing products do with band ratio algorithms.

Nevertheless, the standard approach used nowadays for remote sensing data is inversion exercises, obtaining OACs from remote sensing measurements using different techniques. Amongst these, inversion methods based on artificial neural network analysis are presently being increasingly used to retrieve OACs (Schiller and Doeffer, 1999). But major issues arise from this technique, since its constituent retrieval is based on constituent IOP values obtained from the literature the accuracy of which is often not reported. Even though the statistical approach is robust, the reliability of the retrieval result is dependent on experimental observations of constituent IOPs where no uncertainty ranges are given. The insights gained from this thesis can therefore also be applied to improving the specification of SIOPs used in satellite ocean colour product retrieval algorithms.

Appendix A

SIOPs

	Regression		Point by point			
λ	a_{chl}*	a_{chl}*c.i.	a_{chl}*mean	a_{chl}*median	a_{chl}*max	a_{chl}*min
400	0.0446	0.0040	0.0503	0.0466	0.1349	-0.0001
405	0.0462	0.0040	0.0533	0.0483	0.1381	0.0049
410	0.0489	0.0042	0.0567	0.0525	0.1491	0.0026
415	0.0510	0.0042	0.0593	0.0536	0.1508	0.0087
420	0.0525	0.0043	0.0611	0.0557	0.1527	0.0005
425	0.0541	0.0042	0.0631	0.0573	0.1538	0.0115
430	0.0562	0.0045	0.0661	0.0605	0.1586	0.0186
435	0.0588	0.0045	0.0693	0.0632	0.1704	0.0213
440	0.0592	0.0046	0.0695	0.0643	0.1675	0.0216
445	0.0569	0.0045	0.0674	0.0624	0.1612	0.0187
450	0.0540	0.0043	0.0643	0.0592	0.1524	0.0188
455	0.0524	0.0043	0.0622	0.0560	0.1451	0.0177
460	0.0520	0.0042	0.0617	0.0549	0.1441	0.0168
465	0.0518	0.0042	0.0613	0.0551	0.1426	0.0177
470	0.0508	0.0041	0.0603	0.0542	0.1458	0.0160
475	0.0489	0.0039	0.0574	0.0522	0.1372	0.0160
480	0.0465	0.0038	0.0545	0.0503	0.1304	0.0161
485	0.0439	0.0036	0.0512	0.0468	0.1196	0.0132
490	0.0413	0.0035	0.0481	0.0442	0.1097	0.0130
495	0.0387	0.0032	0.0449	0.0409	0.1016	0.0101
500	0.0360	0.0030	0.0413	0.0365	0.0904	0.0105
505	0.0334	0.0027	0.0381	0.0339	0.0848	0.0092
510	0.0308	0.0025	0.0349	0.0320	0.0800	0.0064
515	0.0285	0.0023	0.0321	0.0298	0.0718	0.0078
520	0.0268	0.0022	0.0297	0.0278	0.0689	0.0015
525	0.0250	0.0021	0.0278	0.0256	0.0637	0.0056
530	0.0234	0.0020	0.0257	0.0233	0.0621	0.0054
535	0.0218	0.0019	0.0241	0.0223	0.0598	0.0003
540	0.0204	0.0018	0.0226	0.0197	0.0590	0.0048
545	0.0189	0.0017	0.0210	0.0184	0.0572	0.0028
550	0.0170	0.0017	0.0189	0.0160	0.0548	0.0015
555	0.0153	0.0016	0.0173	0.0145	0.0525	0.0004
560	0.0135	0.0016	0.0153	0.0125	0.0483	-0.0001
565	0.0120	0.0015	0.0138	0.0116	0.0467	-0.0031
570	0.0111	0.0014	0.0128	0.0113	0.0457	-0.0062
575	0.0106	0.0013	0.0124	0.0109	0.0435	-0.0024
580	0.0105	0.0013	0.0122	0.0104	0.0422	-0.0020
585	0.0105	0.0012	0.0122	0.0105	0.0406	-0.0029
590	0.0106	0.0012	0.0122	0.0105	0.0399	-0.0027
595	0.0104	0.0011	0.0120	0.0104	0.0397	-0.0044
600	0.0100	0.0011	0.0115	0.0103	0.0375	-0.0025
605	0.0100	0.0011	0.0114	0.0104	0.0372	-0.0023
610	0.0102	0.0010	0.0117	0.0105	0.0373	-0.0026
615	0.0109	0.0010	0.0125	0.0110	0.0366	0.0019
620	0.0113	0.0010	0.0126	0.0111	0.0359	0.0009

625	0.0116	0.0010	0.0129	0.0117	0.0358	0.0001
630	0.0118	0.0010	0.0131	0.0120	0.0340	-0.0026
635	0.0122	0.0010	0.0136	0.0123	0.0344	0.0022
640	0.0123	0.0010	0.0137	0.0122	0.0327	0.0039
645	0.0122	0.0010	0.0137	0.0122	0.0330	0.0033
650	0.0124	0.0010	0.0138	0.0126	0.0326	0.0046
655	0.0137	0.0010	0.0151	0.0137	0.0345	0.0053
660	0.0173	0.0011	0.0192	0.0176	0.0399	0.0086
665	0.0234	0.0014	0.0260	0.0243	0.0506	0.0126
670	0.0292	0.0017	0.0325	0.0303	0.0577	0.0165
675	0.0310	0.0019	0.0347	0.0326	0.0692	0.0165
680	0.0279	0.0017	0.0312	0.0293	0.0606	0.0161
685	0.0211	0.0013	0.0230	0.0212	0.0457	0.0113
690	0.0131	0.0009	0.0140	0.0134	0.0333	0.0027
695	0.0075	0.0007	0.0079	0.0072	0.0210	-0.0030
700	0.0045	0.0006	0.0048	0.0043	0.0141	-0.0078
705	0.0030	0.0005	0.0032	0.0029	0.0123	-0.0067
710	0.0021	0.0005	0.0023	0.0022	0.0093	-0.0074
715	0.0017	0.0004	0.0017	0.0016	0.0079	-0.0083
720	0.0012	0.0003	0.0012	0.0011	0.0064	-0.0063
725	0.0008	0.0003	0.0008	0.0007	0.0062	-0.0069
730	0.0005	0.0003	0.0004	0.0004	0.0048	-0.0068
735	0.0003	0.0002	0.0001	0.0003	0.0036	-0.0066
740	0.0002	0.0001	0.0001	0.0000	0.0023	-0.0025
745	0.0001	0.0001	0.0000	0.0000	0.0017	-0.0040
750	0.0000	0.0000	0.0000	0.0000	0.0000	0.0000

	Regression		Point by point			
λ	a_{det}*	a_{det}* c.i.	a_{det}* mean	a_{det}* edian	a_{det}* max	a_{det}* min
400	0.0409	0.0086	0.0538	0.0485	0.4386	0.0101
405	0.0396	0.0083	0.0519	0.0469	0.4210	0.0110
410	0.0386	0.0081	0.0504	0.0448	0.4083	0.0113
415	0.0372	0.0078	0.0487	0.0435	0.3952	0.0116
420	0.0356	0.0076	0.0462	0.0415	0.3823	0.0100
425	0.0340	0.0072	0.0442	0.0390	0.3667	0.0113
430	0.0322	0.0069	0.0418	0.0370	0.3507	0.0099
435	0.0303	0.0066	0.0393	0.0350	0.3355	0.0088
440	0.0285	0.0063	0.0372	0.0326	0.3199	0.0076
445	0.0264	0.0060	0.0344	0.0299	0.3030	0.0066
450	0.0246	0.0057	0.0321	0.0275	0.2858	0.0055
455	0.0228	0.0054	0.0299	0.0255	0.2736	0.0029
460	0.0214	0.0051	0.0280	0.0234	0.2591	0.0035
465	0.0199	0.0049	0.0262	0.0216	0.2482	0.0020
470	0.0185	0.0048	0.0243	0.0202	0.2384	0.0004
475	0.0173	0.0046	0.0229	0.0183	0.2281	-0.0028
480	0.0163	0.0044	0.0217	0.0167	0.2183	-0.0011
485	0.0151	0.0042	0.0204	0.0170	0.2098	-0.0031
490	0.0142	0.0040	0.0191	0.0150	0.2031	-0.0031
495	0.0134	0.0039	0.0179	0.0145	0.1936	-0.0045
500	0.0127	0.0037	0.0170	0.0133	0.1849	-0.0049
505	0.0121	0.0036	0.0160	0.0120	0.1768	-0.0061
510	0.0115	0.0035	0.0150	0.0110	0.1711	-0.0060
515	0.0108	0.0033	0.0142	0.0109	0.1622	-0.0068
520	0.0101	0.0032	0.0134	0.0105	0.1552	-0.0074

525	0.0094	0.0031	0.0126	0.0092	0.1487	-0.0082
530	0.0088	0.0029	0.0117	0.0081	0.1408	-0.0081
535	0.0083	0.0028	0.0110	0.0076	0.1341	-0.0089
540	0.0077	0.0027	0.0101	0.0066	0.1281	-0.0098
545	0.0072	0.0026	0.0093	0.0057	0.1209	-0.0096
550	0.0066	0.0024	0.0086	0.0054	0.1133	-0.0099
555	0.0060	0.0023	0.0077	0.0045	0.1047	-0.0118
560	0.0055	0.0022	0.0070	0.0047	0.0985	-0.0115
565	0.0051	0.0021	0.0065	0.0042	0.0916	-0.0119
570	0.0047	0.0019	0.0059	0.0034	0.0845	-0.0116
575	0.0044	0.0019	0.0054	0.0032	0.0794	-0.0114
580	0.0043	0.0018	0.0053	0.0030	0.0740	-0.0108
585	0.0041	0.0017	0.0050	0.0029	0.0710	-0.0113
590	0.0038	0.0016	0.0046	0.0025	0.0670	-0.0105
595	0.0035	0.0016	0.0042	0.0024	0.0635	-0.0102
600	0.0032	0.0014	0.0038	0.0025	0.0586	-0.0098
605	0.0028	0.0014	0.0034	0.0017	0.0551	-0.0094
610	0.0025	0.0013	0.0030	0.0017	0.0529	-0.0095
615	0.0022	0.0012	0.0027	0.0017	0.0494	-0.0092
620	0.0021	0.0012	0.0026	0.0018	0.0471	-0.0089
625	0.0019	0.0011	0.0024	0.0013	0.0453	-0.0086
630	0.0018	0.0011	0.0023	0.0014	0.0423	-0.0083
635	0.0017	0.0010	0.0022	0.0012	0.0402	-0.0081
640	0.0016	0.0010	0.0020	0.0011	0.0382	-0.0082
645	0.0015	0.0009	0.0018	0.0010	0.0351	-0.0075
650	0.0014	0.0009	0.0017	0.0011	0.0341	-0.0072
655	0.0013	0.0008	0.0016	0.0010	0.0320	-0.0072
660	0.0013	0.0008	0.0016	0.0011	0.0308	-0.0067
665	0.0013	0.0008	0.0016	0.0009	0.0300	-0.0060
670	0.0011	0.0008	0.0014	0.0008	0.0280	-0.0060
675	0.0007	0.0007	0.0009	0.0006	0.0270	-0.0061
680	0.0003	0.0007	0.0006	0.0004	0.0280	-0.0061
685	0.0002	0.0006	0.0002	-0.0001	0.0214	-0.0063
690	-0.0001	0.0005	-0.0003	-0.0003	0.0156	-0.0068
695	-0.0003	0.0005	-0.0003	-0.0002	0.0169	-0.0065
700	-0.0004	0.0005	-0.0005	-0.0004	0.0148	-0.0061
705	-0.0005	0.0004	-0.0006	-0.0006	0.0107	-0.0056
710	-0.0006	0.0004	-0.0008	-0.0006	0.0094	-0.0057
715	-0.0007	0.0004	-0.0009	-0.0007	0.0077	-0.0083
720	-0.0006	0.0003	-0.0008	-0.0008	0.0055	-0.0039
725	-0.0005	0.0002	-0.0005	-0.0005	0.0056	-0.0032
730	-0.0004	0.0002	-0.0004	-0.0003	0.0036	-0.0029
735	-0.0003	0.0001	-0.0003	-0.0003	0.0018	-0.0025
740	-0.0001	0.0001	-0.0001	-0.0002	0.0023	-0.0011
745	-0.0001	0.0001	-0.0001	-0.0001	0.0019	-0.0010
750	0.0000	0.0000	0.0000	0.0000	0.0000	0.0000

	Regression		Point by point			
λ	a_{mss}*	a_{mss}* c.i.	a_{mss}* mean	a_{mss}*median	a_{mss}* max	a_{mss}* min
400	0.0537	0.0027	0.0544	0.0514	0.0854	0.0401
405	0.0525	0.0026	0.0531	0.0505	0.0824	0.0393
410	0.0511	0.0025	0.0515	0.0489	0.0796	0.0383
415	0.0496	0.0024	0.0501	0.0477	0.0770	0.0371

420	0.0481	0.0024	0.0483	0.0463	0.0748	0.0357
425	0.0462	0.0022	0.0465	0.0448	0.0717	0.0342
430	0.0445	0.0021	0.0445	0.0431	0.0680	0.0328
435	0.0426	0.0021	0.0424	0.0410	0.0651	0.0307
440	0.0407	0.0020	0.0405	0.0391	0.0617	0.0296
445	0.0390	0.0019	0.0385	0.0371	0.0588	0.0267
450	0.0373	0.0018	0.0366	0.0355	0.0555	0.0255
455	0.0357	0.0018	0.0350	0.0337	0.0531	0.0240
460	0.0343	0.0017	0.0335	0.0320	0.0511	0.0227
465	0.0329	0.0016	0.0320	0.0307	0.0489	0.0215
470	0.0317	0.0016	0.0306	0.0294	0.0466	0.0192
475	0.0305	0.0015	0.0295	0.0285	0.0451	0.0188
480	0.0294	0.0015	0.0283	0.0274	0.0430	0.0175
485	0.0284	0.0014	0.0272	0.0264	0.0418	0.0175
490	0.0273	0.0014	0.0262	0.0255	0.0397	0.0166
495	0.0263	0.0014	0.0251	0.0244	0.0386	0.0152
500	0.0253	0.0013	0.0240	0.0235	0.0368	0.0150
505	0.0243	0.0013	0.0230	0.0226	0.0353	0.0135
510	0.0232	0.0012	0.0219	0.0217	0.0334	0.0126
515	0.0223	0.0012	0.0210	0.0208	0.0318	0.0123
520	0.0214	0.0011	0.0201	0.0199	0.0301	0.0115
525	0.0205	0.0011	0.0192	0.0193	0.0283	0.0108
530	0.0196	0.0010	0.0183	0.0184	0.0276	0.0102
535	0.0187	0.0010	0.0173	0.0176	0.0256	0.0091
540	0.0177	0.0010	0.0164	0.0167	0.0244	0.0083
545	0.0167	0.0009	0.0154	0.0158	0.0228	0.0076
550	0.0157	0.0008	0.0145	0.0149	0.0214	0.0082
555	0.0147	0.0008	0.0134	0.0137	0.0199	0.0059
560	0.0137	0.0008	0.0125	0.0129	0.0186	0.0053
565	0.0128	0.0007	0.0116	0.0120	0.0172	0.0045
570	0.0120	0.0007	0.0108	0.0112	0.0159	0.0047
575	0.0112	0.0007	0.0100	0.0104	0.0149	0.0036
580	0.0105	0.0006	0.0094	0.0098	0.0141	0.0029
585	0.0100	0.0006	0.0088	0.0091	0.0131	0.0026
590	0.0094	0.0006	0.0083	0.0086	0.0123	0.0024
595	0.0089	0.0005	0.0079	0.0083	0.0114	0.0020
600	0.0085	0.0005	0.0074	0.0079	0.0107	0.0015
605	0.0080	0.0005	0.0070	0.0075	0.0102	0.0014
610	0.0077	0.0005	0.0067	0.0071	0.0098	0.0014
615	0.0073	0.0005	0.0064	0.0068	0.0094	0.0010
620	0.0069	0.0005	0.0060	0.0065	0.0091	0.0009
625	0.0066	0.0004	0.0057	0.0061	0.0086	0.0010
630	0.0063	0.0004	0.0054	0.0058	0.0081	0.0008
635	0.0059	0.0004	0.0052	0.0056	0.0077	0.0004
640	0.0057	0.0004	0.0049	0.0054	0.0074	0.0006
645	0.0054	0.0004	0.0047	0.0052	0.0072	0.0001
650	0.0051	0.0004	0.0044	0.0049	0.0067	0.0002
655	0.0049	0.0003	0.0042	0.0047	0.0064	0.0001
660	0.0047	0.0003	0.0040	0.0044	0.0062	-0.0001
665	0.0044	0.0003	0.0038	0.0041	0.0059	0.0000
670	0.0042	0.0003	0.0036	0.0037	0.0056	0.0013
675	0.0038	0.0003	0.0033	0.0034	0.0052	-0.0005
680	0.0035	0.0003	0.0029	0.0030	0.0047	-0.0007
685	0.0031	0.0002	0.0026	0.0027	0.0043	-0.0006

690	0.0027	0.0002	0.0022	0.0024	0.0037	-0.0009
695	0.0024	0.0002	0.0020	0.0021	0.0036	-0.0007
700	0.0021	0.0002	0.0017	0.0019	0.0034	-0.0012
705	0.0019	0.0002	0.0015	0.0016	0.0029	-0.0008
710	0.0016	0.0002	0.0012	0.0013	0.0026	-0.0002
715	0.0013	0.0001	0.0010	0.0011	0.0021	-0.0005
720	0.0011	0.0001	0.0008	0.0009	0.0017	-0.0007
725	0.0009	0.0001	0.0006	0.0007	0.0013	-0.0006
730	0.0007	0.0001	0.0005	0.0006	0.0010	-0.0003
735	0.0005	0.0001	0.0003	0.0004	0.0007	-0.0005
740	0.0003	0.0001	0.0003	0.0003	0.0006	-0.0003
745	0.0002	0.0000	0.0001	0.0001	0.0005	-0.0003
750	0.0000	0.0000	0.0000	0.0000	0.0000	0.0000

	Regression		Point by point			
λ	a_{cdom}*	a_{cdom}* c.i.	a_{cdom}*mean	a_{cdom}*median	a_{cdom}* max	a_{cdom}* min
400	1.6277	0.0567	1.6594	1.6050	4.2363	0.6603
405	1.5760	0.0491	1.5976	1.5736	3.2184	0.6703
410	1.5099	0.0398	1.5605	1.5312	3.1611	0.8440
415	1.4374	0.0376	1.5003	1.4735	2.8789	0.7155
420	1.3534	0.0356	1.3917	1.3740	2.8249	0.7500
425	1.2696	0.0293	1.3431	1.2661	3.6184	0.9163
430	1.1318	0.0292	1.1659	1.1563	1.8002	0.7975
435	1.0712	0.0255	1.0927	1.0701	1.7293	0.6400
440	1.0000	0.0000	1.0000	1.0000	1.0000	1.0000
445	0.9189	0.0215	0.9197	0.9126	1.8068	0.4507
450	0.8470	0.0218	0.8635	0.8478	2.0518	0.4487
455	0.7869	0.0214	0.8279	0.7907	2.2763	0.4338
460	0.7404	0.0206	0.7418	0.7434	1.5964	0.3291
465	0.6964	0.0194	0.6861	0.6937	1.3904	-0.0335
470	0.6486	0.0212	0.6510	0.6564	1.5746	0.0273
475	0.6031	0.0218	0.5798	0.5961	0.9196	-0.5716
480	0.5682	0.0214	0.5642	0.5726	1.0196	0.1376
485	0.5509	0.0193	0.5556	0.5431	1.2505	-0.0240
490	0.5030	0.0225	0.5037	0.5128	0.9512	-0.0035
495	0.4795	0.0203	0.4773	0.4833	1.2096	-0.1535
500	0.4569	0.0240	0.4604	0.4552	0.9386	-0.2556
505	0.4417	0.0202	0.4498	0.4389	1.1124	0.0432
510	0.4052	0.0200	0.3952	0.3987	0.7008	-0.2626
515	0.4065	0.0198	0.4090	0.4019	0.8517	-0.1943
520	0.3750	0.0202	0.3721	0.3775	0.7471	-0.2059
525	0.3531	0.0206	0.3427	0.3548	0.7711	-0.2385
530	0.3567	0.0215	0.3530	0.3591	0.6815	-0.1177
535	0.3285	0.0182	0.3276	0.3243	0.8224	-0.3183
540	0.3178	0.0191	0.3112	0.3208	0.6238	-0.2824
545	0.3044	0.0225	0.3072	0.3120	0.7240	-0.1517
550	0.2970	0.0176	0.2997	0.3047	0.6001	-0.1413
555	0.2800	0.0186	0.2821	0.2674	0.7057	-0.3141
560	0.2713	0.0172	0.2585	0.2714	0.5037	-0.4324
565	0.2539	0.0179	0.2479	0.2498	0.8860	-0.2163
570	0.2425	0.0184	0.2443	0.2360	0.7354	-0.1840
575	0.2239	0.0201	0.2203	0.2329	0.6524	-0.3950
580	0.2334	0.0158	0.2434	0.2349	0.5837	-0.0323

585	0.2154	0.0192	0.1969	0.2111	0.8335	-0.6181
590	0.2092	0.0209	0.2097	0.2115	0.7186	-0.7942
595	0.1979	0.0179	0.2023	0.1924	0.7825	-0.2631
600	0.1814	0.0153	0.1749	0.1681	0.3863	-0.2189
605	0.1768	0.0167	0.1674	0.1730	0.3683	-0.5867
610	0.1884	0.0166	0.1951	0.1978	0.5132	-0.1712
615	0.1883	0.0155	0.2059	0.2059	1.2577	-0.0444
620	0.1752	0.0150	0.1892	0.1824	0.9390	-0.0625
625	0.1606	0.0143	0.1781	0.1692	0.8062	-0.0092
630	0.1674	0.0140	0.1802	0.1705	0.5110	-0.0285
635	0.1640	0.0158	0.1872	0.1781	0.6985	-0.0408
640	0.1488	0.0146	0.1617	0.1523	0.7323	-0.0859
645	0.1487	0.0150	0.1674	0.1558	1.0534	-0.1694
650	0.1387	0.0143	0.1491	0.1404	0.6839	-0.1469
655	0.1322	0.0131	0.1594	0.1458	1.2924	-0.0346
660	0.1160	0.0156	0.1304	0.1309	0.5480	-0.2190
665	0.1298	0.0136	0.1511	0.1368	0.9282	-0.0743
670	0.1154	0.0139	0.1393	0.1215	1.0087	-0.1988
675	0.1142	0.0141	0.1268	0.1152	0.5633	-0.0738
680	0.1049	0.0169	0.1249	0.1122	0.6457	-0.0438
685	0.0911	0.0132	0.1026	0.0900	0.3225	-0.0386
690	0.0778	0.0120	0.0897	0.0877	0.4224	-0.0484
695	0.0551	0.0143	0.0620	0.0669	0.2724	-0.4701
700	0.0514	0.0124	0.0572	0.0456	0.4055	-0.0991
705	0.0247	0.0216	0.0171	0.0315	0.1864	-1.2802
710	0.0150	0.0128	0.0115	0.0108	0.3420	-0.1793
715	0.0000	0.0000	0.0000	0.0000	0.0000	0.0000
720	-0.0100	0.0103	-0.0216	-0.0188	0.1626	-0.5685
725	-0.0434	0.0139	-0.0565	-0.0411	0.3061	-0.8103
730	-0.0906	0.0180	-0.1412	-0.1142	0.1762	-1.5762
735	-0.1363	0.0194	-0.1636	-0.1382	0.1239	-1.4859
740	0.0052	0.0206	0.0394	0.0306	0.4735	-0.2258
745	0.1125	0.0226	0.1875	0.1706	1.0683	-0.1456
750	0.1735	0.0239	0.2545	0.2348	1.0544	-0.0604

	Regression		Point by point			
λ	b_{chl}*	b_{chl}* c.i.	b_{chl}* mean	b_{chl}*median	b_{chl}* max	b_{chl}* min
412	0.42217	0.061388	0.54527	0.48526	1.9638	0.14838
440	0.40265	0.058958	0.51978	0.45986	1.8239	0.13842
488	0.40287	0.05895	0.51975	0.45838	1.8844	0.13305
510	0.40658	0.058912	0.52388	0.45949	1.8625	0.13666
532	0.40693	0.058587	0.52306	0.45626	1.8573	0.14055
555	0.40546	0.057409	0.52025	0.45555	1.8311	0.14029
650	0.39045	0.05489	0.50076	0.4322	1.7827	0.13463
676	0.36912	0.053778	0.47641	0.40927	1.7753	0.12416
715	0.38751	0.053459	0.49284	0.42825	1.8022	0.13612

	Regression		Point by point			
λ	b_{mss}*	b_{mss}* c.i.	b_{mss}* mean	b_{mss}*median	b_{mss}* max	b_{mss}* min
412	0.35498	0.023274	0.37224	0.34449	0.60682	0.26577

440	0.35637	0.022279	0.36734	0.33671	0.58876	0.25173
488	0.36379	0.021638	0.37116	0.34453	0.56699	0.26558
510	0.36663	0.021617	0.37114	0.34691	0.55677	0.2659
532	0.36767	0.021498	0.37039	0.34454	0.54621	0.26385
555	0.36847	0.020942	0.36917	0.34345	0.53424	0.26189
650	0.36493	0.019556	0.35931	0.3332	0.49032	0.25649
676	0.36157	0.01984	0.35352	0.32944	0.47936	0.25103
715	0.36338	0.019197	0.35479	0.33483	0.48486	0.25792

	Regression		Point by point			
λ	bb/bchl*	bb/bchl* c.i.	bb/bchl*mean	bbchl* median	bbchl* max	bbchl* min
676	0.004758	0.001143	0.005717	0.005802	0.040437	0.000829

	Regression		Point by point			
λ	bb/bmss*	bb/bmss* c.i.	bb/bmss*mean	bb/bmss* median	bb/bmss* max	bb/bmss* min
676	0.008557	0.000639	0.004094	0.008632	0.014311	0.000569

References

AHN, Y.H., A. BRICAUD AND A. MOREL, Light backscattering efficiency and related properties of some phytoplankters, *Deep-Sea Research*, 39, pp. 1835-1855, 1992.

ALLALI, K., A. BRICAUD, M. BABIN, A. MOREL AND P. CHANG, A new method for measuring spectral absorption coefficients of marine particles, *Limnol. Oceanogr.,* 40, pp. 1526-1532, 1995.

AUSTIN, R.W., Coastal Zone Color Scanner radiometry, *Proceedings of the Society of Photo-Optical Instrumentation Engineers*, 208, pp. 170-177, 1979.

BABIN, M., A. MOREL, V. FOURNIER-SICRE, F. FELL AND D. STRAMSKI, Light scattering properties of marine particles in coastal and open ocean waters as related to the particle mass concentration, *Limnol. Oceanogr.,* 48, pp. 843-859, 2003.

BABIN, M., AND D. STRAMSKI, Light absorption by aquatic particles in the near-infrared spectral region, *Limnol. Oceanogr.*, 47, pp. 911-915, 2002.

BABIN, M., AND D. STRAMSKI, Variations in the mass-specific absorption coefficient of mineral particles suspended in water, *Limnol. Oceanogr.*, 49, pp. 756-767, 2004.

BABIN, M., D. STRAMSKI, G.M. FERRARI, H. CLAUSTRE, A. BRICAUD, G. OBOLENSKY, N. HOEPFFNER, Variations in the light absorption coefficients of phytoplankton, nonalgal particles, and dissolved organic matter in coastal waters around Europe, *J. Geophys. Res. (C Oceans),* 108, 2003.

BALCH, W.M., KILPATRICK, K.A., AND C.C. TREES, The 1991 coccolithophore bloom in the Central North Atlantic. 1. Optical properties and factors affecting their distribution, *Limnol. Oceanogr.,* 41, pp. 1669-1683, 1996.

BOWDEN, K.F., Physical Oceanography of the Irish Sea, 67 pp, 1955.

BOWERS, D.G., BOUDJELAS, S., AND G.E.L. HARKER, The distribution of fine suspended sediments in the surface waters of the Irish Sea and its relation to tidal stirring, *International Journal of Remote Sensing,* 19, pp. 2789-2805, 1998.

BOWERS, D.G., HARKER, G.E.L., AND B. STEPHAN, Absorption spectra of inorganic particles in the Irish Sea and their relevance to remote sensing of chlorophyll, *International Journal of Remote Sensing,* 17, pp. 2449-2460, 1996.

BOWERS, D.G., AND E.G. MITCHELSON-JACOB, Inherent optical properties of the Irish Sea determined from underwater irradiance measurements, *Estuarine, Coastal and Shelf Science,* 43, pp. 433-447, 1996.

BRICAUD, A., M. BABIN, A. MOREL, AND H. CLAUSTRE, Variability in the chlorophyll-specific absorption coefficients of natural phytoplankton: Analysis and parameterization, *J. Geophys. Res. (C Oceans)*, 100, pp. 13,321-13,332, 1995.

BRICAUD, A., A. MOREL, AND L. PRIEUR, Absorption by dissolved organic matter of the sea (yellow substance) in the UV and visible domains, *Limnol. Oceanogr.* 26, pp. 43-53, 1981.

BRICAUD, A., AND D. STRAMSKI, Spectral absorption coefficients of living phytoplankton and nonalgal biogenous matter: A comparison between the Peru upwelling area and the Sargasso Sea, *Limnol. Oceanogr.* 35, pp. 562-582, 1990.

BUCHAN, S., G.D. FLOODGATE, AND D.J. CRISP, Studies on the seasonal variation of the suspended matter in the Menai Straits. I. The inorganic fraction, *Limnol. Oceanogr.* 12, pp. 419-431, 1967.

BUKATA, R.P., J.H. JEROME, K.Y. KONDRATYEV, AND D.V. POZDNYAKOV, *Optical properties and remote sensing of inland and coastal waters*, CRC Press, Inc., 2000 Corporate Blvd., N.W., Boca Raton, FL 33431, 1995.

BULGARELLI, B., G. ZIBORDI, AND J.F. BERTHON, Measured and modelled radiometric quantities in coastal waters: toward a closure, *Applied Optics* 42, pp. 5365-5381, 2003.

CARDER, K. L., S. K. HAWES, K. A. BAKER, R. C. SMITH, R. G. STEWARD, AND B. G. MITCHELL, Reflectance model for quantifying chlorophyll a in the presence of productivity degradation products, *J. Geophys. Res. (C Oceans).* 96, pp. 0,599-611, 1991.

CARDER, K.L., STEWARD, R.G., G.R. HARVEY AND P.B. ORTNER, Marine humic and fulvic acids: Their effects on remote sensing of ocean chlorophyll, *Limnol. Oceanogr.* 34, pp. 68-81, 1989.

CHAMI, M., D. MCKEE, E. LEYMARIE AND G. KHOMENKO, Influence of the angular shape of the volume-scattering function and multiple scattering on remote sensing reflectance, *Applied Optics* 45, pp. 9210-9220, 2006.

CHANG, G.C., T.D. DICKEY, C.D. MOBLEY, E. BOSS AND W.S. PEGAU, Toward closure of upwelling radiance in coastal waters, *Applied Optics* 42, pp. 1574-1582, 2003.

CIOTTI, A.M., M.R. LEWIS AND J.J. CULLEN, Assessment of the relationships between dominant cell size in natural phytoplankton communities and the spectral shape of the absorption coefficient, *Limnol. Oceanogr.* 47, pp. 404-417, 2002.

CLAUSTRE, H., HOOKER, S. B., VAN HEUKELEM, L., BERTHON, J. -F., BARLOW, R., RAS, J., SESSIONS, H., TARGA, C., THOMAS, C. S., VAN DER LINDE, D. AND MARTH, J. -C., An intercomparison of HPLC phytoplankton pigment methods using in situ samples: application to remote sensing and database activities, *Mar. Chem.* 85, pp. 41-61, 2004.

COBLE, P.G., Characterization of marine and terrestrial DOM in seawater using excitation emission matrix spectroscopy, *Mar. Chem.* 51, pp. 325-346, 1996.

COTA, G.F., W.O. SMITH, JR. AND B.G. MITCHELL, Photosynthesis of Phaeocystis in the Greenland Sea, *Limnol. Oceanogr.* 39, pp. 948-953, 1994.

FUJI, M., E. BOSS AND F. CHAI, The value of adding optics to ecosystem models: a case study, *Biogeosciences* 4, pp. 817-835, 2007.

GALLEGOS, C.L., D.L. CORRELL AND J.W. PIERCE, Modeling spectral diffuse attenuation, absorption, and scattering coefficients in a turbid estuary, *Limnol. Oceanogr.* 35, pp. 1486-1502, 1990.

GARVER, S.A., AND D.A. SIEGEL, Inherent optical property inversion of ocean color spectra and its biogeochemical interpretation. 1. Time series from the Sargasso Sea, *J. Geophys. Res. (C Oceans)* 102, pp. 18,607-618,625, 1997.

GORDON, H. R., O. B. BROWN, R. H. EVANS, J. W. BROWN, R. C. SMITH, K. S. BAKER, AND D. K. CLARK, A semianalytic radiance model of ocean color, *J. Geophys. Res. Atmospheres* 93, pp. 10909-10924, 1988.

GORDON, H.R., AND K.Y. DING, Self-shading of in-water optical-instruments, *Limnol. Oceanogr.* 37, pp. 491-500, 1992.

GORDON, H.R. AND A.Y. MOREL, Remote assessment of ocean color for interpretation of satellite visible imagery. A review, 1983.

GOULD, R.W., R.A. ARNONE AND P.M. MARTINOLICH, Spectral dependence of the scattering coefficient in case 1 and case 2 waters, *Applied Optics* 38, pp. 2377-2383, 1999.

GOWEN, R.J., D.K. MILLS, M. TRIMMER AND D.B. NEDWELL, Production and its fate in two coastal regions of the Irish Sea: the influence of anthropogenic nutrients, *Marine Ecology-Progress Series* 208, pp. 51-64, 2000.

GOWEN, R.J., B.M. STEWART, D.K. MILLS AND P. ELLIOTT, Regional differences in stratification and its effect on phytoplankton production and biomass in the northwestern Irish Sea, *J. Plankton Res.* 17, pp. 753-769, 1995.

GREGG, W.W., AND K.L. CARDER, A simple spectral solar irradiance model for cloudless maritime atmospheres, *Limnol. Oceanogr.* 35, pp. 1657-1675, 1990.

HILL, A.E., R. DURAZO AND D.A. SMEED, Observations of a cyclonic gyre in the western Irish Sea, *Cont. Shelf Res.* 14, pp. 479-490, 1994.

HIRATA, T., J. AIKEN, N. J. HARDMAN-MOUNTFORD, T. J. SMYTH, AND R. G. BARLOW, An absorption model to determine phytoplankton size classes from satellite ocean colour. *Remote Sensing of the Environment* 112 (6), pp. 3153-3159, 2008.

HORSBURGH, K.J., A. E. HILL, J. BROWN, L. FERNAND, R. W. GARVINE AND M. M. P. ANGELICO, Seasonal evolution of the cold pool gyre in the western Irish Sea, *Prog. Oceanogr.* 46, pp. 1-58, 2000.

HUOT, Y., C.A. BROWN, AND J. J. CULLEN, New algorithms for MODIS sun-induced chlorophyll fluorescence and a comparison with present data products. *Limnol. Oceanogr.*: *Methods,* 3, pp. 108-130, 2005.

IOCCG, Remote Sensing of Inherent Optical Properties: Fundamentals, Tests of Algorithms, and Aplications. 2006.

ITURRIAGA, R., AND D.A. SIEGEL, Microphotometric characterization of phytoplankton and detrital absorption properties in the Sargasso Sea, *Limnol. Oceanogr.* 34, pp. 1706-1776, 1989.

JEFFREY, S.W., AND G.F. HUMPHREY, New spectrophotometric equations for determining chlorophylls a, b, c1 and c2 in higher plants, algae and natural phytoplankton. Biochemie und Physiologie der Pflanzen, 167, pp. 191-194, 1975.

JERLOV, N.G., *Marine Optics*, Elsevier. Amsterdam-Oxford-New York. 1976.

JONES, T.A., Multiple regression with correlated independent variables. *Math. Geol*. 4**,** pp. 203-208, 1972.

KIEFER, D.A., R.J. OLSON AND W.H. WILSON, Reflectance spectroscopy of marine phytoplankton. Part 1. Optical properties as related to growth rate, *Limnol. Oceanogr.* 24, pp. 664-672, 1979.

KIEFER, D.A., AND J.B. SOOHOO, Spectral absorption by marine particles of coastal waters of Baja California, *Limnol. Oceanogr.* 27, pp. 492-499, 1982.

KIRK, J.T.O., *Light and photosynthesis in aquatic ecosystems*, 2nd edition, Cambridge University Press. 1994.

KISHINO, M., M. TAKAHASHI, N. OKAMI AND S. ICHIMURA, Estimation of the spectral absorption coefficients of phytoplankton in the sea, 1985.

KOWALCZUK, P., Seasonal variability of yellow substance absorption in the surface layer of the Baltic Sea, *J. Geophys. Res. (C Oceans)* 104, pp. 30047-30058, 1999.

LEATHERS, R.A., AND T.V. DOWNES, Self-shading correction for upwelling sea-surface radiance measurements made with buoyed instruments, *Optics Express* 8, pp. 561-570, 2001.

LEE, Z.P., K.L. CARDER AND R.A. ARNONE, Deriving inherent optical properties from water color: a multiband quasi-analytical algorithm for optically deep waters, *Applied Optics* 41, pp. 5755-5772, 2002.

LETELIER, R.M., AND M.R. ABBOTT, An analysis of chlorophyll fluorescence algorithms for the moderate resolution imaging spectrometer (MODIS), *Remote Sensing of Environment* 58, pp. 215-223, 1996.

LOISEL, H., AND A. MOREL, Light scattering and chlorophyll concentration in case 1 waters: A reexamination, *Limnol. Oceanogr*. 43, pp. 847-858, 1998.

MCKEE, D., M. CHAMI, I. BROWN, V. SANJUAN CALZADO, D. DORAXAN, AND A. CUNNINGHAM, The role of measurement uncertainties in observed variability in the spectral backscattering ratio for mineral-rich coastal waters, *Applied Optics (accepted)*, 2009.

MCKEE, D., AND A. CUNNINGHAM, Evidence for wavelength dependence of the scattering phase function and its implication for modeling radiance transfer in shelf seas, *Applied Optics* 44, pp. 126-135, 2005.

MCKEE, D., AND A. CUNNINGHAM, Identification and characterisation of two optical water types in the Irish Sea from in situ inherent optical properties and seawater constituents, *Estuarine Coastal and Shelf Science* 68, pp. 305-316, 2006.

MCKEE, D., A. CUNNINGHAM AND S. CRAIG, Estimation of absorption and backscattering coefficients from in situ radiometric measurements: theory and validation in case II waters, *Applied Optics* 42, pp. 2804-2810, 2003.

MCKEE, D., A. CUNNINGHAM AND S. CRAIG, Semi-empirical correction algorithm for AC-9 measurements in a coccolithophore bloom, *Applied Optics* 42, pp. 4369-4374, 2003.

MCKEE, D., A. CUNNINGHAM, J. SLATER, K.J. JONES AND C.R. GRIFFITHS, Inherent and apparent optical properties in coastal waters: a study of the Clyde Sea in early summer, *Estuarine, Coastal and Shelf Science* 56, pp. 369-376, 2003.

MCKEE, D., A. CUNNINGHAM AND A. DUDEK, Optical water type discrimination and tuning remote sensing band-ratio algorithms: Application to retrieval of chlorophyll and Kd(490) in the Irish and Celtic Seas, *Estuarine Coastal and Shelf Science* 73, pp. 827-834, 2007.

MCKEE, D., A. CUNNINGHAM AND K.J. JONES, Optical and hydrographic consequences of freshwater run-off during spring phytoplankton growth in a Scottish fjord, *J. Plankton Res.* 24, pp. 1163-1171, 2002.

MCKEE, D., A. CUNNINGHAM, D. WRIGHT AND L. HAY, Potential impacts of nonalgal materials on water-leaving Sun induced chlorophyll fluorescence signals in coastal waters, *Applied Optics* 46**,** pp. 7720-7729, 2007.

MCKEE, D., J. PISKOZUB AND I. BROWN, Scattering error corrections for in situ absorption and attenuation measurements, *Optics Express* 16, pp. 19480-19492, 2008.

MCKINNEY, E.S.A., C.E. GIBSON AND B.M. STEWART, Planktonic diatoms in the north-west Irish Sea: A study by automatic sampler, *Biology and Environment-Proceedings of the Royal Irish Academy* 97B, pp. 197-202, 1997.

MEYERS-SCHULTE, K.J., AND J.I. HEDGES, Molecular evidence for a terrestrial component of organic matter dissolved in ocean water, *Nature* 321, pp. 61-63, 1986.

MITCHELL, B.G., Algorithms for determining the absorption coefficient of aquatic particles using the quantitative filter technique (QFT). *Ocean Optics X*, Proc SPIE, p. 1302, 1990.

MITCHELL, B.G., AND D.A. KIEFER, *Determination of absorption and fluorescence excitation spectra for phytoplankton*, Marine phytoplankton and productivity. Springer 157-169, 1984.

MITCHELL, B.G., AND D.A. KIEFER, Chlorophyll a specific absorption and fluorescence excitation spectra for light-limited phytoplankton, *Deep-Sea Research Part a-Oceanographic Research Papers* 35**,** pp. 639-663, 1988.

B.G. MITCHELL AND D.A. KIEFER, Variability in pigment specific particulate fluorescence and absorption-spectra in the northeastern pacific-ocean, *Deep-Sea Research Part a-Oceanographic Research Papers* 35, pp. 665-689, 1988.

MOBLEY, C.D., *Light and Water. Radiative transfer in natural waters*, Academic Press. New York 592 pp, 1994.

MOBLEY, C.D., L.K. SUNDMAN AND E. BOSS, Phase function effects on oceanic light fields, *Applied Optics* 41, pp. 1035-1050, 2002.

MOISAN, T.A., AND B.G. MITCHELL, Photophysiological acclimation of Phaeocystis antarctica Karsten under light limitation, *Limnol. Oceanogr.* 44**,** pp. 247-258, 1999.

MOREL, A., *Optical aspects of oceanography*. In: N.G. Jerlov and E. Steeman Nielson, Editors, Academic, New York, 1974.

MOREL, A., Optical modeling of the upper ocean in relation to its biogenous matter content (case 1 water), *J. Geophys. Res. (C Oceans)* 93**,** pp. 10749-10768, 1988.

MOREL, A., AND A. BRICAUD, Theoretical results concerning light absorption in a discrete medium, and application to specific absorption of phytoplankton, *Deep Sea Research Part A. Oceanographic Research Papers* 28**,** pp. 1375-1393, 1981.

MOREL, A., AND R.C. SMITH, Relation between total quanta and total energy for aquatic photosynthesis, *Limnol. Oceanogr.* 19, pp. 591-600, 1974.

MUELLER, J.L., ET AL., Ocean Optics Protocols For Satellite Ocean Color Sensor Validation, Revision 4, Volumes 1 - 7, SeaWIFS Technical Report Series, NASA/TM-2003-2162, 2003.

NELSON, J.R., AND S. GUARDA, Particulate and dissolved spectral absorption on the continental shelf of the southeastern United States, *J. Geophys. Res. (C Oceans)* 100, pp. 8715-8732, 1995.

PEGAU, W.S., D. GRAY AND J.R.V. ZANEVELD, Absorption and attenuation of visible and near-infrared light in water: dependence on temperature and salinity, *Applied Optics* 36, pp. 6035-6046, 1997.

PETZOLD, T.J., Volume scattering functions for selected ocean waters., *SIO Reference Series*, Scripps Institution of Oceanography, 1972.

PISKOZUB, J., P.J. FLATAU AND J.V.R. ZANEVELD, Monte Carlo study of the scattering error of a quartz reflective absorption tube, *Journal of Atmospheric and Oceanic Technology* 18, pp. 438-445, 2001.

POPE, R.M., AND E.S. FRY, Absorption spectrum (380 -700 nm) of pure water. II. Integrating cavity measurements, *Applied Optics* 36, pp. 8710-8723, 1997.

PRIEUR, L., AND S. SATHYENDRANATH, An Optical Classification of Coastal and Oceanic Waters Based on the Specific Spectral Absorption Curves of Phytoplankton

Pigments, Dissolved Organic Matter, and Other Particulate Materials, *Limnol. Oceanogr.* 26, pp. 671-689, 1981.

REYNOLDS, R.A., D. STRAMSKI AND B.G. MITCHELL, A chlorophyll-dependent semianalytical reflectance model derived from field measurements of absorption and backscattering coefficients within the Southern Ocean, *J. Geophys. Res. (C Oceans)* 106, pp. 7125-7138, 2001.

ROESLER, C.S., Theoretical and experimental approaches to improve the accuracy of particulate absorption coefficients derived from the quantitative filter technique, *Limnol. Oceanogr.* 43, pp. 1649-1660, 1998.

ROESLER, C.S., M.J. PERRY AND K.L. CARDER, Modeling in situ phytoplankton absorption from total absorption spectra in productive inland marine waters, *Limnol. Oceanogr.* 34, pp. 1510-1523, 1989.

SATHYENDRANATH, S., L. LAZZARA AND L. PRIEUR, Variations in the spectral values of specific absorption of phytoplankton, *Limnol. Oceanogr.* 32, pp. 403-415, 1987.

SCHILLER, H., AND R. DOEFFER, Neural network for emulation of an inverse model operational derivation of Case II water properties from MERIS data, *Int. J. Remote Sensing*, 20 (9), pp. 1735-1746, 1999.

SIEGEL, D.A., S. MARITORENA, N.B. NELSON, D.A. HANSELL AND M. LORENZI-KAYSER, Global distribution and dynamics of colored dissolved and detrital organic materials, *J. Geophys. Res. (C Oceans)* 107, 2002,

SIMPSON, J.H., AND J.R. HUNTER, Fronts in the Irish Sea, *Nature* 250, pp. 404-406, 1974.

SMITH, R.C., AND K.S. BAKER, Optical properties of the clearest natural waters (200-800 nm), *Applied Optics* 20, pp. 177-184, 1981.

SNYDER, W.A., R. A. ARNONE, C. O. DAVIS, W. GOODE, R. W. GOULD, S. LADNER, G. LAMELA, W. J. RHEA, R. STAVN, M. SYDOR AND A. WEIDEMANN, Optical scattering and backscattering by organic and inorganic particulates in US coastal waters, *Applied Optics* 47, pp. 666-677, 2008.

SOSIK, H.M. AND B.G. MITCHELL, Light absorption by phytoplankton, photosynthetic pigments and detritus in the California Current System, *Deep-Sea Res. (1 Oceanogr. Res. Pap.)* 42, pp. 1717-1748, 1995.

SPINRAD, R.W., K.L. CARDER AND M.J. PERRY, *Ocean Optics*, Oxford University Press, New York, 1994.

STAVN, R.H. AND S.J. RICHTER, Biogeo-optics: particle optical properties and the partitioning of the spectral scattering coefficient of ocean waters, *Applied Optics* 47, pp. 2660-2679, 2008.

STRAMSKI, D., Artifacts in measuring absorption spectra of phytoplankton collected on a filter, *Limnol. Oceanogr.* 35, pp. 1804-1809, 1990.

STRAMSKI, D., A. BRICAUD AND A. MOREL, Modeling the inherent optical properties of the ocean based on the detailed composition of the planktonic community, *Applied Optics* 40, pp. 2929-2945, 2001.

D. STRAMSKI AND A. MOREL, Optical-properties of photosynthetic picoplankton in different physiological states as affected by growth irradiance, *Deep-Sea Res. (1 Oceanogr. Res. Pap.)* 37, pp. 245-266, 1990.

STRAMSKI, D. AND J. TEGOWSKI, Effects of intermittent entrainment of air bubbles by breaking wind waves on ocean reflectance and underwater light field, *J. Geophys. Res. (C Oceans)* 106, pp. 31345-31360, 2001.

SULLIVAN, J. M., M. S. TWARDOWSKI, J. R. V. ZANEVELD, C. M. MOORE, A. H. BARNARD, P. L. DONAGHAY AND B. RHOADES, Hyperspectral temperature and salt dependencies of absorption by water and heavy water in the 400-750 nm spectral range, *Applied Optics* 45, pp. 5294-5309, 2006.

TASSAN S. AND G.M. FERRARI, An alternative approach to absorption measurements of aquatic particles retained on filters, *Limnol. Oceanogr.* 40, pp. 1358-1368, 1995.

TASSAN, S., G.M. FERRARI, A. BRICAUD AND M. BABIN, Variability of the amplification factor of light absorption by filter-retained aquatic particles in the coastal environment, *J. Plankton Res.* 22, pp. 659-668, 2000.

TILSTONE, G.H., T.J. SMYTH, R.J. GOWEN, V. MARTINEZ-VICENTE AND S.B. GROOM, Inherent Optical Properties of the Irish Sea and Their Effect On Satellite Primary Production Algorithms, *J. Plankton Res.* 27, pp. 1127-1148, 2005.

TRIMMER, M., R.J. GOWEN AND B.M. STEWART, Changes in sediment processes across the western Irish Sea front, *Estuarine, Coastal and Shelf Science* 56, pp. 1011-1019, 2003.

ULLOA, O., S. SATHYENDRANATH AND T. PLATT, Effect of the particle-size distribution on backsattering ratio in seawater, *Applied Optics* 33, pp. 7070-7077, 1994.

VIDUSSI, F., H. CLAUSTRE, B.B. MANCA, A. LUCHETTA AND J.C. MARTY, Phytoplankton pigment distribution in relation to upper thermocline circulation in the eastern Mediterranean Sea during winter, *J. Geophys. Res. (C Oceans)* 106, pp. 19,939-19,956, 2001.

YENTSCH, C.S., AND D.A. PHINNEY, A bridge between ocean optics and microbial ecology, *Limnol. Oceanogr.* 34, pp. 1694-1705, 1989.

ZANEVELD, J.R.V., J.C. KITCHEN AND C. MOORE, The scattering correction on reflecting-tube absorprtion meters. *Ocean Optics XII*, SPIE, pp. 44-55, 1994.